UNIVERSITY OF NAPLES FEDERICO II

SCHOOL OF DOCTORATE IN CHEMICAL SCIENCES

Structure and properties of polyolefin-based multilayer films for healthcare applications and management of quality control.

by

Diego Tufano

Tutors:

Prof. Claudio De Rosa

Prof. Finizia Auriemma

Opponent:

Prof. Gerardino D'Errico

Abstract

Different blends of various grades of polyethylene (low density PolyEthylene (LDPE), linear low density PolyEthylene (LLDPE) and medium density PolyEthylene (MDPE), specialty of etherophasic copolymers propylene-ethylene and inorganic additives, as talc and calcium carbonate, were used for the production of multilayered films for healthcare applications. These films were obtained through the blow extrusion process using a pilot plant at company Blu Plast. This study was aimed to the improvement of the characteristic of soft-touch and mechanical performance of films used as back-sheet, whitout resorting surface treatment.

Moreover, the management system of quality control of the company Blu Plast was implemented.

INDEX

CHAPTER 1
Introduction

CHAPTER 2
Extrusion

CHAPTER 3
Experimental parts

CHAPTER 4
Structural and thermal characterization

CHAPTER 5

CHAPTER 1

INTRODUCTION

1.1 Plastics

Plastics are commercially used materials that are based on polymers or prepolymers, from which they are obtained after physical compounding and/or chemical hardening. The name plastics (from Greek *πλαστική τέχνη* = to form, to shape) refers to their easy processibility and shaping that allows them to be cast, pressed, or extruded into a variety of shapes, such as films, plates, tubes, bottles, boxes, and much more.

The history of synthetic plastics is relatively recent, since the industrial production of the main resins dates back to the 1930-1940 years, and in about half century, the use of plastics in many different applications increased enormously, thanks to their low cost of production and versatility.

In the 1930s synthetic polymers, as polyvinyl chloride and polystyrene, were produced commercially, although they were known many years before.

The rapid growth of macromolecular chemistry and plastics production happens from the 1950s, as a results of many factors, as the significant industrial development, the growth of world population, the average increase in standard of living and the replacement of older materials by plastics. The main impulse to the industrial production of synthetic plastics was, hoewever, when for the first time Natta and Ziegler obtained highly crystalline polymers by polymerization of ethylene (1953) and propylene (1954) by using catalysts based on transition metals. The use of Ziegler – Natta catalysts enabled the polymerization of propylene and other α-olefins to solid, crystalline and stereoregular polymers. The commercial production of isotactic polypropylene (iPP) began in Italy, the Federal Republic of Germany, and the

United States in 1957. The use of these catalysts and the availability of inexpensive feedstocks from petroleum refining led to rapid growth of the polymer industry (Tables 1.1 and 1.2)[1]. Plastics are the leader in this growth, followed by synthetic fibers and synthetic elastomers.

Table 1.1. *World production of polymers(in 10^6t/a).*

Type	1940	1950	1960	1970	1980	1990
Plastic	0.36	1.62	6.7	31.0	59.0	100
Fibers						
Synthetic	0.005	0.069	0.70	5.0	11.5	15.7
Semisynthetic	1.1	1.6	2.6	3.4	3.3	3.2
Natural**	8.7	8.0	12.8	14.0	17.7	18*
Elastomers						
Synthetic	0.043	0.54	1.94	5.9	8.7	9.1*
Natural	1.44	1.9	2.02	3.1	3.9	4.9*

*Estimated - ** Textile fibers only

Table 1.2. *Production of plastics, world population, and consumption per capita (in 10^6t/a).*

Region/country	1950	1960	1970	1980	1990
European	0.3	2.3	11.5	19.7	30
Community					
US	1.1	2.8	9.1	16.1	30
Japan	0.04	0.7	5.3	7.5	13
Est Europe	0.1	0.5	4.0	6.9	13
Other	0.07	0.3	1.1	8.8	14
Total	1.6	6.7	31.0	59.0	100
World population, x10^6	2532	3062	3730	4498	5320
Per capita consumption (kg)	0.6	2.2	8.3	13.1	18.8

1.2 Polyethylene

The polyethylene (PE) was synthesized by accident for the first time in 1898 by German chemist Hans von Pechman, who was studying the diazomethane. His colleagues, Eugen Bamberger and Friedrich Tschirner, analyzed the white substance similar to wax on the walls of the container and discovered it contained long chains of $-CH_2-$; they decided to call this substance polymethylene.

The first patent in 1936 and small-scale production in 1939 was due again to the chance observation in 1933 by an ICI research team that traces of a waxy polymer were formed when ethylene and benzaldehyde were subjected to a temperature of 170 °C and a pressure of 190 MPa. The polymers made in this way, by using free radical initiators, were partially crystalline, and measurement of the density of the product was quickly established as a means of determining the crystallinity. Due to the side reactions occurring at the high temperatures employed, the polymer chains were branched, and densities of 0.915 – 0.925 g/cm^3 were typically obtained. The densities of completely amorphous and completely crystalline polyethylene would be 0.88 and 1.0 g/cm^3, respectively.

During the 1950s three research groups working independently discovered three different catalysts which allowed the production of essentially linear polyethylene at low pressure and temperature. These polymers had densities in the region of 0.96 g/cm^3, and became known as high-density polyethylenes (HDPE), in contrast to the polymers produced by the extensively commercialized high-pressure process, which were named low-density polyethylenes (LDPE).[2]

These discoveries laid the basis for the coordination catalysis of ethylene polymerization, which has continued to diversify. Of the three catalytic systems develloped at Standard Oil (Indiana), Phillips Petroleum, and by Karl

Ziegler at the Max-Planck-Institut für Kohlenforschung, the latter two, based on chromium dioxide and titanium halide and organic compounds of aluminum, respectively, have been extensively commercialized. More recently the observation that traces of water can dramatically increase the polymerization rate of certain Ziegler catalysts has led to major developments in soluble coordination catalysts and later their supported variants.[2]

The coordination catalysts allowed for the first time the copolymerizaton of ethylene with other olefins such as butene, which by introducing side branches reduces the crystallinity and allows a low-density polyethylene to be produced at comparatively low pressures. Although Du Pont of Canada introduced such a process in 1960, worldwide the products remained a smallvolume specialty until 1978 when Union Carbide announced their Unipol process and coined the name linear low-density polyethylene (LLDPE). In addition to developing a cheaper production process, Union Carbide introduced the concept of exploiting the different molecular structure of the linear product to make tougher film. Following this lead, LLDPE processes have been introduced by many other manufacturers.[2]

More recently (1983) Walter Kaminsky described a new catalyst, based on metallocene complexes, which combined ideal molecular weight distribution and composition distribution with high yield. The basic form of the catalyst was bis(cyclopentadienyl)dimethylzirconium with a massive excess of methyl aluminoxane as cocatalyst. [3]

The metallocene and the Ziegler catalysts have both demonstrated an excellent flexibility in the synthesis of polyethylene, of other polyolefins and of ethylene copolymers, bases of the wide range of the different grades of polyethylene.

The reason of the great diffusion of polyethylene and other polyelefins is essentially due to the low cost (Table 1.3), easy processability, low specific

weight and good mechanical properties (Table 1.4)[4], from which a wide versatility of use derives (Tables 1.5).

Table 1.3. *Energy cost of production of oil equivalent.*

Packaging	Energy cost (tons eq. of oil)
1 million of shoppers of polyethylene	4.1
1 million of shoppers of paper	7.6
1 million of PVC bottles of 1l	97.0
1 million of glass bottles of 1l	230.0
1 million of HDPE bottles of 0.75l	109.0
1 million of glass bottles of 0.75 l	161.0

Table 1.4. *Properties of some typical polyethylenes (data from Repsol Quimica).*

Property	LDPE	HDPE	LLDPE	Method	Standard
Polymer grade	Repsol PE077/A	Hoechst GD-4755	BP LL 0209		
Melt Flow Index (MFI), g/600 s	1.1	1.1	0.85	190°C/2.16Kg	ASTM D1238
High load MFI, g/600 s	57.9	50.3	24.8	190°C/2.16Kg	ASTM D1238
Die swell ratio (SR)	1.43	1.46	1.11		
Density, Kg/m^3	924.3	961.0	922.0	slow annealed	ASTM D1505
Crystallinity, %	40	67	40	DSC	
Temperature of fusion, °C	110	131	122	DSC	
Vicat softening point, °C	93	127	101	5 °C/h	ASTM D1525
Short branches**	23	1.2	26	IR	
Comonomer		butene	butene	NMR	
Molecular mass*					
M_w	200 000	136 300	158 100	SEC	
M_n	44 200	18 400	35 800	SEC	
Tensile yield strenght, MPa	12.4	26.5	10.3	50 mm/min	ASTM D638
Tensile rupture strenght,MPa	12.0	21.1	25.3		
Elongation at rupture, %	653	906	811		
Modulus of elasticity, MPa	240	885	199	flexure	ASTM D790
Impact energy					
Unnotched, KJ/m^2	74	187	72		ASTM D256
Notched, KJ/m^2	61	5	63		ASTM D256
Permittivity at 1 MHz	2.28				ASTM D1531
Loss tangent at 1 MHz	100x10^{-6}				ASTM D1531
Volume resistivity, Ω•m	10^{16}				
Dielectric strenght, KV/mm	20				

*Corrected for effects of long branching by on-line viscometry - ** Number of methyl group per 1000 carbon atoms.

Table 1.5. *Uses of Polyethylene.*

Containers	Plastics
Glasses, bowl	PVC, PP, HDPE, PS
Trays	PS, PE
Semi-rigid bottles	LDPE, HDPE
Rigid bottles	HDPE, PP, PVC, PET
Transparent bottles	PVC, PET
Jerry can	HDPE, LDPE
Barrel	HDPE
Disposable case	PP, PS
Packing box, case	PP, HDPE
Stretch film	LDPE, PVC
Film for wrapping	PVC, LDPE, HDPE, PP
Film for lamination	PP, PET, PA, LDPE, HDPE
Coatings	LDPE, PP, PVDC
Bags	LDPE, PP, HDPE
Sacks	PVC, LDPE, HDPE

1.2.1 Molecule Structure and morphology.

Polyethylene was classified on the basis of the molecular weight distribution and degree of branching. There are three main grades of polyethylene based on density and structure, as shown in Table 1.6.

Table 1.6. *Grades of Polyethylene.*

Grade	Density g/cm^3
Low Density (LDPE)	0.910-0.925
Linear Low Density (LLDPE)	0.926-0.940
High Density (HDPE)	0.941-0.959

Figure 1 shows schematic structures for the three polyethylenes, with the main features exaggerated for emphasis.

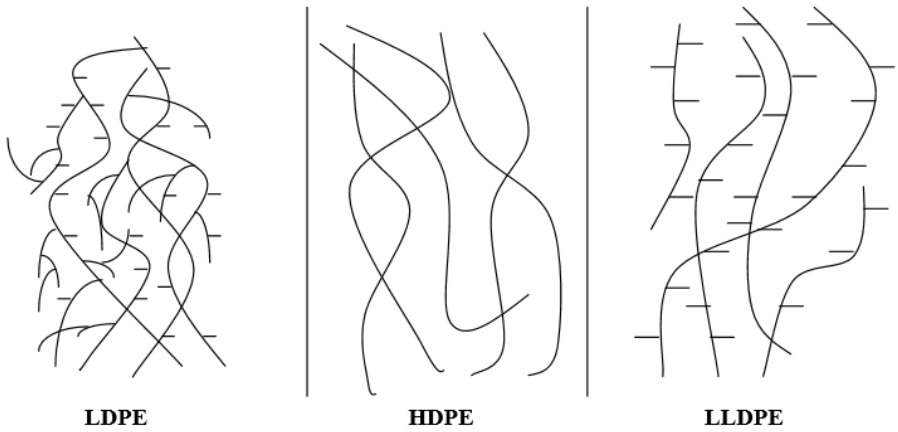

Figure 1: *Schematic molecular structure of PE: LDPE, Low-Density PolyEthylene;* HDPE, *High-Density PolyEthylene; LLDPE, Linear Low-Density PolyEthylene.*

Low Density PolyEthylene, LDPE. It is generally synthesized through radical polymerization and is characterized by a random branching structure, with long chain branching (LCB) and short chain branching (SCB). The SCB are not uniform in length but are mainly four (butyl) or two (ethyl) carbon atoms long.[5] The ethyl branches probably occur in pairs, and there may be some clustering of other branches.[5] The molecular weight distribution (MWD) is moderately broad.

The presence of branching and the lower crystallinity makes LDPE a material more ductile and less stiff compared to HDPE. The physical properties of LDPE depend of the molecular weight, the molecular weight distribution, the frequency of short chain branching, the frequency and length of long-chain branching. [6a] It is used primarily for the production of films, coatings, pipes and cables, and molding applications.

High Density PolyEthylene, HDPE. It is generally synthesized through coordination polymerization with a Ziegler Natta catalyst system and is essentially free of both long and short branching, although very small amounts may be deliberately incorporated to achieve specific product targets. The MWD depends on the catalyst type but is typically of medium width.

Due to the almost absence of branching, HDPE has high intermolecular forces and greater rigidity. The low melting point and high chemical stability facilitate the processability of the HDPE by conventional techniques. Some of the most common applications include containers and articles obtained by injection molding and blow molding, films, coatings, pipes and tubes, obtained by cast or blown extrusion.[6b]

Linear Low Density PolyEthylene, LLDPE. It is normally obtained by copolymerization of ethylene with greater α-olefins (e.g. butene, hexene, octene) by Ziegler-Natta catalysts, and generally represented by formula $[-CH_2-CH_2-CH_2-CH-(C_{n-2}H_{2(n-2)+1})]$, where *n* represents the number of carbon atoms of the comonomer.[6c] It is characterized by chain branching of uniform length randomly distributed along a given chain, but there is a spread of average concentrations between chains, the highest concentrations of branches being generally in the shorter chains.[7] The catalysts used to minimize this effect generally also produce fairly narrow MWDs.

LLDPE is used in packaging especially for film, bags and sheets. Injection molding is the second largest product area for LLDPE.[6c]

The share percentage of market and the consumption, in tons, of the various PE grades in the United States are reported in Table 1.7.

Table 1.7. *Market compared HDPE, LDPE and LLDPE, in North America (10^3t).*[6]

Market Area	**LDPE**	**LLDPE**	**HDPE**
Extrusion			
Film for packaging	1022	1180	164
Film no pakaging	506	1010	753
Coatings	420	13	/
Sheets	56	18	333
Pipes and cables	/	/	710
Injection molding	150	277	1177
Blow	29	9	2066
Other uses	1470	1760	867

The only stable local chain conformation of PE at low temperature is the trans-planar chain configuration with C-C bond length of 0.154 nm, and C C C bond angle of 112°. This local chain conformation also prevails in the melt and solution. The principal crystalline form of linear PE is the orthorhombic (a = 7.40 Å, b = 4.93 Å and c = 2.54 Å)[8a], like the linear paraffins, with theoretical density of 1.00 g/cm^3. A second crystalline form is the pseudomonoclinic[8b] with theoretical density of 0.965 g/cm^3. The former is typical of most articles made of HDPE, while the latter forms during low temperature stretching and orientation of films, and is thus always present in PE film. It is stable only below 50°C; annealing at 80–100°C restores the orthorhombic form.

1.3 Isotactic Polypropylene

The stereospecific polymerization of propylene by Giulio Natta in 1954 is one of the most commercially significant scientific breakthroughs in the polymer chemistry. Natta's discovery that a Ziegler catalyst, based on a solid transition-metal halide, usually TiCl3, and an organoaluminum alkylating agent, such as AlR_3 or AlR_2Cl (R = ethyl or buthyl), later known as Ziegler–Natta catalysts, could be used to produce highly isotactic polypropylene, led to the first commercial processes for the production of this polymer by Montecatini in Italy and Hercules in the United States in 1957.

The attractive properties and relatively low cost of polypropylene produced using this technology led to its rapid commercial acceptance. Consequently, Karl Ziegler and Giulio Natta were awarded the Nobel Prize in Chemistry in 1963.

The commercial potential of olefin polymerization was recognized by many of the leading companies, leading to a tremendous amount of activity and the invention of a number of competing technologies in the early 1950s. These technologies were not, however, economically competitive with those based on Ziegler–Natta catalysts.

1.3.1 Catalytic System for propene polymerization

Early work[9a] by the Natta school used pure $TiCl_3$ made by hydrogen reduction of $TiCl_4$, followed by ball milling to give a high surface area.

$$TiCl4 + ½\ H2 \rightarrow TiCl_3 + HCl$$

A more active form is made by reduction with aluminum powder, followed by ball milling.

$3\ TiCl_4 + Al \rightarrow TiCl_3{\cdot}AlCl_3$

Much of the aluminum chloride is present as a true solid solution in the crystalline violet δ-$TiCl_3$.[9b-d] This catalyst has a larger surface area of 10 – 40

m^2/g and is commercially available from several companies. Nowadays, a Lewis base, such as an ester or ketone, may be introduced at the milling stage to increase stereospecificity.

Another important route dispenses with ball milling by reducing a hydrocarbon solution of $TiCl_4$ with an organoaluminum compound below room temperature. Di- and trialkylaluminum compounds are suitable. In this process $TiCl_3$ precipitates in the brown, β form. Heating to 80 – 120 °C completes the reduction and transforms this solid to the required δ-$TiCl_3$ form. Several hydrocarbon washes remove some of the aluminum compounds to leave an active, stereospecific catalyst. A useful aspect of this technique is that conditions can be selected to precipitate spherical catalyst particles. Subsequent propene polymerization then yields spherical polymer particles that exhibit good flow characteristics. This ability to replicate the shape of catalyst particles is quite general in Ziegler – Natta polymerization. Polymer forms throughout the agglomerate of small catalyst clusters, expanding the particle uniformly in all dimensions as polymerization continues.

Major refinements in alkyl-reduced $TiCl_3$ systems were made by Solvay (second generation catalysts) with formation of a spongelike structure δ-form characterized by a large surface area (150 m^2/g) and porosity (>0.2 cm^3/g) which gave a 4 – 5-fold increase in activity.[10]

Continued interest in olefin polymerization led to the invention of the supported high yield, high stereoregularity catalyst systems based on activated $MgCl_2$, by Montedison in Italy and Mitsui Petrochemical Industries in Japan (third generation catalysts).[11]

A particle-form supported catalyst may be prepared as follows:[11]

1. A spheroidal support is prepared by making a fine dispersion of molten (125 °C) magnesium chloride ethanolate complex in hot kerosene containing

sorbitan distearate as surfactant. The dispersion is quenched by pumping into kerosene at -15 °C to give particles with a diameter of 5 – 30 μm.

2. A slurry of the particles is added to neat $TiCl_4$ at 20 °C.

3. Diisobutyl phthalate (17% v/w) is added and the mixture heated to 120°C.

4. Decant, and heat with further $TiCl_4$ to 130 °C; isolate by hot filtration and washing. The product contains 2.3 wt% Ti, 63 wt% Cl, 20 wt% Mg, and 9.9 wt% diisobutyl phthalate.

For the polymerization of propene, triethylaluminum is used as a cocatalyst, and phenyltriethoxysilane as an additional external Lewis base stereoregulator. By 1980, commercial plants were achieving 20 – 30 kg polymer per gram catalyst, and the isotactic index progressively improved from 88 to 99 % (Table 1.6).

These catalysts form the basis of advanced technology plants in which deashing (removal of catalyst residues) and atactic polymer separation can be eliminated entirely.[11] This led to the development of a number of low cost polymerization processes, spurring a dramatic increase in production capacity. Today, these catalyst systems are used to produce polypropylene in every major region of the world.

More recently in the early 1980s, Sinn and Kaminsky[12] serendipitously discovered that replacing triethylaluminum with methyaluminoxane (MAO) enormously increased the polymerization rate of ethylene when combined with a substituted zirconocene dichloride, but gave an atactic polypropylene. Low stereospecificity, as well as poor reactivity and polymerization temperature restrictions were solved by further molecular tailoring of the matallocene catalysts.

Metallocences suitable for isotactic PP manufacture generally seem to be based on zirconocenes supported on inert solids to preserve particle size and shape. Sophisticated chemistry is needed to prepare the base metallocenes,

many of which have been made only in laboratory-scale equipment. An additional constraint is the heavy patenting, already amounting to more than 900 applications since 1984. Hoechst, Exxon, Fina, Mitsui, and BASF together hold half of these.

The great versatility of metallocenes has been demonstrated in trials that yielded improved and novel polymers. Currently, these polymers are produced in relatively limited amounts for a number of specialty applications.

An overview of the different catalyst development phases for the propene polymerization to isotactic polymer is given in Table 1.8.[13]

Table 1.8. *Catalyst Development*

System	Catalyst performance		Plant process
	Activity, Kg PP/g catalyst	I.I.*, wt %	
1st Generation **1957-1970** **$TiCl_3$ • $AlEt_2Cl$**	0.8-1.2	88-93	deash and remove atactic
2nd Generation **1970-1980** **$TiCl_3$ •$AlEt_2Cl$ + Lewis base (solvay)**	3-5	92-97	deash/deactivate, atactic usually remains
3rd Generation **1980-1990** **MgCl2-supported** **TiCl4•$AlEt_3$**	5-20	≥ 98	no deash and no atactic removal
4th Generation **1995** **Metallocene/MAO systems**	ca. 20	?	no deash and no atactic removal MMD ca. 2-4

*Isotactic index (% insoluble in boiling heptane).

1.3.2 Properties and uses of isotactic polypropylene

Isotactic polypropylene is one of the most widely used polymers in the world because of the widespread availability and low cost of monomer, low manufacturing cost, and attractive polymer properties. These properties can be modified to be suitable for a wide variety of applications.

iPP can be processed by almost all commercial fabrication techniques. Approximately 30,000,000 ton was consumed worldwide in 2001.

iPP is used in a wide range of applications for its remarkable properties such as hardness, high tensile strength and chemical resistance. Some properties of iPP homopolymer are reported in Table 1.9.[13]

The market concerns processes for extrusion of polypropylene is dominated by the production of fibers and films especially in Europe and United State. Its applications show a increasing use in the field of "nonwoven fabrics". The Table 1.10 shows the main uses of polypropylene, on the basis of sales in North America in 1996 (in 10^6 t/y).[13]

Table 1.9. *Mechanical and thermal properties of PP Origin "Propathene" (with permission of ICI Chemicals & Polymers)*

System	Method	Temperature	Homopolymer				Impact copolymer		Random Copolymer LXF 301
			GSE 16	GWM 22	LYM42	LZM55/52	GWM 101	GWM 213	
Melt Flow Index (230 °C/2.16 Kg), g/10 min (dg/min)	ISO 1133		1.00	4.00	12.00	33.00	6.00	2.00	7.50
Tensile yield stress, MPa	ISO 527		33.50	34.50	34.50	34.00	27.00	23.50	25.00
Flex. Modulus, GPa	ISO 178 (10mm/min)		1.45	1.50	1.50	1.55	1.15	1.00	0.85
Izod impact strenght, KJ/m²	ISO 180 (0.25 mm notch radius)	23 °C	4.50	4.50	4.00	3.00	9.50	no break	5.00
		0 °C	3.00	3.00	2.50	2.00	5.50	10.00	2.50
		-20 °C	2.00	2.00	2.00		3.50	7.50	
		-40 °C						5.00	
Instrumented drop weight impact strenght, J	ICI method	23 °C					7.00	10.00	10.00
		0 °C					6.00	11.00	2.00
		-20 °C					6.00	11.00	2.00
		-40 °C						9.50	
Embrittlement temperature, °C	ICI method		> 23	> 23	> 23	> 23	-20.00	-45.00	
Rockwell hardness	ISO2039/ASTM D785 R scale		93.00	95.00	95.00	95.00	90.00	75.00	
Vicat softening temperature (10N force), °C	ISO 306A, BS 2782: 120A		154.00	154.00	154.00	154.00	147.00	142.00	135.00
Heat distortion temperature, °C	ISO 75A & /B								
A - 1.8 MPa			65.00	65.00	65.00	68.00	60.00	50.00	46.00
B – 0.45 MPa			100.00	100.00	100.00	102.00	95.00	90.00	71.00

Table 1.10. *Market data (1996) of poyipropylene in North America (10^6t/y).*[13]

Market Area	PP
Extrusion	
Coatings	5
Fibers and filaments	1463
Film (up to 0.25 mm)	
Oriented	503
Non oriented	111
Tubes and pipes	
Sheets (over 0.25 mm)	110
Wires and cables	5
Other	43
Injection molding	
Appliances	139
Consumer products	565
Rigid packaging	523
Transport	186
Other	131
Blow	79
Other uses	1177

1.3.3 Polymorphism of isotactic polypropylene

i-PP presents a complex polymorphism in the solid state, complicated by the presence of disorder. Three crystalline forms have been identified so far, named α, β and γ, and a mesomorphic form.[14-22] They all are characterized by chains in a 3_1 $(TG)_n$ helical conformation, where T and G stand for backbone torsion angles in trans and gauche states, respectively.

Commercial iPP, prepared with the traditional heterogeneous Ziegler-Natta catalytic systems, generally crystallizes in the stable α form.[23] The γ form may be obtained only under special conditions, i.e., by crystallization from the melt at elevated pressures (about 5000 atm)[23,24] or by crystallization at atmospheric pressure of low molecular weight samples[25] and of copolymers containing small amounts (in the range 5-20 mol %) of other olefins.[26]

iPP samples prepared with homogeneous metallocene catalysts crystallize more easily in the γ form, even at atmospheric pressure and for high molecular weight samples.[27-30] The different polymorphic behavior of iPP samples prepared with heterogeneous and homogeneous catalysts is related to the different type and distribution along the chains of insertion mistakes, that is, stereodefects and regiodefects, generated by the different kinds of catalytic systems. The distribution of defects, in turn, influences the average length of the crystallizable (fully isotactic) sequences.[28-30]

The α-form of isotactic polypropylene. The crystalline α form is generally obtained from melt-crystallization procedures and in drawn fibers.[23] Depending on the thermal and mechanical history, either melt-crystallized samples or drawn fibers, may present different degrees of structural disorder, indicating that they are crystallized in modifications, which can usefully be considered as intermediate between two ideal forms, the limit-ordered and the limit-disordered model structures.[31,32]

As first proposed by Natta and Corradini1 and confirmed by successive studies,[15-17] the α form of i-PP can be described in terms of a monoclinic unit cell (*b* unique axis, chain axis c = 6.5 Å), containing four chains in a 3_1 helical conformation. Left- and right-handed helices, schematized as triangles in the projection perpendicular to *c* of Figure 1.1, are packed in the unit cell in such a way that isochiral chains are piled along *a* forming *a*-*c* rows of parallel

chains, with the chains belonging to adjacent *a*-*c* rows stacked along *b* being enantiomorphous. A pair of adjacent *a*-*c* rows (delimited by the vertical dashed lines in Figure 1.1) is named a bilayer; within the bilayers, the helices face each other along *b* side by side.

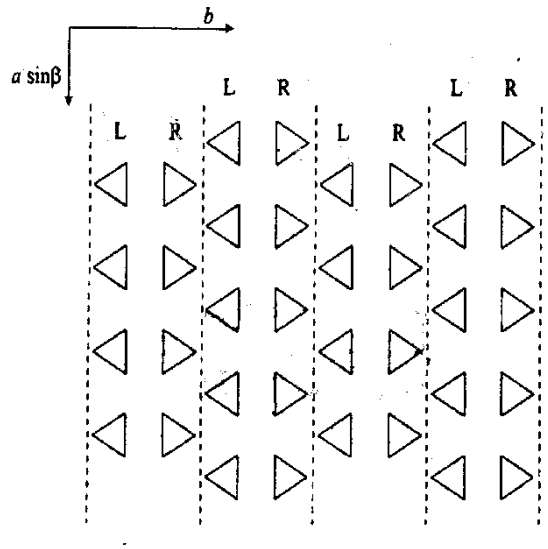

Figure 1.1 *Mode of packing of right- (R) and left- (L) handed 3/1 helices (schematized as triangles) viewed along the c axis in the α form of i-PP. The vertical dashed lines delimit bilayers.*

The γ form of isotactic polypropylene. The crystal structure the γ form is unusual and represents the first example of packing of nonparallel chains.[18-19]

The chains in the helical 3/1 conformation are oriented with the chain axes parallel to the two diagonals in the *ab* plane of the orthorhombic unit cell proposal by Brückner and Meille (a_γ=8.54Å, b_γ=9.93Å, c_γ=42.41Å).[18] The chain axes form an angle of 81.4° and the space group is *Fddd*, consistent with the presence of positional up/down disorder of the isomorphous helices.[18,19]

The value of 81.4° is similar to the angle formed by branched lamellae in iPP samples crystallized in the α form.[23] The growth of branched lamellae in iPP samples crystallized in the α form is a phenomenon well documented in the literature and consists in the epitaxial growth of daughter lamellae on lamellae crystallized in the α form (mother lamellae), so that the c_α and a_α axes of the daughter lamellae are oriented parallel to the a_α e c_α of the mother lamellae, respectively, forming an angle of about 80° between the chain axes.

Figure 1.2A shows the projection of the structural model proposed for the γ form of iPP in a plane perpendicular to the diagonal $\mathbf{a}_\gamma+\mathbf{b}_\gamma$, so to better distinuguish between helices tilted by about 80°. The projection in the $a_\alpha \sin\beta_\alpha$-$b_\alpha$ plane of the structural model proposed for the α form is reported in Figure 1.2B for comparison.

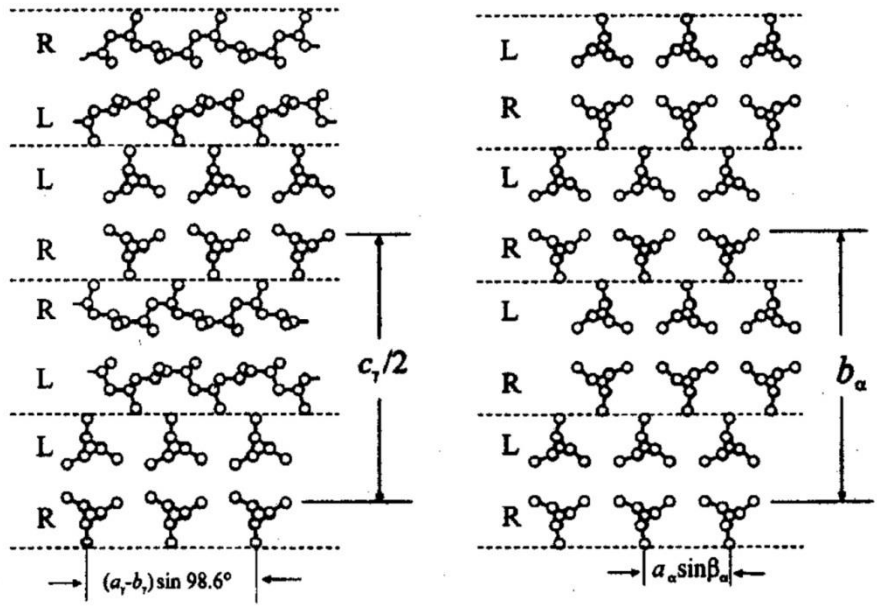

Figure 1.2 *Mode of packing of right- (R) and left- (L) handed 3/1 helices in the γ (A) and α (B) form of i-PP.*

The X-ray diffraction profiles of the α and γ forms are very similar, due to the close resemblance bettween the packing chain model for Figure 1.2. The only difference is in the third diffraction peak (indicated with an arrow in Figure 1.3, which corresponds to *d*=4.77Å (2θ = 18.6°) for αform, to a *d*=4.43Å (2θ = 20.1°) for the γ form.

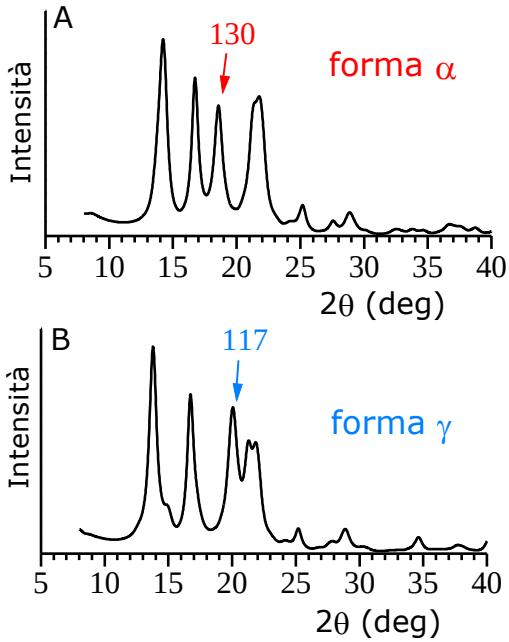

Figure 1.3 *X-ray diffraction profiles of the α (A) and γ (B) form of iPP.*

1.4 Heterophase copolymers of propylene

iPP has unique characteristics as low density, high chemical resistance, good toughness and ability to be oriented. One of the disadvantages of iPP is its fragility, especially at low temperatures.

It has long been recognized that incorporation of an ethylene-propene rubber (EP) fraction into a PP matrix, results in a dramatic improvement in the impact properties of material, even at low temperatures, without excessive deterioration of its rigidity. This results from a multiphase morphology of the PP/EP system, consisting of spherical rubber domains embedded in a semicrystalline polypropylene matrix, which is particularly effective in dissipating the impact energy, possibly via both crazing and shear yielding mechanism.

This multiphase PP/EP materials, named etherophasic copolymers of propene, initially were produced by mechanical blending of iPP and EP rubbers. More recently, they have been obtained by direct synthesis in the polymerization reactor, through a sequential polymerization, where the step of polymerization of the homopolymer iPP is followed by a step of copolymerization in presence of ethylene.[33-36]

Tthe introduction of the elastomeric component produces increase in the impact resistance and decrease of stiffness and hardness of the iPP homopolymer.

The properties of the etherophase copolymers depends on many factors, as nature and composition of the rubber phase, its molecular weight and molecular weight distribution, volume and size of the rubber domains.[33,35,36]

The nature of the rubber phase determines the deformation behavior of the particles dispersed in the PP matrix and their ability to absorb and redistribute the energy; the concentration and the particle size of the the rubber domains (i.e. their number) defines the probability of intercepting the fracture line and

activating the mechanism of opposition to its propagation. The molecular weight of the rubber phase is crucial to control the particles size of the domains in the PP matrix.[33-36]

High amount of PP increases the glass transition temperature (T_g) and reduces the impact resistance of the material, whereas with increasing the amount of EP rubber the T_g decreases and the impact resistance improves, but too high concentrations of ethylene in the EP copolymers can induce the crystallization of long polyethylene sequences.

In general, the properties and application of the etherophase copolymers depend on the relative ratio between rigid, thermoplastic, and elastomeric phase:

1. High Stiffness/Impact materials are obtained for high content of thermoplastic phase (ca. 70 wt%);
2. Soft and supersoft materials for high content of rubber phase (ca. 70 wt%);
3. Thermoplastic elastomers (TPEs) for high content of rubber phase (at least 70 wt%) with ethhylene content of ca. 60wt%.

The development of innovative polymerization processes, as the Catalloy process,[36-37] has allowed the obtaining of every kind of etherophase matereial from super-rigid homopolymers with wide molecular weight distribution, to transparent high-impact and low seal copolymers, up to soft and supersoft materials.

The Catalloy process, working in the presence of isospecific heterogeneous catalysts based on magnesium chloride-supported titanium tetracholoride and electorn donors, is based on a modular technology, consisting of three independent reactors operating in gas phase, allowing the polymerization of different monomers (e.g. propene, ethylene, butene), separately or in series. A

scheme of the Catalloy plants, developped at the Montell Company, is shown in Figure 1.4.

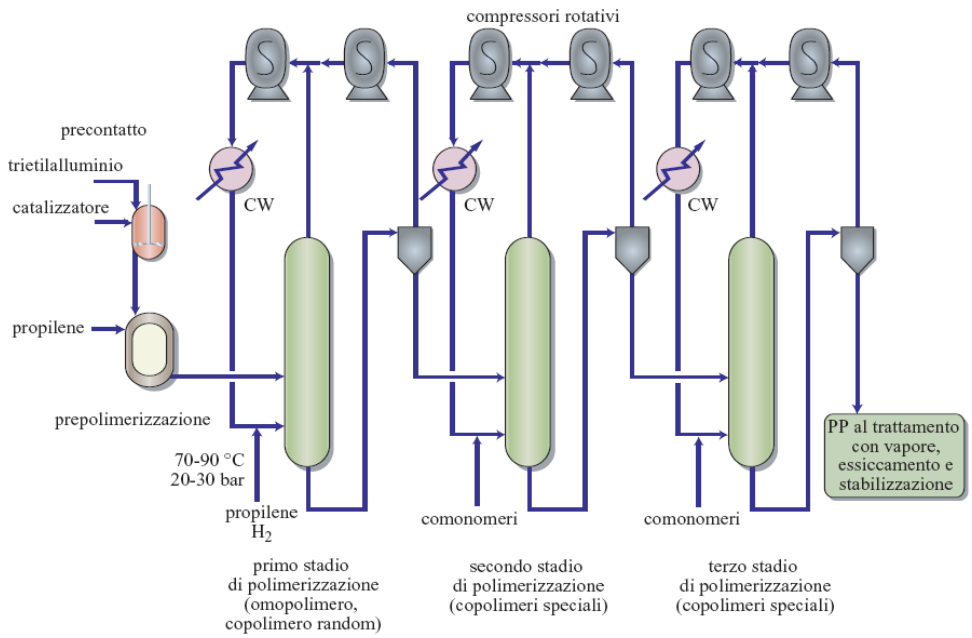

Figure 1.4 *Catalloy plants developed by Montell.*

The main features of the Catalloy process are low energy consumption, high product quality and low manufacturing cost, compared to products obtained by compounding technologies.

Another important aspect is that the Catalloy process exploits the Reactor Granule Technology (RGT), an innovative technology of synthesis capable of controlling and fine tuning both catalyst chemistry and physics, in particular the morphology and porosity of the solid catalyst particle, and the distribution of the active centers in the catalyst particle.[33]

The RGT has been defined as “a controlled, reproducible polymerization of olefinic monomers on an active magnesium cholride supported catalyst, to give a growing, sperical polymer granule that provides a porous reaction bed

within which other monomers can be introduced and polymerized to form a polyolefin alloy".[38] In the RGT the polymer grain tends to reproduce the architecture (shape, structural hierarchy and porosity) of the parent catalyst grain, enlarging of course its size as polymerization yield increases (see Figure 1.5). Thus shape, size and porosity of the catalyst macroparticle can be predicted, designed and tailored to meet a specific product and/or process requirement.[35,36]

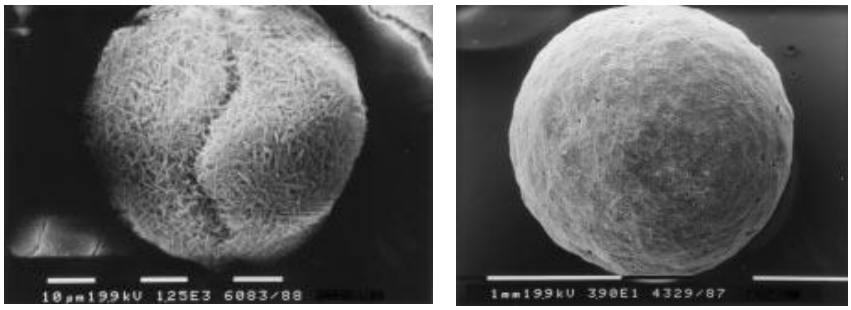

Figure 1.5 *SEM micrographs of (A): a prepolymerized catalyst grain (polypropene/catalyst 0.3 wt/wt) after extraction with hot xylene; (B) a polypropene grain. Polypropylene/ catalyst 20000/1 w/w.*[35]

1.5 The plastics in healthcare applications

Polyolefins especially PE and PP are used in the field of sanitation for:

- Syringes
- Containers for blood and medical liquids
- Containers for drugs
- Traverse
- Outer layer of napkins ("*back sheet*") for adults and childrens

In this area are required special features such as:

- High purity of the components
- No dangerous additives
- Good machine and lamination ability and Good resistance to tear
- Opacity (for films)
- Transparency (for containers)

According to the market demands, the films used as back-sheet in healthcare applications have to ensure good characteistics of "soft touch". This term is generally used to indicate feeling of softness to the touch so that the films appear as a tissue and not as plastic when they are in contact with skin.

“Soft touch” features also ensure a suitable surface in order to allow an excellent adhesion to cellulose and tissues "nonwoven", used in healthcare applications.

The PE-based films, used as back-sheets for fabrication of napkins, are subjected to surface treatments through hot embossing.

This technique induces a surface modification by impressing on it a permanent pattern (micrometric dimensions) consisting of motifs that stick out on one side and are indented on the opposite side of the film. The purpose of embossing is to change the physical characteristics of several materials, such as leather, fabric, paper, plastic, wood and particular metals as aluminum foil. After the embossing treatment, these materials appear more valuable, for example, the paper becomes more absorbent and the aluminum foil more malleable.

In the case of PE-based back-sheet films, hot embossing may also have drastic effects on the mechanical properties up to obtain films with higher flexibility and with cloth-like appearance that mimic that one of non woven materials. The change in the mechanical properties are possibly due to the

high embossing temperature, close to the melting temperature of the polymer, which induces local melting of crystals with consequent decrease of rigidity and improvement of flexibility.

A typical rotary machine for embossing is showed in Figure 1.6.

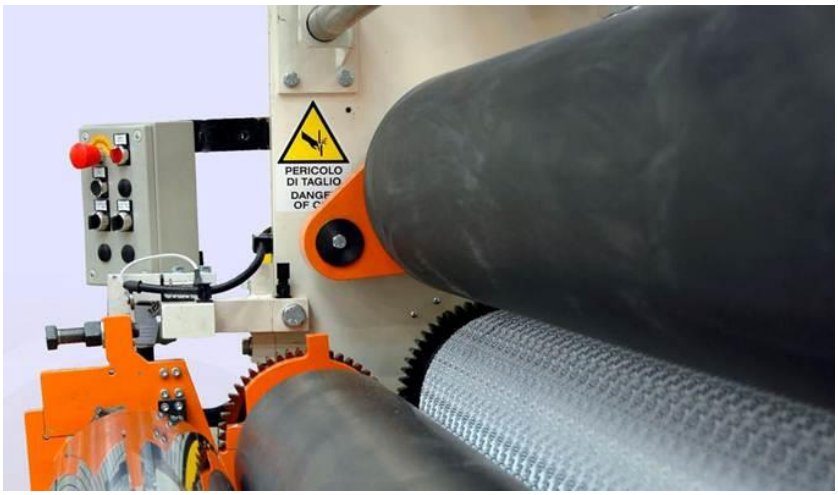

Figure 1.6 *Rotary machine for embossing.*

1.6 Objectives

The objective of this PhD is the development of new polyolefin-based mono and multilayered films, for healthcare applications, produced by extrusion and/or co-extrusion process.

The main goal is obtaining films having mechanical performances and soft-touch characteristics similar to those of the commercial micro-embossing films, without resorting to micro-embossing. In fact, although the use of micro-embossing provides good soft-touch performance to the polyolefins films, it also imply additional costs to the overall process.

In particular, the structure and the physical properties of smooth, not embossed, polyolefin based films used as back sheets (not breathable) of napkins for adult and hospital draw-sheets have been studied.

These films, represent one of three types of materials of the structure of napkins. In fact, napkins usually have a layered structure consisting of a layer (top sheet) of a "nonwoven" material, an inner layer (internal sheet) consisting of cellulose with a super adsorbent polymer, and an outer layer (back sheet) consisting of a polyolefin based film (Figure 1.7).

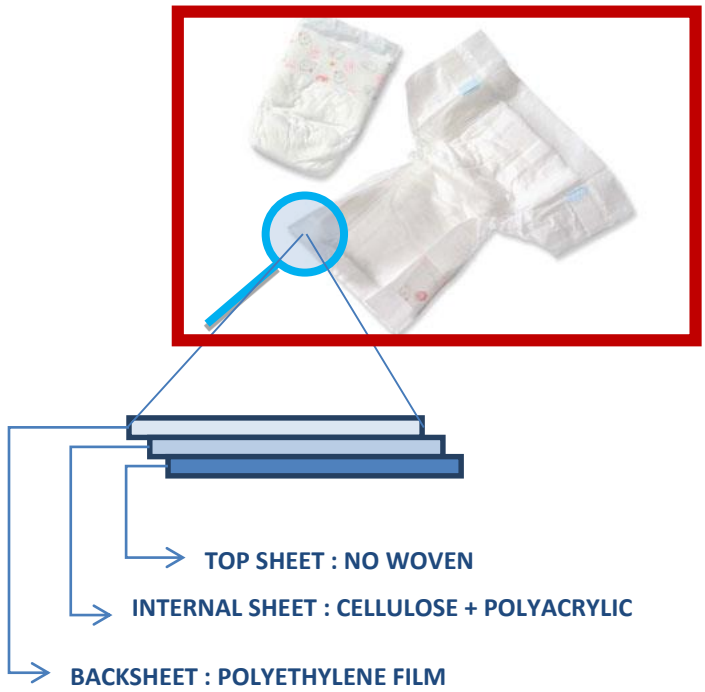

Figure 1.7 *Layered structure of napkins*

A difficulty is to correlate the soft-touch characteristic of the films to physical and measurable parameters. The first part of the research activity has been, hence, aimed at identifying the the physical properties responsible for the characteristic of soft touch of a polyolefin based film and the parameters

directly or indirectly linked to it. To this purpose, three commercial micro-embossed polyethylene films, already present on the market, have been characterized.

Based on the results obtained for the micro-embossed films, we have explored the possibility to produce polyolefin films having similar soft-touch characteristics by a single-step process, thus eliminating the additional cost of the embossing process.

The approach relies on the know-how acquired so far in the field of polymer blends, co-extrusion and in the use of co-polymers of ethylene.

PE films, modified with the addition of inorganic additives and/or mixed with copolymers of ethylene have been prepared and characterized and in order to obtain material having suitable physical parameters correlated to good properties of soft touch.

To this aim, different blends of various kinds of PE, specialty ethylene/propylene etherophase copolymers and inorganic additives have been used to prepare films with thickness of nearly 70 μm, by a tubular-blown extrusion process. These films have been characterized as far as mechanical, thermal properties, morphology and crystallinity. The surface texture of the films have been also analyzed by optical microscopy, atomic force microscopy and using a profilometer. The properties of the films were then compared to those of the commercial micro-embossed polyethylene films.

In order to create a surface having good soft-touch properties without resorting to micro-embossing, the films have been prepared by mixing to the polymer grades special fillers such as talc and calcium carbonate. The particle size distribution, the apparent density and purity, of the additives have been selected in such a way to create motifs sticking out and indenting the film surface (bulges and valleys), able to mimic the surface roughness of commercial films produced with micro-embossing technique.

The thesis project has been performed in collaboration with the Blu Plast s.r.l. company.

Moreover, the process of production of mono and multilayered polyolefin films by the tubular-blown process plants at the Blu Plast company has been improved and the management of their quality control system has been implemented.

1.7 Company Overview

Blu Plast S.r.l. company was founded from Brillante's family.

It produces polyethylene film with blown process for many technical and industrial applications.

Its core business is focused on the production of:

- Film for lamination in food packaging
- Film for lamination in health care
- Printed shrink film
- Printed film for tissue packaging
- Film for protective film
- Polyethylene film for industrial purpose

About 22.000 Tons/year di PE film are produced in the two sites in Italy, Zingonia (BG) and Pagani (SA) where the following study was carried out.

The company uses the latest technology of extrusion and coextrusion for the production of blown film. It has also a five layers Pilot Line in Pagani plant used for the development of new PE-based film employed in healthcare applications.

The constant economic and commercial competition and the search for a product in line with the European regulatory requirements induces the company to optimize the quality control system.

CHAPTER 2

EXTRUSION

2.1 Extrusion Principles

One of the most common methods of processing plastics is Extrusion using a screw inside a barrel as illustrated in Fig. 2.1 The plastic, usually in the form of granules or powder, is fed from a hopper on to the screw. It is then conveyed along the barrel where it is heated by conduction from the barrel heaters and shear due to its movement along the screw flights.

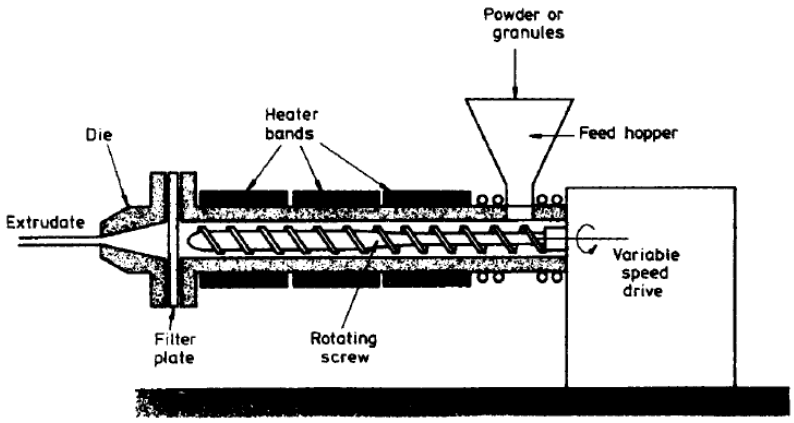

Fig. 2.1 *Schematic view of single screw extruder*

The depth of the screw channel is reduced along the length of the screw so as to compact the material. At the end of the extruder the melt passes through a die to produce an extrudate of the desired shape.

Basically an extruder screw has three different zones (Figure 2.2):

- **Feed Zone:** The function of this zone is to preheat the plastic and convey it to the subsequent zones. The design of this section is important since the constant screw depth must supply sufficient material to the metering zone so as not to starve it, but on the other hand not supply so much material that the metering zone is overrun. The optimum design is related to the nature and shape of the feedstock, the geometry of the screw and the frictional properties of the screw and barrel in relation to the plastic.
- **Compression Zone:** In this zone the screw depth gradually decreases so as to compact the plastic. This compaction has the dual role of squeezing any trapped air pockets back into the feed zone and improving the heat transfer through the reduced thickness of material.
- **Metering Zone:** In this section the screw depth is again constant but much less than the feed zone. In the metering zone the melt is homogenised so as to supply at a constant rate, material of uniform temperature and pressure to the die. This zone is the most straight-forward to analyse since it involves a viscous melt flowing along a uniform channel.

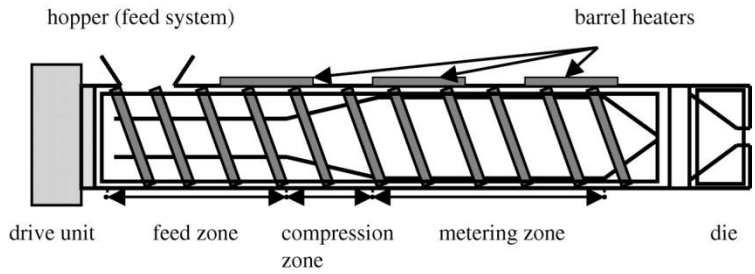

Fig. 2.2 *Different zones in screw extruder*

Another feature of an extruder is the presence of a gauze filter after the screw and before the die. This effectively filters out any inhomogeneous material which might otherwise clog the die.

As the plastic moves along the screw, it melts by the following mechanism. Initially a thin film of molten material is formed at the barrel wall. As the screw rotates, it scrapes this film off and the molten plastic moves down the front face of the screw flight. When it reaches the core of the screw it sweeps up again, setting up a rotary movement in front of the leading edge of the screw flight.

Initially the screw flight contains solid granules but these tend to be swept into the molten pool by the rotary movement. As the screw rotates, the material passes further along the barrel and more and more solid material is swept into the molten pool until eventually only melted material exists between the screw flights.

As the screw rotates inside the barrel, the movement of the plastic along the screw is dependent on whether or not it adheres to the screw and barrel. In theory there are two extremes. In one case the material sticks to the screw only and therefore the screw and material rotate as a solid cylinder inside the barrel. This would result in zero output and is clearly undesirable. In the second case the material slips on the screw and has a high resistance to rotation inside the barrel. This results in a purely axial movement of the melt and is the ideal situation. In practice the behaviour is somewhere between these limits as the material adheres to both the screw and the barrel.

The useful output from the extruder is the result of a drag flow due to the interaction of the rotating screw and stationary barrel. Superimposed on this is a flow due to the pressure gradient which is built up along the screw. Since the high pressure is at the end of the extruder the pressure flow will reduce the output. In addition, the clearance between the screw flights and the barrel

allows material to leak back along the screw and effectively reduces the output.

The external heating and cooling on the extruder also plays an important part in the melting process. The thermal state of the melt in the extruder is frequently compared with two ideal thermodynamic states. One is where the process may be regarded as adiabatic. This means that the system is fully insulated to prevent heat gain or loss from or to the surroundings. If this ideal state was to be reached in the extruder it would be necessary for the work done on the melt to produce just the right amount of heat without the need for heating or cooling. The second ideal case is referred to as isothermal. In the extruder this would mean that the temperature at all points is the same and would require immediate heating or cooling from the barrel to compensate for any loss or gain of heat in the melt. In practice the thermal processes in the extruder fall somewhere between these ideals. Extruders may be run without external heating or cooling but they are not truly adiabatic since heat losses will occur. Isothermal operation along the whole length of the extruder cannot be envisaged if it is to be supplied with relatively cold granules.

2.2 Co-Extrusion

As a result of the wide range of requirements which occur in practice it is not surprising that in many cases there is no individual plastic which has the correct combination of properties to satisfy a particular need.

Therefore it is becoming very common in the manufacture of articles such as packaging film, gaskets and window frames that a multi-layer plastic composite will be used. This is particularly true for extruded film and thermoforming sheets. In co-extrusion two or more polymers are combined in a single process to produce a multilayer film. These co-extruded films can either be produced by a blown film or a cast film process as illustrated in Figs

2.3 (a) and (b). The cast process using a slot die and chill roll to cool the film, produces a film with good clarity and high gloss. The film blowing process, however, produces a stronger film due to the transverse orientation which can be introduced and this process offers more flexibility in terms of film thickness.

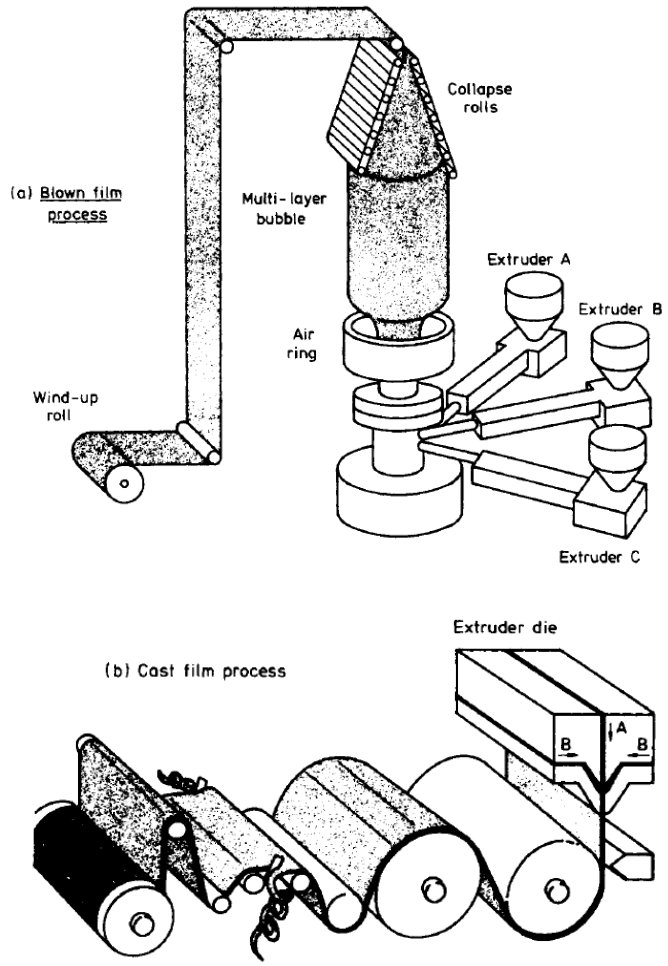

Fig. 2.3 *Co-Extrusion of plastic film*

The main reason for producing multi-layer co-extruded films is to get materials with better barrier properties, particularly in regard to gas permeation.

The production of multilayer structures of polymers and other materials (paper, aluminum foil) is obtained with the lamination technique, which involves the production of the individual films in rolls and then a step of coupling through the use of adhesives.

2.3 Film Blowing

Although plastic sheet and film may be produced using a slit die, by far the most common method nowadays is the film blowing process illustrated in Fig. 2.4. The molten plastic from the extruder passes through an annular die and emerges as a thin tube. A supply of air to the inside of the tube prevents it from collapsing and indeed may be used to inflate it to a larger diameter.

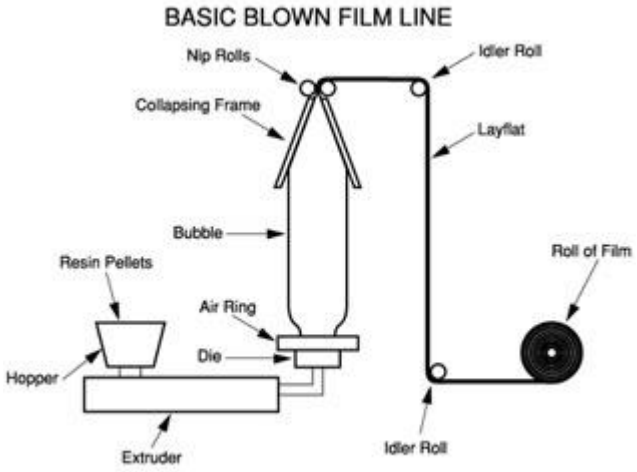

Figure 2.4 *Film blowing process*

Initially the bubble consists of molten plastic but a jet of air around the outside of the tube promotes cooling and at a certain distance from the die exit, a freeze line can be identified (Figure 2.5). Eventually the cooled film passes through collapsing guides and nip rolls before being taken off to storage drums or, for example, gussetted and cut to length for plastic bags.

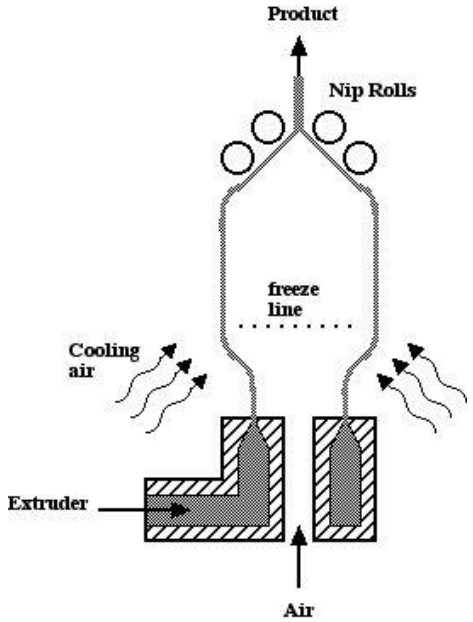

Figure 2.5 *Freeze Line in blowing extrusion*

The major advantage of film blowing is the ease with which biaxial orientation can be introduced into the film. The pressure of the air in the bubble determines the ***blow-up*** and this controls the circumferential orientation. In addition, axial orientation may be introduced by increasing the nip roll speed relative to the linear velocity of the bubble. This is referred to as ***draw-down***. It is possible to make a simple estimate of the orientation in blown film by considering only the effects due to the inflation of the bubble. Since the volume flow rate is the same for the plastic in the die and in the bubble, then for unit time

$$\pi D_d h_d L_d = \pi D_b h_b L_b$$

where ***D, h*** and ***L*** refer to diameter, thickness and length respectively and the subscript ***'d'*** is for the die and ***'b'*** is for the bubble.

So the orientation in the machine direction, O_{MD}, is give by

$$O_{MD} = \frac{L_b}{L_d} = \frac{D_d h_d}{h_b D_b} = \frac{h_d}{h_b B_R}$$

where ***BUR*** = blow-up ratio *(D_b/D_d)*

Also the orientation in the transverse direction, $\boldsymbol{O_{TD}}$, is given by

$$O_{TD} = \frac{D_d}{D_b} = B_R$$

Therefore the ratio of the orientations may be expressed as

$$\frac{O_{MD}}{O_{TD}} = \frac{h_d}{h_b (B_R)^2}$$

2.3.1 Additives

Usually, in most of extrusion processes are used additional resins to modify and / or improve performaces of the films, such as:

- SLIP: additives used to decrease the COF (Coefficient of Friction) of films; these slip agents migrate through the film and they are balanced between the matrix and the surface of the same. This migration is dependent on the polymer, the thickness, and environmental conditions (temperature and humidity).
- ANTI-BLOCKING: based on synthetic silicates, natural or mineral fillers (Talc or $CaCO_3$) that dispersed through the film change the surface state by decreasing COF, but they have a negative influence on the optical properties (opacity).
- ANTI-OXIDANTS (phosphites and phenols): additives used primarily during the extrusion process to protect the polymers by oxidation.
- POLYMERS PROCESSING AID (Fluoro-Polymer): improve the flow of the polymer for a better surface appearance during extrusion .
- COLOURS (example: TiO_2): used as a masterbatch to change the color of the film.

CHAPTER 3

Experimental part

3.1 Materials

Three commercial embossed films available in the market and used as back-sheet, have been analyzed and their properties have been compared to those of the new production films.

The characteritisc of the commercial embossed films, named as Film 1, Film 2 and Film 3, are reported in Table 3.1. In particular, Film 1 was produced by cast process, whereas Film 2 and Film 3 were produced by blowing process.

Table 3.1 *Characteristics of the three analyzed commercial embossed films.*

Samples	Type	Process	Effective Thickness (μ)	Apparent Thickness (μ)	perception Soft Touch
Film1	embossed	cast	35	45	Excellent
Film 2	embossed	blown	26	26	Good
Film 3	embossed	blown	33	33	Good

Since these film were subjected to the embossing procedure, they present on the surface a permanent pattern formed by bulges and valleys, well visible from the images obtained by an optical microscope (see Figure 4.14 - 4.16 of Chapter 4). Therefore, the films have an apparent thickness depending on the type of pattern imprinted on the surface (the height of the bulges and the depth of the valleys) and an effective thickness, corresponding to the thickness of the flat films before the embossing process. The values of apparent thickness, supplied by the film producers, and the effective

thickness, measured with a micrometer in different areas of the film, are reported in Table 3.1 for the three analyzed films.

The soft-touch perception of the embossed films indicated in Table 3 refers to the feeling of softness to the touch, evaluated by simply handling the films, with respect to a tissue (excellent indicates that the film have equal soft-touch perception of the tissue).

Three different sets of multilayered films, with thickness in the range 25 - 70 μm, have been produced by using blends of various grades of PE, different ethylene-propylene etherophase copolymers and inorganic additives, as calcium carbonate ($CaCO_3$) and talc ($Mg_3Si_4O_{10}(OH)_2$). They are listed in Tables 3.2 and 3.3.

In particular, the first sets of samples (Test 1 – Test 4) includes films having a total thickness of 70 μm, same mixture of different PE grades, but different amounts of $CaCO_3$, from 0% (sample Test 1) to 40 wt% (sample Test 4), as shown in Table 3.2. The films were produced by the pilot plant at the Blu Plast Company (see Paragraph 3.2).

The second set of samples (Test 4 – Test 4-4) consists in films having same composition of film of Test 4, with 40wt% of $CaCO_3$, but different thicknesses, from 70 μm (sample Test 4) to 25 μm (sample Test 4-4), as indicated in Table 3.2.

Table 3.2 *First and second sets of samples, with different amount of $CaCO_3$ and different thickness.*

Thickness (μm)	**$CaCO_3$ (wt%)**			
	0	**20**	**30**	**40**
70	Test 1	Test 2	Test 3	Test 4
50				Test 4-2
35				Test 4-3
25				Test 4-4

The third sets of samples (Test 5 - Test 7) consists in films having total thickness of 70 μm, same mixture of different PE grades, but different for the amounts and kind of of inorganic additives, as $CaCO_3$ and talc, and for the presence of small amount of an elastomeric ethylene/propylene copolymers (PE-PP), as shown in Table 3.3.

Table 3.3 *Third sets of samples, with different amount and kind of inorganic fillers (talc and $CaCO_3$) and different etherophasic ethylene-propylene copolymers (PE-PP1 and PE-PP2).*

Thickness (μm)	30%$CaCO_3$ + Talc	40%$CaCO_3$ + PE-PP 1	50%$CaCO_3$ + PE-PP 1 + PE-PP 2	40%$CaCO_3$ + PE-PP 2
70	Test 5	Test 6	Test 6 BIS	Test 7

All the films of Tables 3.2 and 3.3 were produced by the pilot plant at the Blu Plast Company (see Paragraph 3.2).

3.2 Extrusion process parameters of the samples

The pilot plant used for the production of the samples of Table 3.2 and 3.3 is a five-layers blown extrusion plant.

The scheme of the plant is shown in Figure 3.1 where A, B, C, D and E indicate the five extruders. The extruders and the extruder head can be divided in different zones, indicated in Figure 3.1 as Z1 - Z7. In particular, the extruders A and E constitue the inner and outer layers, respectively, whereas the extruders B, C and D constitute the central layers, having same composition. Therefore, the films can be considered as 3-layered films, even if they are produced by a 5-layers co-extrusion plant.

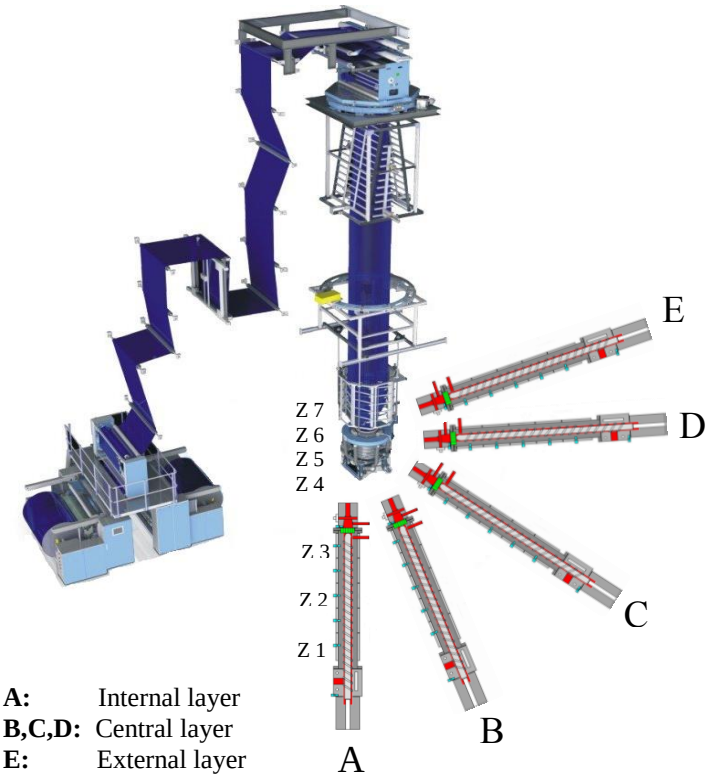

Figure 3.1 *Scheme of the 5-layers pilot plant used for the production of the samples of Table .3.2 and 3.3, with indication of the various extrusion zones Z1 - Z7.*

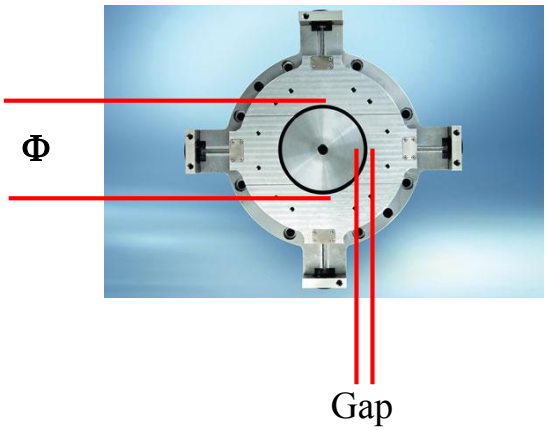

Figure 3.3 *Extrusion Heads*

The head of the extruder, in particular the shape and the dimensionof the annular gap of the die (Figure 3.2), plays a fundamental role on the film properties. The width of the annular die gap (Gap) determines the thickness of the film coming out from the extruder, values of Gap within the range from 0.6 mm (for thin film) to 1.6 mm (for thick film) are generally used. The final thickness depends on the values of *Blow-Up Ratio* and *Draw-Down Ratio* (BUR and DDR, see Chapter 2). The diameter of the tubular films, depending on the circunference of the bubble, are generally from several centimetres up to three meters.

The process parameters of the pilot plant used for the production of the films are reported in Table .3.4. The extruder head has fixed values of Gap = 1.5 mm and die diameter Φ = 130 mm. All films were extruded with a bubble circumference of 1200 mm corresponding to a BUR value of 2.9 (Table 3.4).

The thickness of the films depends on the DDR value. For the first and third set of samples, having thickness of 70 μm, DDR was fixed to 7.3; for the second set of samples, having thickness of 50, 35 and 25 μm, the DDR values was increased to 10.2, 14.6 and 20.4, respectively (Table 3.4).

The values of temperatures in the extruder zones and in the head are reported in Table .3.5. For the films containing inorganic fillers the temperatures in the various zones were increased to improve the dispersion of the inorganic phase in the polymeric matrix.

Table 3.4 *Process Parameters used for the production of the samples of Table 3.2 and 3.3. Circunferenze of the bubble, Blow-Up and Draw-Down Ratios (BUR and DDR), width of the anular gap (Gap) and diameter of the die (Φ) of the extruder head.*

Samples	Circumference Bubble (mm)	Thickness (μm)	BUR	DDR	Gap (mm)	Φ (mm)
Test 1	1200	70	2.9	7.3	1.5	130
Test 2	1200	70	2.9	7.3	1.5	130
Test 3	1200	70	2.9	7.3	1.5	130
Test 4	1200	70	2.9	7.3	1.5	130
Test 4-2	1200	50	2.9	10.2	1.5	130
Test 4-3	1200	35	2.9	14.6	1.5	130
Test 4-4	1200	25	2.9	20.4	1.5	130
Test 5	1200	70	2.9	7.3	1.5	130
Test 6	1200	70	2.9	7.3	1.5	130
Test 6 Bis	1200	70	2.9	7.3	1.5	130
Test 7	1200	70	2.9	7.3	1.5	130

Table 3.5 *Temperatures in the different extrusion zone of Figure 3.1 and head and rate of the screw turn.*

Samples	Extrusor	Zone 1 T(°C)	Zone 2 T(°C)	Zone 3 T(°C)	Extruder Head T(°C)				Turn Screw (rpm)
					Z4	Z5	Z6	Z7	
Test 1	A	190	190	190	190	190	190	190	90
	B / C / D	190/190/190	190/190/190	190/190/190					
	E	190	190	190					
Test 2	A	205	205	205	205	210	207	208	90
	B / C / D	205/208/205	205/208/208	205/208/208					
	E	205	208	205					
Test 3	A	205	210	205	208	210	210	210	90
	B / C / D	205/210/205	205/212/208	205/210/208					
	E	210	212	210					
Test 4	A	205	210	205	208	210	210	210	90
	B / C / D	205/210/205	205/212/208	205/210/208					
	E	210	212	210					
Test 4-2	A	205	210	205	201	201	202	201	60
	B / C / D	205/210/205	205/212/208	205/210/208					
	E	210	210	210					
Test 4-3	A	205	210	205	201	201	202	201	30
	B / C / D	205/210/205	205/212/208	205/210/208					
	E	210	210	210					
Test 4-4	A	205	210	205	201	201	202	201	15
	B / C / D	205/210/205	205/212/208	205/210/208					
	E	210	210	210					

The polymeric basic structure of all samples has been obtained using a mixture of different grades of polyethylene: low-density PE (LDPE), linear-low-density PE (copolymer with butene C4-LLDPE) and medium-density polyethylene (MDPE), supplied by Polimeri Europa and listed in Table 3.6.

Table 3.6 *Characteristics of the three different grades of PE used for the preparation of the multilayerd films from the MDS of Polimeri Europa.*

Samples	**Type**	**Supplier**	**MFI (g/10min)**	***d*** **(g/cm^3)**	***T*$_m$ (°C)**
LDPE	Riblene FF 34	Polimeri Europa	0.75	0.924	114
C4-LLDPE	Flexirene FG 20 F	Polimeri Europa	1.0	0.918	120
MDPE	Eraclene FB 506	Polimeri Europa	0.8	0.939	129

The inorganic fillers were added as masterbatch, in particular calcium carbonate was added as masterbatch constituted by 80% of calcium carbonate and 20% of LDPE, while talc was added as masterbatch constituted by 60% of talc and 40% of LDPE.

The Test 1 sample does not contain calcium carbonate, for the Test 2 – Test 4 samples different amounts of masterbatch containing calcium carbonate were added in the inner and outer layers from 25 to 65 wt%, with the aim of improving the characteristics of the soft touch, maintaining constant the composition of the central layers (Table 3.7).

Table 3.7 Layer composition of the first set of samples (Test 1 – Test 4).

Sample	A	B	C	D	E
Test 1 (0% $CaCO_3$)	LDPE	C4-LLDPE	C4-LLDPE	C4-LLDPE	LDPE
	C4-LLDPE	LDPE	LDPE	LDPE	C4-LLDPE
	MDPE				MDPE
Test 2 (20% $CaCO_3$)	LDPE	C4-LLDPE	C4-LLDPE	C4-LLDPE	LDPE
	C4-LLDPE	LDPE	LDPE	LDPE	C4-LLDPE
	MDPE	25% $CaCO_3$	25% $CaCO_3$	25% $CaCO_3$	MDPE
	25% $CaCO_3$				25% $CaCO_3$
Test 3 (30% $CaCO_3$)	LDPE	C4-LLDPE	C4-LLDPE	C4-LLDPE	LDPE
	C4-LLDPE	LDPE	LDPE	LDPE	C4-LLDPE
	MDPE	25% $CaCO_3$	25% $CaCO_3$	25% $CaCO_3$	MDPE
	50% $CaCO_3$				50% $CaCO_3$
Test 4 (40% $CaCO_3$)	LDPE	C4-LLDPE	C4-LLDPE	C4-LLDPE	LDPE
	C4-LLDPE	LDPE	LDPE	LDPE	C4-LLDPE
	MDPE	25% $CaCO_3$	25% $CaCO_3$	25% $CaCO_3$	MDPE
	65% $CaCO_3$				65% $CaCO_3$

The second set of samples (Test 4-2 – Test 4-4) has same composition of the sample of Test 4 (40wt% of calcium carbonate) and different thickness.
In the third set of samples different kinds and amounts of inorganic fillers (as talc and calcium carbonate) and different types of etherophase PE/PP copolymers were added. In particular, the sample Test 5 has same composition of the sample Test 4 with small amounts of masterbatch containing talc in the inner and outer layers (Table 3.8). In the sample Test 6 small amounts of an etherophasic copolymer PE-PP1, constituted by 70-75% of elastomeric phase and 25-30% of thermoplastic phase, were added in the inner and outer layers. In the sample Test 7 the percentage of calcium carbonate in the central layers was incresed to 50wt% and small amounts of a supersoft ethylene-propylene etherophasic copolymer PE-PP2, constituted of more than 80% of elastomeric phase, were added. The sample Test 6 BIS has composition of the central layers as Test 7 and the external layers as Test 6.

Table 3.8 Layer composition of the third set of samples (Test 5 – Test 7).

	A	B	C	D	E
Test 5 (30% $CaCO_3$)	LDPE	C4-LLDPE	C4-LLDPE	C4-LLDPE	LDPE
	C4-LLDPE	LDPE	LDPE	LDPE	C4-LLDPE
	MDPE	25% $CaCO_3$	25% $CaCO_3$	25% $CaCO_3$	MDPE
	50% $CaCO_3$				50% $CaCO_3$
	Talc				Talc
Test 6 (40% $CaCO_3$)	LDPE	C4-LLDPE	C4-LLDPE	C4-LLDPE	LDPE
	PE-PP 1	LDPE	LDPE	LDPE	PE-PP 1
	MDPE	25% $CaCO_3$	25% $CaCO_3$	25% $CaCO_3$	MDPE
	65% $CaCO_3$				65% $CaCO_3$
Test 6 BIS (50% $CaCO_3$)	LDPE	C4-LLDPE	C4-LLDPE	C4-LLDPE	LDPE
	PE-PP 1	LDPE	LDPE	LDPE	PE-PP 1
	MDPE	50% $CaCO_3$	50% $CaCO_3$	50% $CaCO_3$	MDPE
	65% $CaCO_3$	PE-PP 2	PE-PP 2	PE-PP 2	65% $CaCO_3$
Test 7 (40% $CaCO_3$)	LDPE	C4-LLDPE	C4-LLDPE	C4-LLDPE	LDPE
	C4-LLDPE	LDPE	LDPE	LDPE	C4-LLDPE
	MDPE	50% $CaCO_3$	50% $CaCO_3$	50% $CaCO_3$	MDPE
	50% $CaCO_3$	PE-PP 2	PE-PP 2	PE-PP 2	50% $CaCO_3$

All samples have been characterized as far as thermal properties, x-ray diffraction, morphology and mechanical properties.

3.3 Thermal and structural analysis

3.3.1 Thermal analysis

Thermal analysis of polyolefin-based multilayer films was performed by differential scanning calorimetry (DSC), in order to detect the melting point, the crystallization temperature and the glass transition temperature. DSC Mettler-822 calorimeter was used with the *intra cooler* system. Few milligrams of the sample were thermally scanned, under nitrogen flow, in an appropriate temperature range. The sample was first heated to a temperature above its melting point, then quenched and finally heated once again until melting. From the DSC curves of the thermal cycle, the temperature of first heating, crystallization and second heating were obtained. The sample was heated at a constant rate of 10°C/min.

The degree of crystallinity of the samples has benne obtained from the DSC measurements through the following expression:

$$x_{c(\mathrm{DSC})} = 100\frac{\Delta H_m}{\Delta H_m^0}$$

with ΔH_m the melting enthalpy of the sample measured from the DSC scans and ΔH_m^0 the thermodynamic melting enthalpy, that is the melting enthalpy of a perfect crystal of PE infinite size and molecular weight (297 J/g).

For the commercial embossed film, a thermogravimetric TGA analysis was performed in order to determine the amount of the inorganic fillers present in these films. The thermogravimetric measurements were performed with a thermobalance TA Instrument SDT 2960, Simultaneous DSC-TGA, in a flow of air by heating the samples at the scan rate of 10 ° C / min up to a temperature of 800 °C.

3.3.2 X-ray diffraction

The structural characterization was performed by X-ray diffraction techniques.

The diffraction powder profiles were obtained with an automatic Philips diffractometer with Ni filtered CuKα radiation (λ = 1.5418 Å). Approximate degrees of crystallinity of the samples have been obtained by considering that the diffraction profiles can be resolved into two contributes A_c and A_a, proportional to the crystalline and amorphous fractions of the samples, respectively.

In the case of the PE films the amorphous contribution has been obtained by the diffraction profile of an amorphous samples of an ethylene-propylene rubber.

The amorphous profiles have been scaled for a suitable factor and subtracted from the X-ray diffraction profiles of the semicrystalline samples, and the degree of crystallinity can be calculated from the ratio of the so-obtained crystalline diffracting area (A_c) and the total area of the original X-ray diffraction profile (A) through the following expression:

$$x_{c(\mathrm{RX})} = 100\frac{A_c}{A} = 100\frac{A - A_a}{A}$$

The X-ray fiber diffraction patterns of the embossed films were recorded on a BAS-MS imaging plate (FUJIFILM) using a cylindrical camera (R = 57.3 mm) and digitized with a digital imaging reader (Perkin Elmer Cyclone Plus).

The X-ray fiber diffraction patterns of the test films were obtained using a Bruker-Nonius KappaCCD diffractometer with a MoKα radiation, monochromatized with a graphite crystal (λ = 0.70926 Å).

3.4 Morphological analysis

3.4.1 Optical Microscopy

The analysis of the film surfaces was performed using a polarizing Optical Microscope “Axioskop 40” by Zeiss, equipped with a digital camera.

3.4.2 Atomic Force Microscopy (AFM)

Atomic force microscopy has been used to examine the inner and outer surface of commercial blown polyethylene films. When this technique has been used, direct-space images of surface lamellae have been obtained, and the surface roughness determined.

The AFM consists of a cantilever with a sharp tip (probe) at its end that is used to scan the specimen surface. The cantilever is typically silicon or silicon nitride with a tip radius of curvature on the order of nanometers. When the tip is brought into proximity of a sample surface, forces between the tip and the sample lead to a deflection of the cantilever according to Hooke's law. Depending on the situation, forces that are measured in AFM include mechanical contact force, van der Waals forces, capillary forces, chemical bonding, electrostatic forces, magnetic forces, Casimir forces, solvation forces, etc. Along with force, additional quantities may simultaneously be measured through the use of specialized types of probe. Typically, the deflection is measured using a laser spot reflected from the top surface of the cantilever into an array of photodiodes (see Figure 3.4).

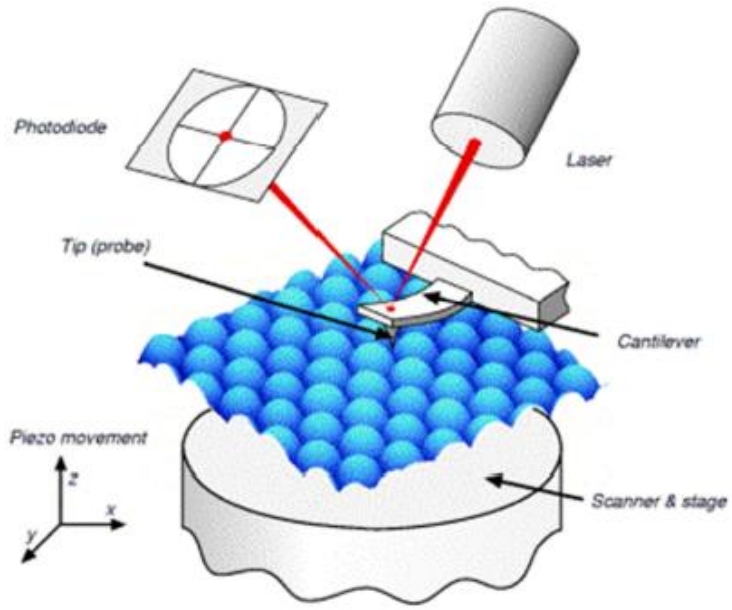

Figure 3.4: *Schematic illustration of an AFM. The tip is attached to a cantilever, and is raster-scanned over a surface. The cantilever deflection due to tip-surface interactions is monitored by a photodiode sensitive to laser light reflected at the tip backside.*

Other methods that are used include optical interferometry, capacitive sensing or piezoresistive AFM cantilevers. These cantilevers are fabricated with piezoresistive elements that act as a strain gauge. Using a Wheatstone bridge, strain in the AFM cantilever due to deflection can be measured, but this method is not as sensitive as laser deflection or interferometry. If the tip was scanned at a constant height, a risk would exist that the tip collides with the surface, causing damage. Hence, in most cases a feedback mechanism is employed to adjust the tip-to-sample distance to maintain a constant force between the tip and the sample.

Traditionally, the sample is mounted on a piezoelectric tube, that can move the sample in the z direction for maintaining a constant force, and the x and y directions for scanning the sample. Alternatively a 'tripod' configuration of

three piezo crystals may be employed, with each responsible for scanning in the x,y and z directions. This eliminates some of the distortion effects seen with a tube scanner. In new designs, the tip is mounted on a vertical piezo scanner while the sample is being scanned in x and y using another piezo block. The resulting map of the area z = f (x, y) represents the topography of the sample. The AFM analysis can be operated in a number of modes, depending on the application. In general, possible imaging modes are divided into static (also called contact) modes and a variety of dynamic (non-contact or "tapping") modes where the cantilever is vibrated.

The AFM images reported in this PhD thesis were obtained at room temperature by a Caliber, Veeco Instruments microscope and were performed in tapping mode. Silicon probes having a tip nominal radius of curvature of 8 nm, with a force constant of 42 N/m were used. The resonance frequency was about 320 kHz with a scan rate of 1 Hz s-1. The sample line was 256 or 512 and the target amplitude was around 0.6 V.

In order to obtain repeatable results different regions of the specimens have been scanned.

In tapping mode, the tip of the cantilever does not contact the sample surface. The cantilever is instead oscillated at a frequency slightly above its resonant frequency where the amplitude of oscillation is typically a few nanometers (<10 nm). The van der Waals forces, which are strongest from 1 nm to 10 nm above the surface, or any other long range force which extends above the surface acts to decrease the resonance frequency of the cantilever. This decrease in resonant frequency combined with the feedback loop system maintains a constant oscillation amplitude or frequency by adjusting the average tip-to-sample distance. Measuring the tip-tosample distance at each (x, y) data point allows the scanning software to construct a topographic image of the sample surface. Non-contact mode AFM does not suffer from tip

or sample degradation effects that are sometimes observed after taking numerous scans with contact AFM. This makes non-contact AFM preferable to contact AFM for measuring soft samples.

3.4.3 Profilometry

A diamond stylus is moved vertically in contact with a sample and then moved laterally across the sample for a specified distance and specified contact force. A profilometer can measure small surface variations in vertical stylus displacement as a function of position. A typical profilometer can measure small vertical features ranging in height from 10 nanometers to 1 millimeter. The height position of the diamond stylus generates an analog signal which is converted into a digital signal stored, analyzed and displayed. The radius of diamond stylus normally ranges from 20 nanometers to 25 μm, and the horizontal resolution is controlled by the scan speed and data signal sampling rate.

In order to measure the thickness of the thin films it was necessary to create a neat step between the investigated materials and the substrate as shown in Figure 3.5.

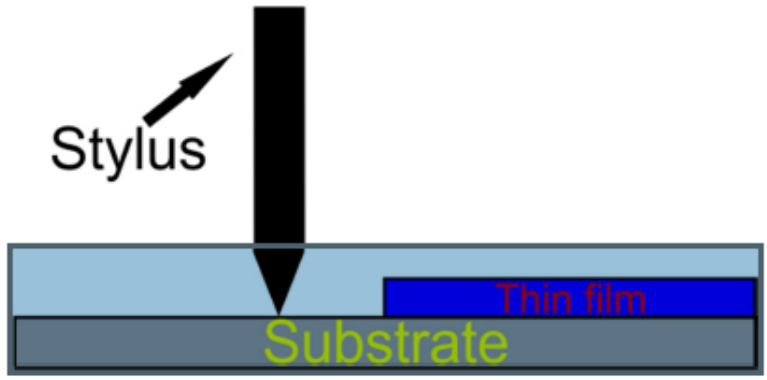

Figure 3.5: *Schematic representation of the profilometric measurements performed over thin films.*

Once that thin films were spin-coated homogeneously all over the surface of the Si wafer, one-half of the substrate covered by the neat or hybrid nanocomposite was cleaned out using acetone thus creating a well-defined step. All the profilometric measurements were obtained using a "ALPHA-STEP IQ – Surface Profile Measuring System" fabricated by KLA Tencor. This instrument is a surface texture measuring system, which could analyze the vertical surface profile of the sample: its roughness, waviness and step height. Measurements were made electromechanically by moving the sample beneath a diamond-tipped stylus (12.5 µm standard radius). KLA Tencor provided accurate height measurements with vertical resolution of 5 Å in a long lateral scan range of 50 µm to 30 mm. The analysis of thin film surface with the profilometer allowed evaluating the arithmetic average value of roughness *Ra* defined by equation:

$$R_a = \frac{1}{n}\sum_{i=1}^{n}|y_i|$$

and allowed also evaluating the square mean roughness *Rq* defined by eqaution:

$$R_{\mathrm{q}} = \sqrt{\frac{1}{n}\sum_{i=1}^{n} y_i^2}$$

Where *n* is the number of the equally spaced points along the trace and *yi* is the vertical distance from the mean line to the i^{th} data point of the stylus trace.

3.5 Mechanical properties

The mechanical tests were performed at room temperature with a dynamometer by Zwick Roell, following the standard test method for tensile properties of thin plastic sheeting ASTM D882-83. Rectangular specimens 50 mm long, 4-5 mm width cut from the films were stretched up to the break.

In the mechanical tests the ratio between the drawing rate and the initial length was fixed equal to 0.1 mm/(mm×min) for the measurement of Young's modulus and 10 mm/(mm×min) for the measurement of stress-strain curves and the determination of the other mechanical properties (stress and strain at yield and at break). The reported stress-strain curves and the values of the mechanical properties are averaged over at least ten independent experiments.

CHAPTER 4

STRUCTURAL AND THERMAL CHARACTERIZATION

4.1 X-ray diffraction analysis

The of X-ray diffraction profiles of the three commercial embossed films of Table 3.1 are reported in Figure 4.1.

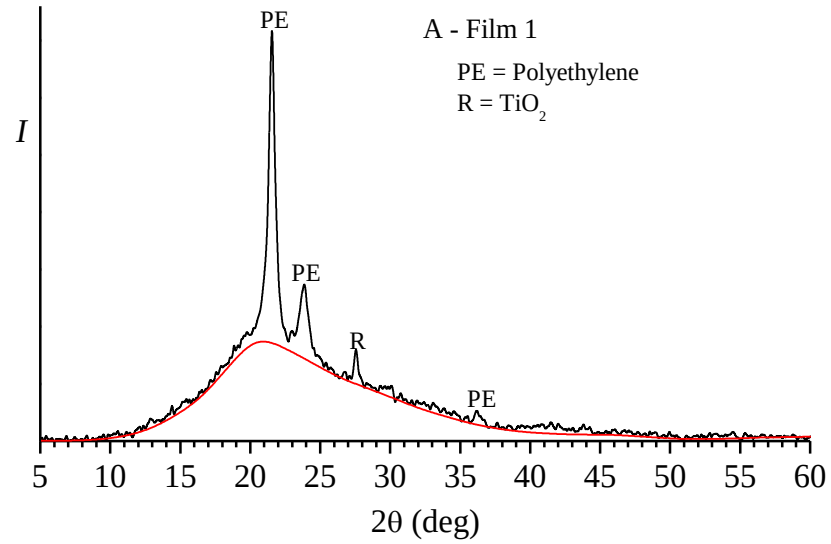

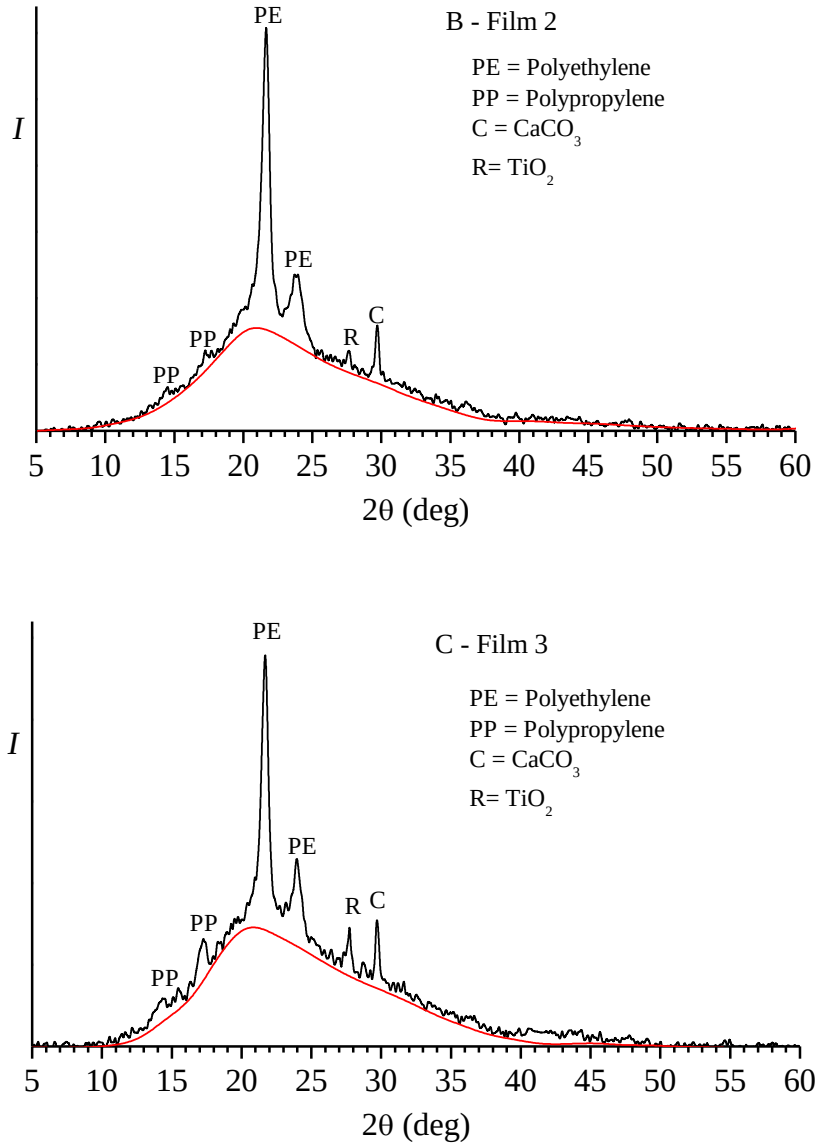

Figure 4.1 *X-ray diffraction profiles of the commercial embossed Film 1 (A), Film 2 (B) and Film 3 (C). The crystalline peaks due to the polyethylene (PE), polypropylene (PP) and inorganic fillers calcium carbonate (C) and titanium dioxide (R) are indicated. The contribution to the diffraction of the amorphous polymeric phase is reported by a red line.*

The diffraction profiles have been analyzed with the software X'Pert High Score Plus, which has allowed to recognize the nature and amount of the crystalline inorganig fillers, by the comparison of the experimental profiles of

Figure 4.1 with those contained in the electronic database PDF-4+ (2012) of the "*International Centre for Diffraction Data*" (ICDD).

All profiles show a diffuse halo, due to the contribution to the diffraction from the amorphous fraction of the polymeric phase; this contribution is shown in Figure 4.1 by a red line.

The diffraction profile of the embossed Film 1 (Figure 4.1 A) presents three peaks at 2θ = 21.4, 24 and 36°, corresponding to 110, 200 and 020 reflections of the orthorhombic crystalline form of PE[8a] and a peak at 2θ = 27.5° corresponding to the main reflection of the titanium dioxide (TiO_2), in the crystalline form rutile, indicated in Figure 4.1 with a R.

The diffraction profiles of the embossed Film 2 (Figure 4.1B) and Film 3 (Figure 4.1C) present, besides the typical reflections of polyethylene (at 2θ = 21.4 and 24°) and of rutile (at 2θ = 27.5°), a peak at 2θ = 29 corresponding to the most intense reflection of the calcium carbonate, in its most common polymorph calcite (C in Figure 4.1) and two less intense peaks at $2\theta \approx 14$ and 17°, corresponding to the 110 and 040 reflections of the crystalline form α of isotactic polypropylene.[14]

The composition of the three films, evaluated by the fractions of the crystalline phases determined by the software X'Pert Hight Score Plus interfaced to the electronic database PDF-4+ of ICDD, is reported for each sample in Table 3.1. The values of the degree of crystallinity (x_c) with respect to the only polymeric phase are also reported. These values have been determined considering that the experimental diffraction profiles of Figure 4.1 are the sum of three contributions: the diffraction from the amorphous polymer (PE or PE + PP) represented by a red line in Figure 4.1, the diffraction from the crystalline polymer (PE or PE+PP) and the diffraction of the crystalline inorganic fillers (calcite and/or rutile). Then, after subtraction of a baseline representative of the background and of the contribution due to

the crystalline inorganic additives, a profile corresponding to the diffraction of the only polymeric pahse is obtained. The degree of crystallinity of the films, with respect to the only polymer, has been evaluated from these profiles, as the ratio between the area of the peaks of the crystalline PE or PE + PP and the total area of the profile, as described in Chapter 2.

The data of Table 4.1 shows that the embossed Film 1 is constituted consists exclusively of PE, with small percentage of titanium dioxide (3 wt%), whereas Film 2 and Film 3 are constituted by PE (70-80 wt%), PP (10-20 wt%) and inorganic fillers as calcium carbonate (2 wt%) and titanium dioxide (1-3 wt%).

The X-ray diffraction data do not allow either to determine the type of polyethylene, LDPE, HDPE, LLDPE or a mixture of different grades, or if the PP is homopolymer iPP or a copolymer of iPP.

All embossed films have similar crystallinity of about 20% (Table 4.1).

Table 4.1. *Compposition of the commercial embossed films. The fraction of the crystalline phases, determined from the experimantal diffraction profiles of Figure 4.1 by the X'Pert High Score Plus software, interfaced to the electronic database PDF-4+ of the "International Centre for Diffraction Data" (ICDD0), after subtraction of the background and amorphous contributions, the crystallinity degrees ($x_{c(RX)}$) with respect to the only polymeric phase, calculated as described in the text and in the Experimental Part, the percentage of the various phases and the relative amount of inorganic (CaCO3 + TiO2) and organic (PE + PP) phases are reported. PE = polyethylene, PP = polypropylene, PE_c and PP_c indicate crystallyne PE and PP, respectively.*

	crystalline phases (wt%)				$x_{c(RX)}$ (%)	Composition (wt%)				Inorganic Phases (wt%)	Organic Phases (wt%)
Samples	**PE_c**	**PP_c**	**$CaCO_3$**	**TiO_2**		**PE**	**PP**	**$CaCO_3$**	**TiO_2**		
Film 1	89	-	-	11	24	97	-	-	3	3	97
Film 2	77	11	8	4	21	85	12	2	1	3	97
Film 3	64	25	7	4	26	70	25	2	3	5	95

The X-ray diffraction profiles of the three set of samples of Table 3.2 and 3.3 are reported in Figures 4.2 and 4.3 respectively

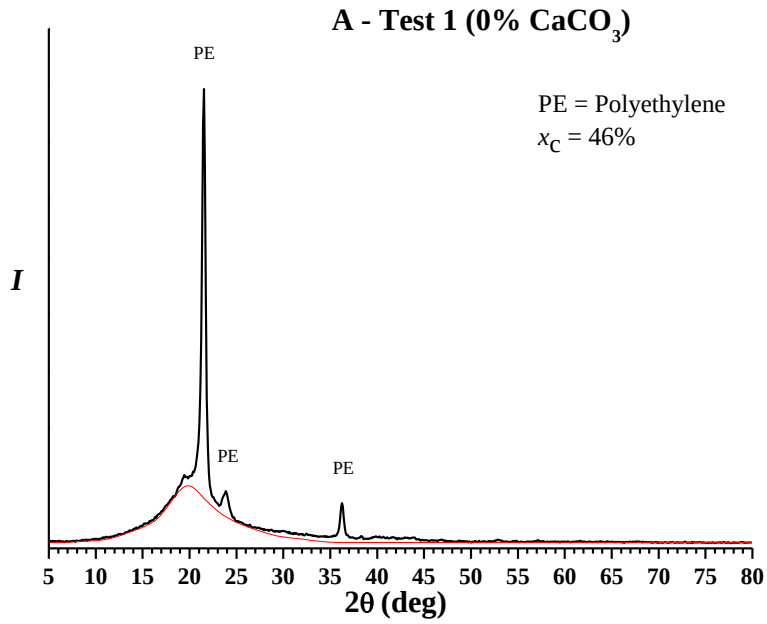

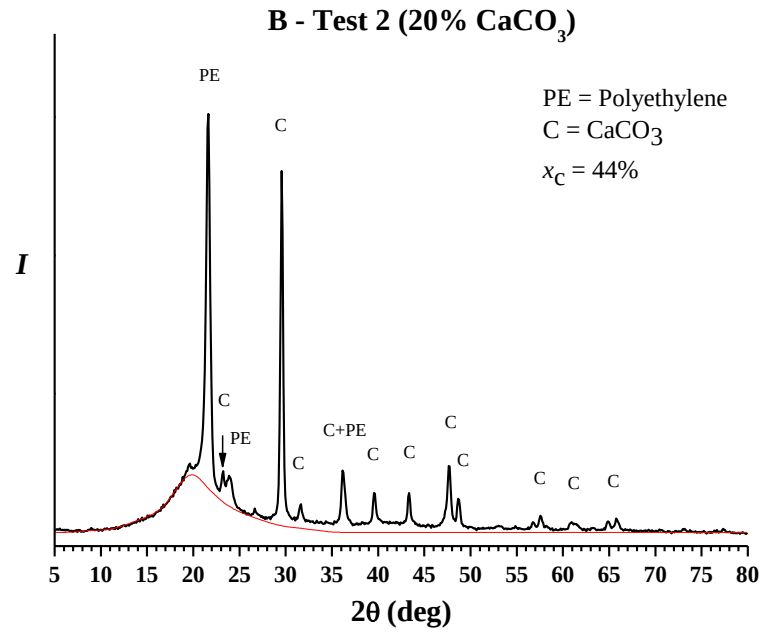

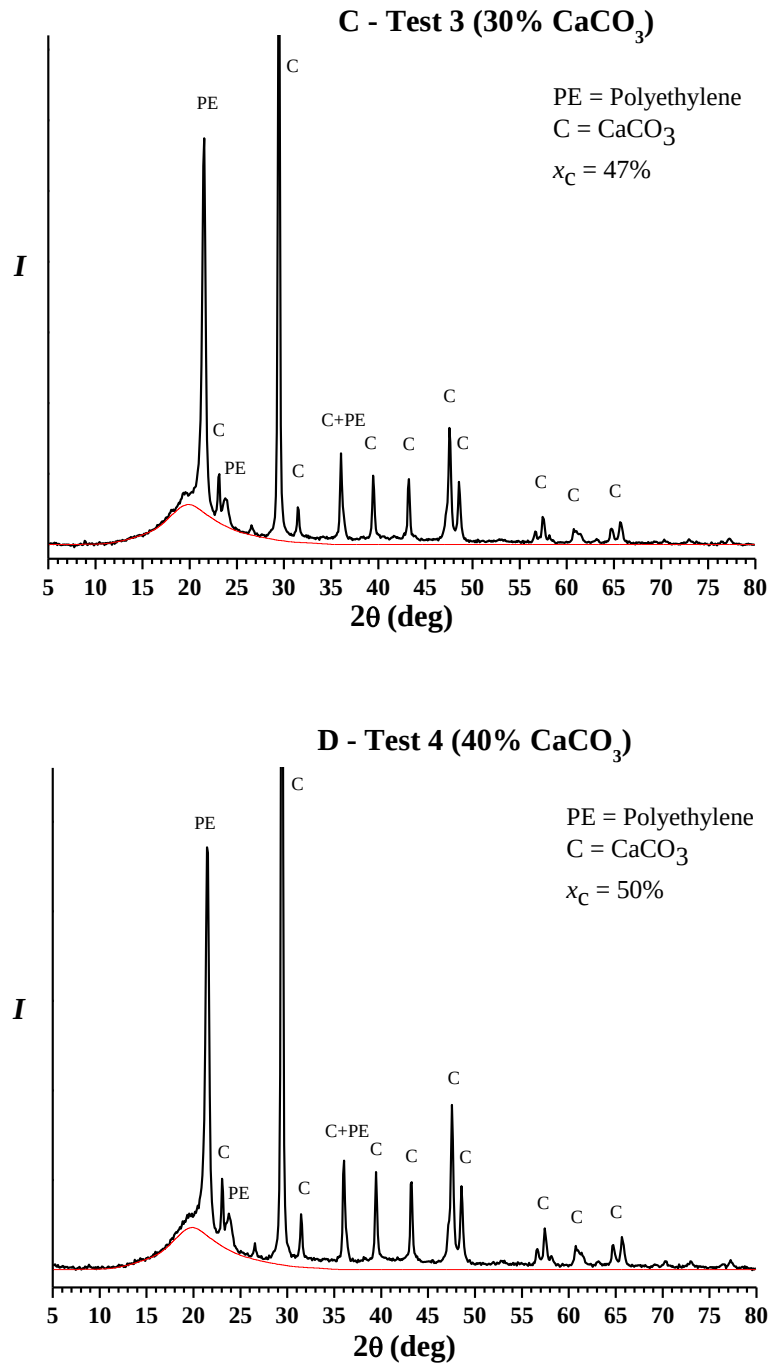

Figure 4.2 *X-ray diffraction profiles of samples Test 1 (A), Test 2 (B), Test 3 (C) and Test 4 (D). The crystalline peaks due to the polyethylene (PE), and calcium carbonate (C) are indicated. The contribution to the diffraction of the amorphous PE is reported by a red line.*

The diffraction profile of the film Test 1, constituted only by a mixture of different PE grades (Table 3.7), show only the reflection of PE at 2θ = 21.4, 24 and 36° (Figure 4.2A).

The diffraciotn profiles of the films Test 2 - Test 7, which contain calcium carbonate (Table 3.7 and Table 3.8) show the presence of numerous peaks at 2θ = 23.0, 29.4, 36, 39.4, 43.2, 47.5 and 48.5, 57.5, 60.8, 64.8 and 65.8° (Figures 4.2B-D and 4.3) due to the crystalline form of calcite (C), whose intensity increases with increasing the amount of calcium carbonate, i.e. going from sample Test 2 to sample Test 4 (Table 3.7) and from sample Test 5 to sample Test 6BIS (Table 3.8).

The diffractrion profiles of the film Test 5, besides the peaks of PE and calcite present also crystalline peaks, whose most intense are at 2θ = 9.5 and 28.7°, due to due to the talc (indicated with T in Figure 4.3A), and the diffraction profiles of the samples Test 6, Test 6BIS and Test 7, which contain also small amounts of the etherophase PP/PE copolymers (Table 3.8), show peaks at 2θ ≈ 14 and 16.8°, typical of the crystalline α form of iPP, of very low intensity (indicated with PP in Figure 4.3B-D).

The presence of the peaks at 2θ = 9.5 and 28.7° in the diffraction profile of the sample Test 6 is due to residue of talc of the previous test, since the tests were performed in succession.

The degree of crystallinity, calculated with respect to only the polymeric phase, varies from 44% to 54% in the various tests. They are reported in the Figures 4.1 – 4.3 for each sample.

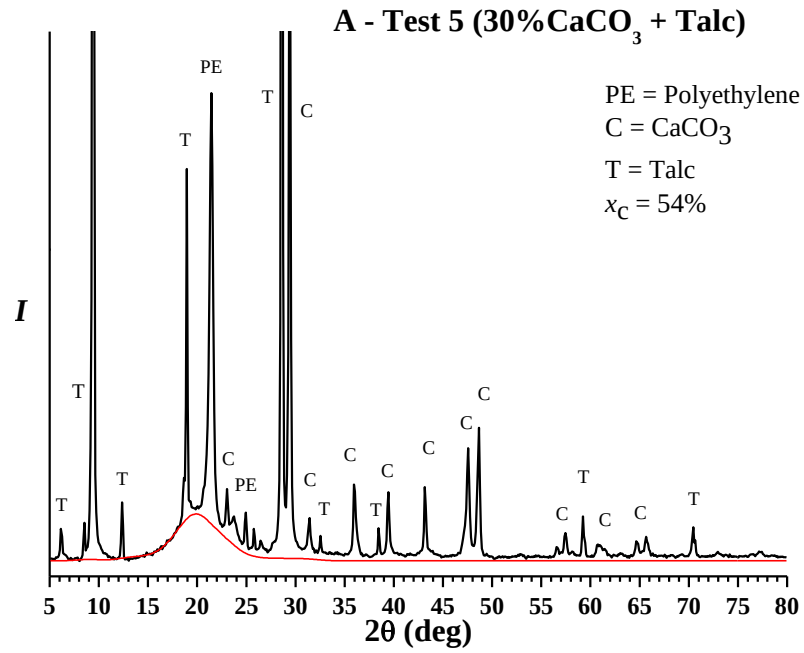
A - Test 5 (30%CaCO3 + Talc)
PE = Polyethylene
C = CaCO3
T = Talc
xc = 54%
I
2θ (deg)

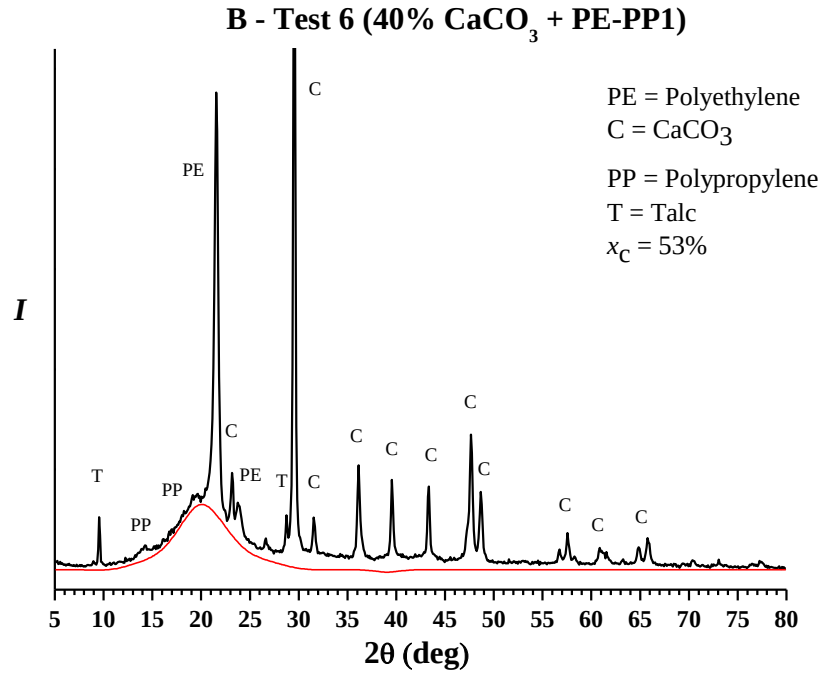
B - Test 6 (40% CaCO3 + PE-PP1)
PE = Polyethylene
C = CaCO3
PP = Polypropylene
T = Talc
xc = 53%
I
2θ (deg)

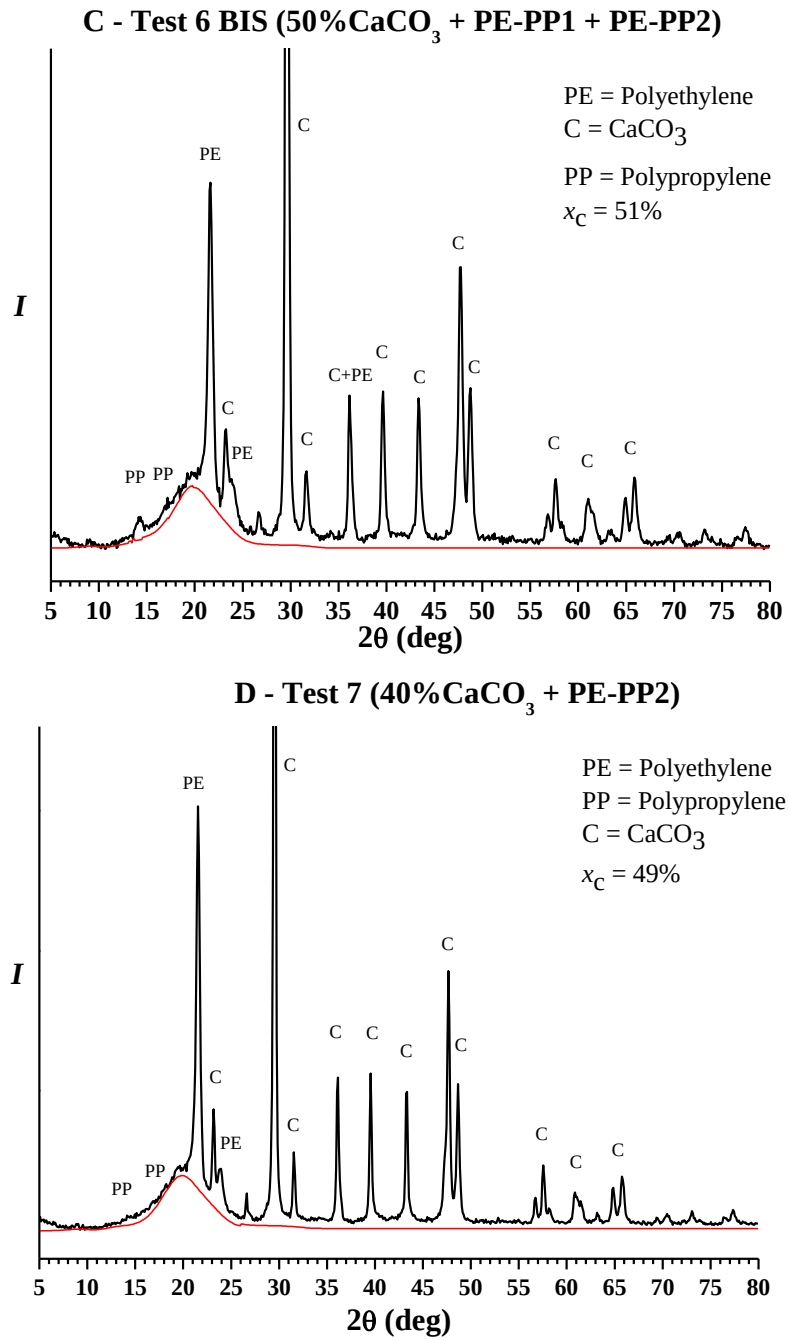

Figure 4.3. *X-ray diffraction profiles of samples Test 5 (A), Test 6 (B), Test 6BIS (C) and Test 7 (D). The crystalline peaks due to the polyethylene (PE), polypropylene (PP), calcium carbonate (C) and talc (T) are indicated. The contribution to the diffraction of the amorphous PE is reported by a red line.*

The diffraction profiles of third set are characterized by the presence of typical reflections of polyethylene (at $2\theta = 21.4°$ and 24), of inorganic additives of calcium carbonate and talc (at $2\theta = 6.1°$, 9.5°, 12.3°, 18.9°, 28.7°, 32.5°, 38.45°, 59.2° and 70.4°) and reflections at $2\theta \approx 14°$ and 16.8°, typical of isotactic polypropylene in the form α.

In the profile of the Test 6 is possible to note the presence of characteristic reflections at $2\theta = 9.5°$ and 28.7° of talc, this is due to the residue of talc of the previous test, since the tests were performed in succession.

The degree of crystallinity, calculated considering only the polymer phase, varies from 44% to 54% in all tests.

4.2 Thermogravimetric and Thermal Analysis

4.2.1 Thermogravimetric Analysis

The thermogravimetric (TGA) curves of the three embossed films are shown in Figure 4.4.

A first weight loss at a temperature of about 450 °C, due to the decomposition of the organic polymeric phase is observed for all samples. The TGA curves of Film 2 and Film 3 present also a second weight loss at temperature of about 650 °C, due to the thermal decomposition of calcium carbonate to calcium oxide, according to the following reaction:

$$CaCO_3 \rightarrow CaO + CO_2$$

that corresponds to a weight loss of 44%.

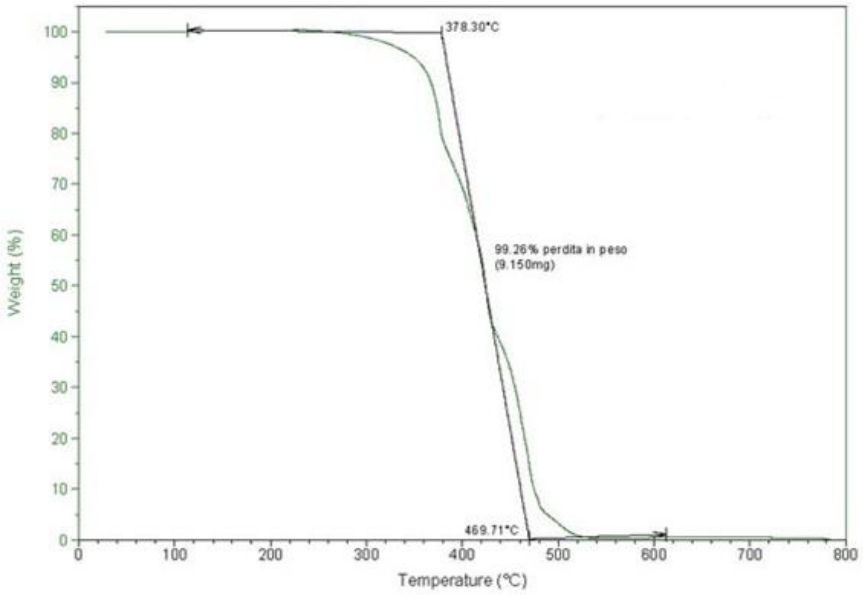

A - Film 1

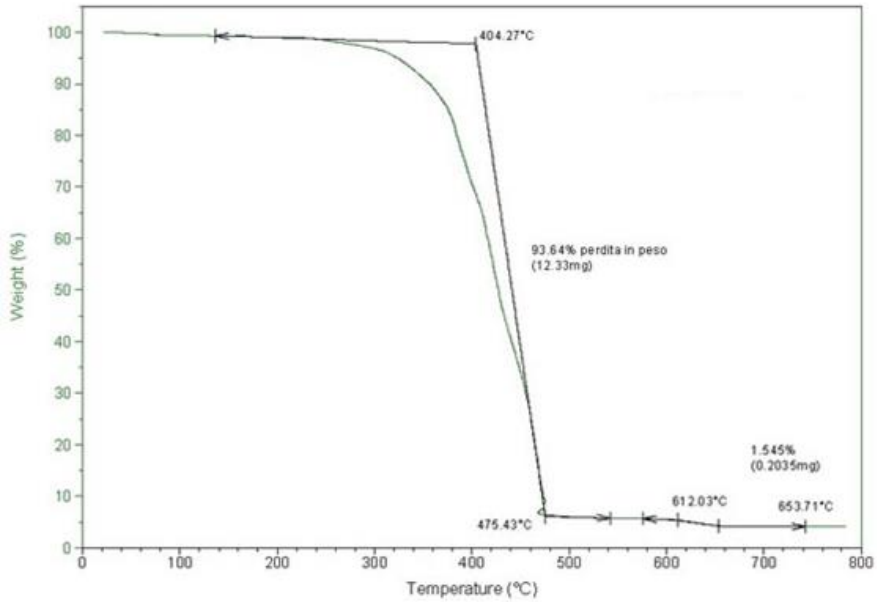

B - Film 2

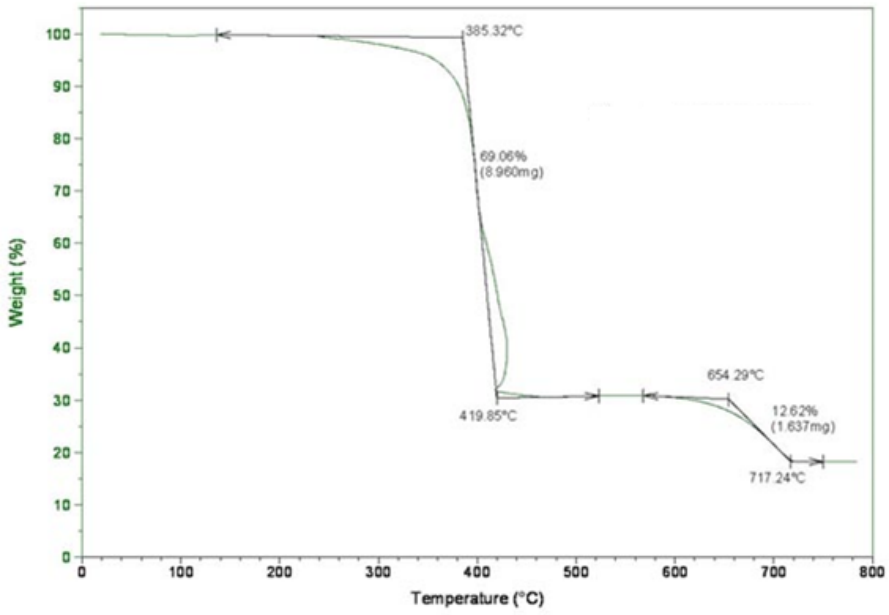

C - Film 3

Figure 4.4. *Thermogravimetric curve of the commercial embossed Fiolm 1 (A), Film 2 (B) and Film 3*

The data obtained by the TGA curves of Figure 4.4 are compared to the percentages of organic and inorganic phase evaluated from the diffraction profiles of Figure 4.1 in Table 4.2. A good agreement between the data obtained by the the two techiques is obtained.

Table 4.2 *Weight loss from TGA curves of Figure 4.4, and percentages of organic and inorganic phase determined from the X-ray diffraction profiles of Figure 4.1 for the three commercial embossed films.*

sample	Weight loss (%) TGA	% Organic Phase (RX)	% Inorganic Phase (RX)
Film 1	99	97	3
Film 2	94	95	5
Film 3	95	97	3

4.2.2 Thermal Analysis

The DSC thermograms of the three commercial embossed films (Film 1, Film 2 and Film 3) and the new production films (samples Test 1 – Test 7), recorded at 10°C / min are reported in Figures 4.5 – 4.7.

The thermograms are composed of the first heating scan of the as-prepared film (red curves) , the cooling scan from the melt (blue curves) and the second heating scan after cooling from the melt (green curves).

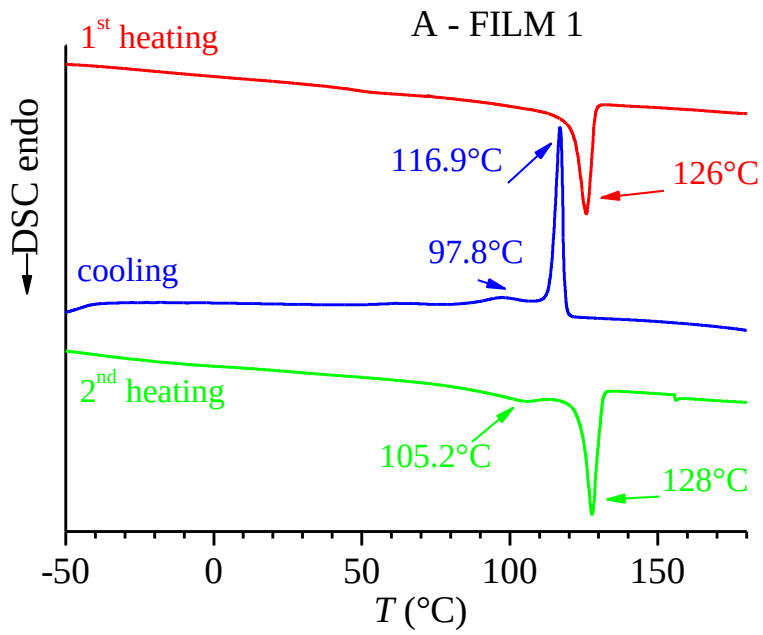

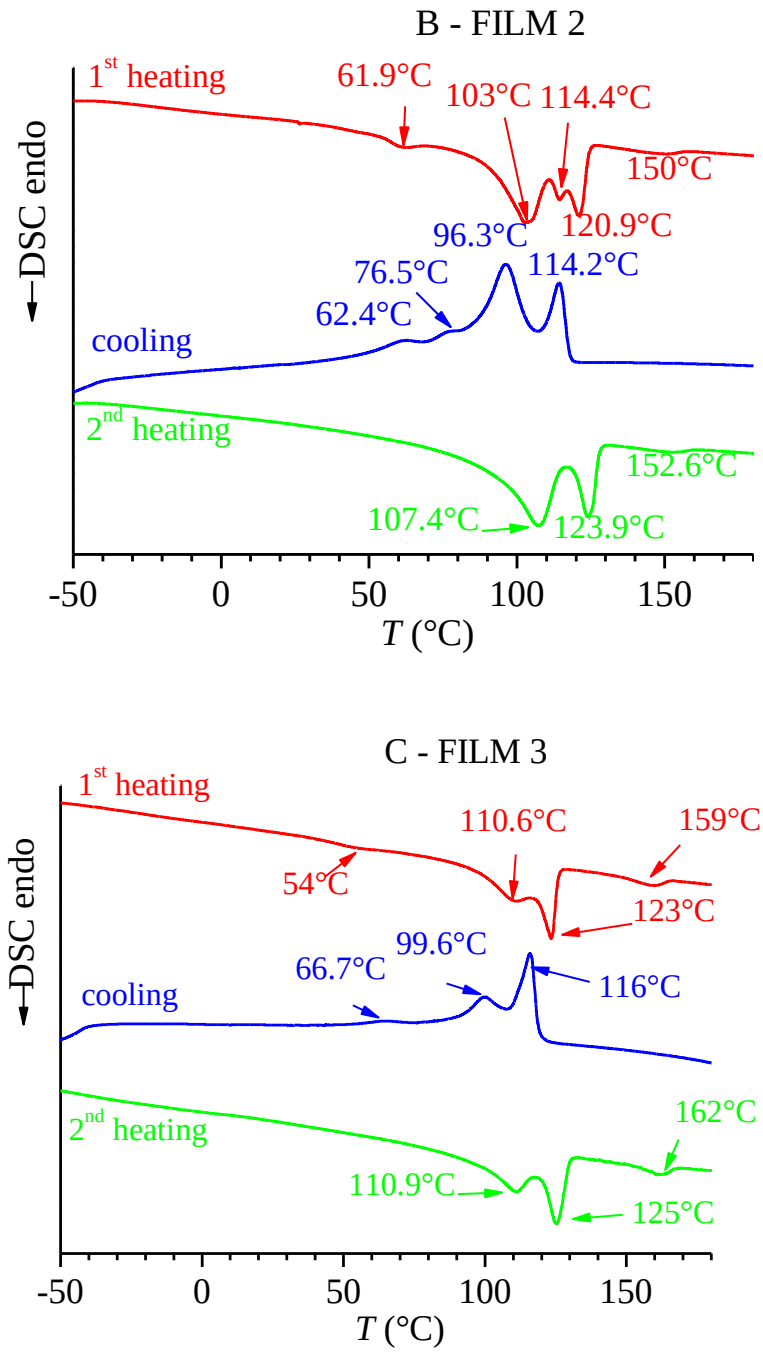

Figure 4.5. *DSC thermograms recorded at 10°C/min of the embossed Film 1 (A), Film 2 (B) and Film 3 (C). The first heating scans (red curves), the cooling scans from the melt (blue curves) and the second heating scans (green curves) are reported. The values of the temperatures relative to the endothermic and exothermic peaks are also indicated.*

The DSC thermograms of the embossed Film 2 and Film 3 are characterized by the presence of endothermic and exhotehermic peaks rather broad and in many cases with double peaks either in the first and second heating curves, in the range 110-120°C, or in the crystallization curves, in the range 60-110°C (Figure 4.5B,C). The presence of multiple peaks indicates that in the films are constituted by different PE grades, in particular LDPE and LLDPE, whose melting and crystallization occurs at different temperatures around 110 - 120°C.

The DSC thermogram of the embossed Film 1, instead, presents neatand narrow melting and crystallization peaks, at temperatures higher than those of the other embossed films. In fact, a single melting peak at 126°C and a single crystallization peak at 117°C is observed in Figure 4.4 A. This indicates that the embossed Film 1 is probably constituted by HDPE, whose melting point occurs at temperature generally higher than LDPE and LLDPE.

Moreover, the thermograms of Film 2 and Film 3 (Figure 4.5B, C) present small endotermic peak at T = 150-160°C, due to the melting of crystals of isotactic polypropylene in the αform.

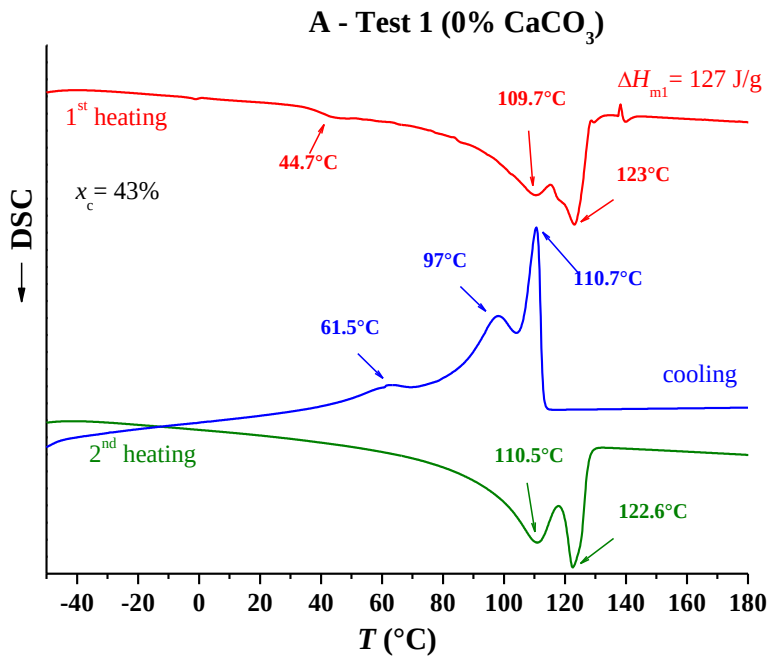
A - Test 1 (0% CaCO3)
ΔHm1 = 127 J/g
1st heating
109.7°C
44.7°C
123°C
xc = 43%
97°C
110.7°C
61.5°C
cooling
2nd heating
110.5°C
122.6°C
DSC
-40 -20 0 20 40 60 80 100 120 140 160 180
T (°C)

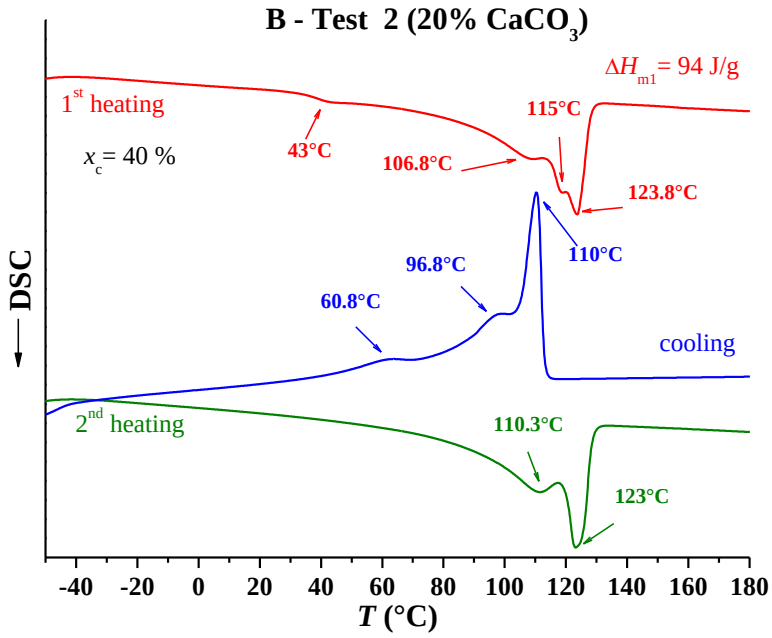
B - Test 2 (20% CaCO3)
ΔHm1 = 94 J/g
1st heating
115°C
43°C
106.8°C
xc = 40 %
123.8°C
110°C
96.8°C
60.8°C
cooling
2nd heating
110.3°C
123°C
DSC
-40 -20 0 20 40 60 80 100 120 140 160 180
T (°C)

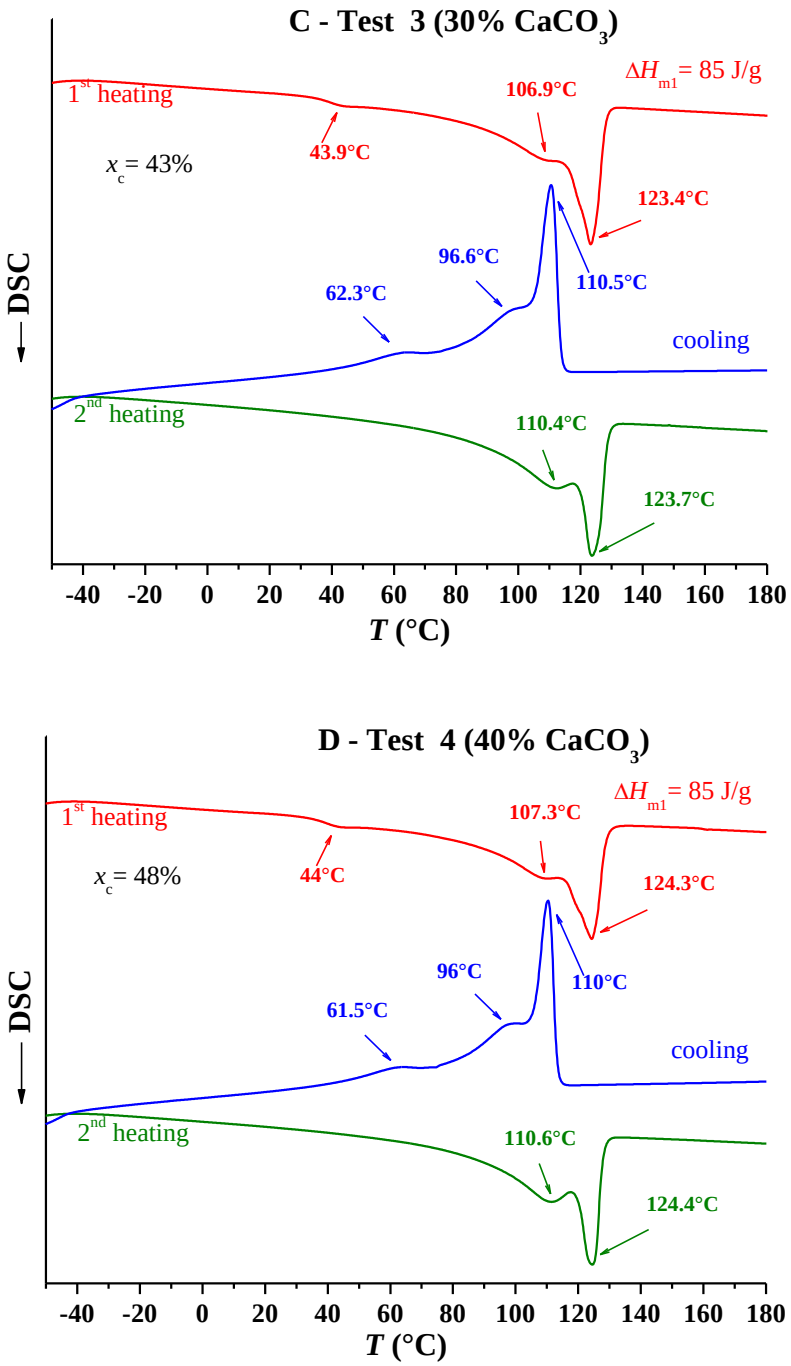

Figure 4.6. *DSC thermograms recorded at 10°C/min of the first set of samples Test 1 (A), Test 2 (B), Test 3 (C) and Test 4 (D). The first heating scans (red curves), the cooling scans from the melt (blue curves) and the second heating scans (green curves) are reported. The values of the temperatures relative to the endothermic and exothermic peaks are also indicated.*

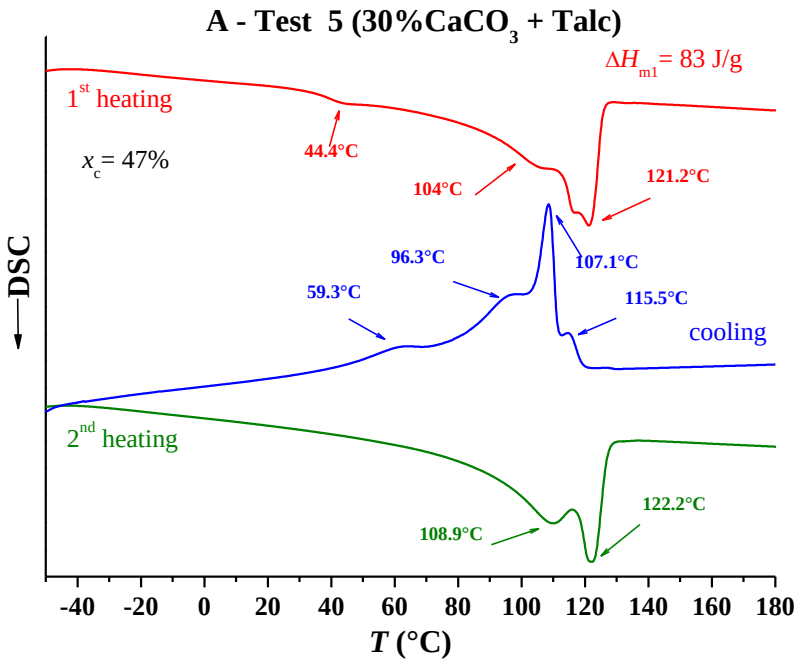
A - Test 5 (30%CaCO3 + Talc)
ΔHm1 = 83 J/g
1st heating
xc = 47%
44.4°C
104°C
121.2°C
96.3°C
107.1°C
59.3°C
115.5°C
cooling
2nd heating
122.2°C
108.9°C
DSC
-40 -20 0 20 40 60 80 100 120 140 160 180
T (°C)

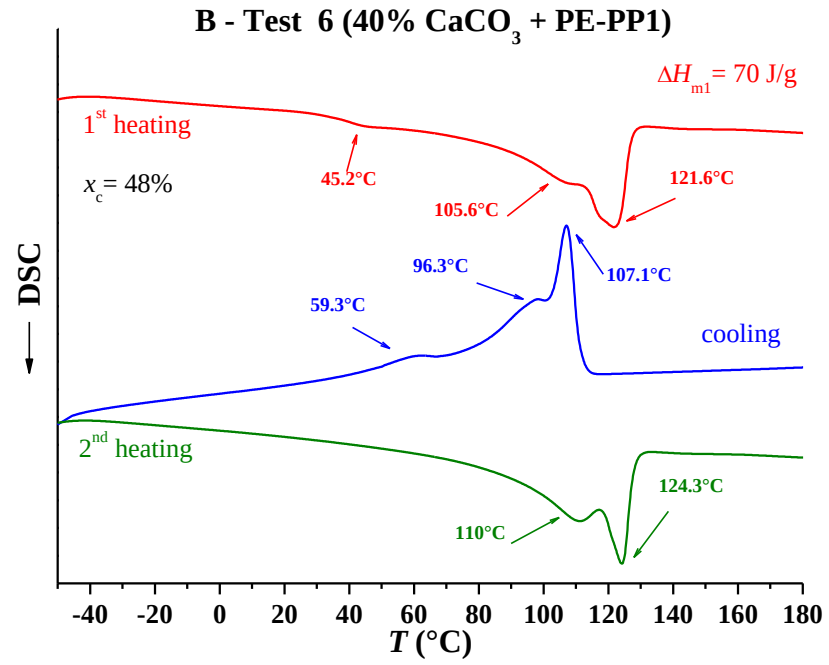
B - Test 6 (40% CaCO3 + PE-PP1)
ΔHm1 = 70 J/g
1st heating
xc = 48%
45.2°C
105.6°C
121.6°C
96.3°C
107.1°C
59.3°C
cooling
2nd heating
124.3°C
110°C
DSC
-40 -20 0 20 40 60 80 100 120 140 160 180
T (°C)

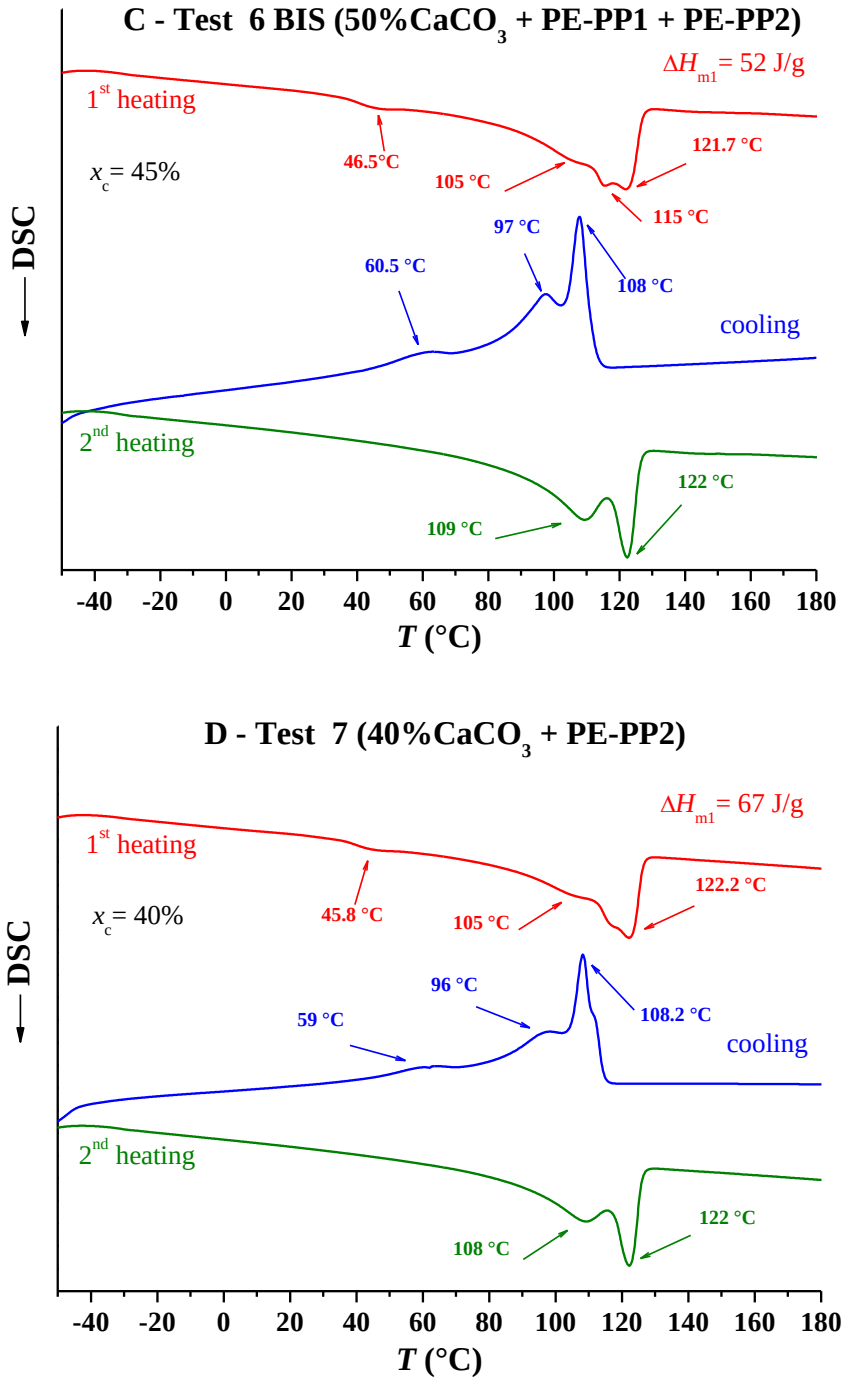

Figure 4.7. *DSC thermograms recorded at 10°C/min of the second and third set of samples Test 5 (A), Test 6 (B), Test 6BIS (C) and Test 7 (D). The first heating scans (red curves), the cooling scans from the melt (blue curves) and the second heating scans (green curves) are reported. The values of the temperatures relative to the endothermic and exothermic peaks are also indicated.*

The DSC thermograms of the three sets of films (Test 1 - Test 7) are similar and all characterized by double endothermic and exhotermic peaks, due to the different PE grades employed for the realization of the films (Tables 3.6 and 3.7), whose crystallization and melting takes place at different temperatures.

The values of melting temperature and enthalpy determined by the first (T_{m1}^{I} and ΔH_{m1}^{I}) and second heating scans (T_{m1}^{II} and ΔH_{m1}^{II}) and of crystallization temperature and enthalpy (T_c and ΔH_c) determined by the cooling scans of thermograms of Figures 4.5 - 4.7 are reported in Table 4.3. For the embossed Film 2 and Film 3 the values of melting temperature and enthalpy observed in the first heating scans, relative to the melting of the PP crystals (T_{m2}^{I} and ΔH_{m2}^{I}), are also reported.

The data of Table 4.1 indicate that the presence of inorganic fillers and elastomeric copolymers does not affect the melting and crystallization behavior of PE, as evident by the comparison of the melting and crystallization temperature and enthalpy of sample Test 1 (constituted by only PE) with those of samples Test 2 - 4 (constituted by PE and calcium carbonate, see Table 3.6), or those of sample Test 5 (constituted by PE, calcium carbonate and talc, see Table 3.7) or those of samples Test 6 - 7 (constituted by PE, calcium carbonate and etherophasae PE-PP copolymer, see Table 3.7).

The degrees of crystallinity, evaluated as described in Chapter 3 from the ratio between the experimental melting enthalpy relative to the first heating scan (ΔH_{m1}) and the thermodynamic melting enthaply of a 100% crystalline PE ($\Delta H^0_{m(PE)}$ = 297 J/g) are reported in Table 4.4 and compared to the crystallinity degrees evaluated by the *X*-ray diffraction data in Table 4.3.

Table 4 .3 *Cristallinity degree evauated from the X-ray diffraction profiles of Fig. 4-2 and 4-3, and DSC thermograms of Fig. 4-6 and 4-7.*

Sample	X_c **(%) (X-ray)**	X_c **(%) (DSC)**
Test 1	46	43
Test 2	44	40
Test 3	47	43
Test 4	50	48
Test 5	54	47
Test 6	53	48
Test 6 BIS	51	45
Test 7	49	40

Table 4.4 *Values of the temperatures of the first (T_m^I) and second (T_m^{II}) melting and crystallization (T_c), and values of the enthalpies of first and second melting (ΔH_m^I e ΔH_m^{II}) and crystallization (ΔH_c) obtained from the thermograms of the various films in Figures 4.4, 4.5 and 4.6.*

Sample	T_{m1}^{I} (°C)	T_{m2}^{I} (°C)	T_c (°C)	T_m^{II} (°C)	T_{m2}^{II} (°C)	ΔH_m^I (J/g)	ΔH_{m2}^I (J/g)	ΔH_c (J/g)	ΔH_m^{II} (J/g)	ΔH_{m2}^{II} (J/g)
Film 1	125.8	-	97.8–116.9	105.2–127.8	-	114.5	-	120.5	111.6	-
Film 2	110.6–123.4	159.1	66.7–99.6 15.9	110.9–125.2	162.3	103.3	5.6	129.4	105.3	4.8
Film 3	60.6–103.2 113.9–121.4	149.4	62.4–76.6 96.4–113.6	105.9–122.6	-	101.6	2.1	117.4	11.1	-
Test 1	44.7–109.7 123	-	61.5–97 110.7	110.5–122.6	-	127	-	125.8	123.5	-
Test 2	43–106.8 115-123.8	-	60.8–96.8 110	110.3– 123	-	94	-	95.8	93.3	-
Test 3	43.9-106.9 123.4	-	62.3-96.6 110.5	110.4-123.7	-	85	-	83.8	82.0	-
Test 4	44-107.3 124.3	-	61.5-96 110	110.6-124.4	-	85	-	84.0	84.5	-
Test 5	44.4-104 121.2	-	59.3-96.3 107.1-115.5	108.9-122.2	-	83	-	83.5	82.6	-
Test 6	45.2-105.6 121.6	-	59.3-96.3 107.1	110-124.3	-	70	-	69.8	68.2	-
Test 6 BIS	46.5-105 115-121.7	-	60.5-97 108	109-122	-	52	-	52.4	50	-
Test 7	45.8-105 122.2	-	59-96 108.2	108-122	-	67	-	66	65	-

4.3 Analysis of the preferred orientation

During the blown extrusion process the material is subjected to tensions both in the direction of extrusion (defined machine direction, MD) and in direction perpendicular to it (defined transverse direction TD). These stresses may generate preferred orientations in both amorphous and crystalline phase.

The analysis of the preferred orientation of the films was performed by X-ray diffraction techniques recording photographs on specimens with a width of 2-3 mm and a length of about 3 cm, cut from the film.

In these samples three directions shown in Figure 4.7 are identified: the machine direction (MD) or “end” direction, corresponding to the direction parallel to the film surface and parallel to the direction of extrusion, the transverse direction (TD) or “edge” direction also parallel to the film surface but perpendicular to MD, and the normal direction (ND) or “through” direction corresponding to the direction perpendicular to the film surface.

For each film three *X*-rays diffraction patterns with the incident *X*-rays parallel to the three directions of the sample "end", "edge" and "through" were recorded.

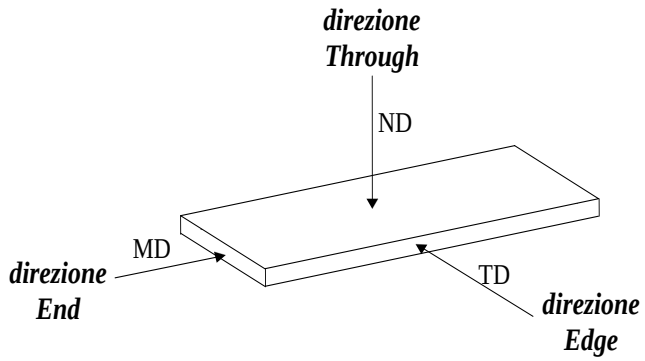

Figura 4.8. *Scheme of a specimen of film with indication of the three directions "end" parallel to MD, "edge" parallel to TD and "through" parallel to ND.*

The bidimensional (2D) X-ray diffraction patterns of the commercial embossed Film 1, Film 2 and Film 3 are reported in the Figures 4.9 - 4.11, respectively, whereas the 2D X-ray diffraction patterns of the samples Test 1 (without inorganic fillers) and Test 4 (with 40%wt of calcium carbonate) are reported in the Figures 4.11 and 4.12, respectively. The other not embossed films present X-ray diffraction patterns similar to those of samples Test 4, for this reason the patterns are not shown.

Parts A of the figures the *X*-ray diffraction pattern obtained with the incident radiation perpendicular to the film surface (image THROUGH) are reported; and parts B and C shown the *X*-rays diffraction patterns obtained withy the incident radiation parallel to the film surface, along the direction "edge", (image EDGE) and direction "end" (image END).

The diffraction patterns of Film 1 (Figure 4.9) are equal and all present only Debye Scherrer rings. In particular, two rings at $2\theta = 21.4°$ e 24° corresponding to the 110 and 200 reflections, respectively, of the PE[8a] and a ring at $2\theta = 27.5°$ due to the rutile (figure 4.1 A) are present. The presence in all the three diffraction patterns of concentric rings with an uniform distribution of the relatively intensities indicates that the Film 1 is isotropic and the crystals of PE and of rutile do not show any preferred orientation.

A slight polarization of the 110 and 200 reflections on the equator is observed in the images "through" (Figure 4.9A) and "edge" (Figure 4.9B), indicating that a slight orientation of the PE crystals with the chain (*c*) axes parallel to the machine direction (MD) is prtesent. However, the degree of orientation is very low.

The X-ray diffraction patterns of the embossed Film 2 and Film 3 are similar. In particular, for both samples the images "through" and "edge" present the 110 and 200 reflections of PE polarized on the equator (Figures 4.10A,B and 4.11A,B), while the images "end" are characterized by the

presence of Debye Scherrer rings (Figures 4.10C and 4.11C). The reflections of the inorganic phases, calcite and rutile, appear in all diffraction patterns as Debye Scherre rings. This indicates taht in these two films the crystals of PE are preferentially oriented with the *c* axes parallel to the machine direction and the crystals of inorganic additives are not oriented. The polarization of the intensity on the equator is more evident for Film 2 than Film 3, indicating that the degree of orientation of the crystalline phase of the PE is higher for this film.

Moreover the patterns of the Film 2 and Film 3 present also a Debye Scherrer ring of very low intensity at $2\theta = 14°$ due to the 110 reflection of the α form of iPP. This indicates that the crystals of iPP are not oriented.

The X-ray diffraction patterns of Figure 4.12 and 4.13, relative to the sample Test 1 (whitout inorganic phase) and Test 4 (with 40% of $CaCO_3$), are similar to those of the embossed. In fact, also in these patterns a slight polarization of the 110 and 200 reflection of PE on the equator is present in the images "through" (Figures 4.12A and 4.13A) and "edge" (Figures 4.12B and 4.12B), indicating a low degree of axial orientation (*c* axes parallel to MD).

Moreover, as in the embossed films for the sample Test 4 the crystalline inorganic additives do not show any orientation and only Debye Scherrer rings are present in all patterns (Figures 4.12 and 4.13).

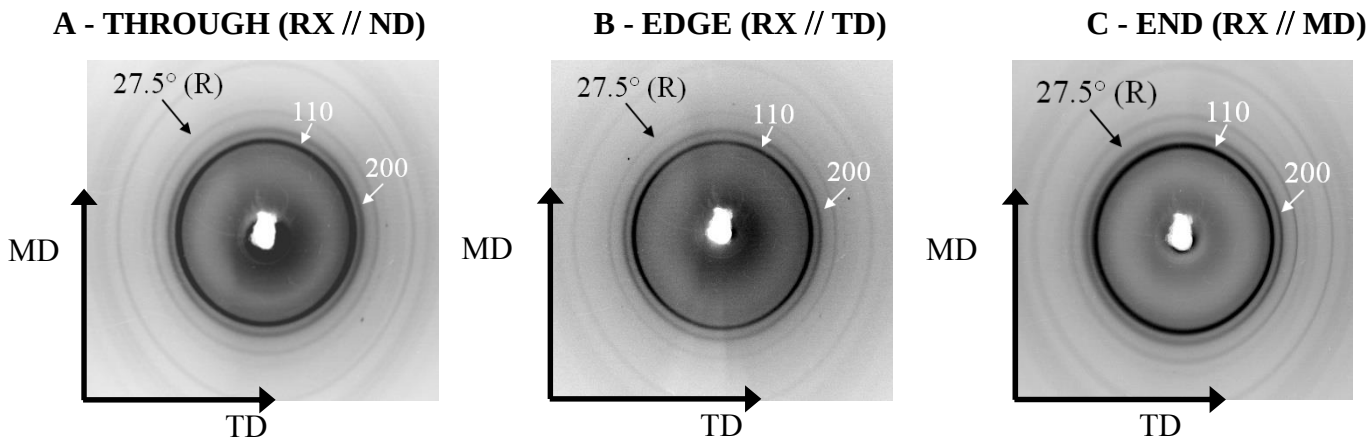

Figure 4.9 *2D X-ray diffraction of the embossed film, Film 1: through (A), edge (B), end (C). Shows the reflections 110 and 200 of the PE and the main reflection diffraction of rutile (R).*

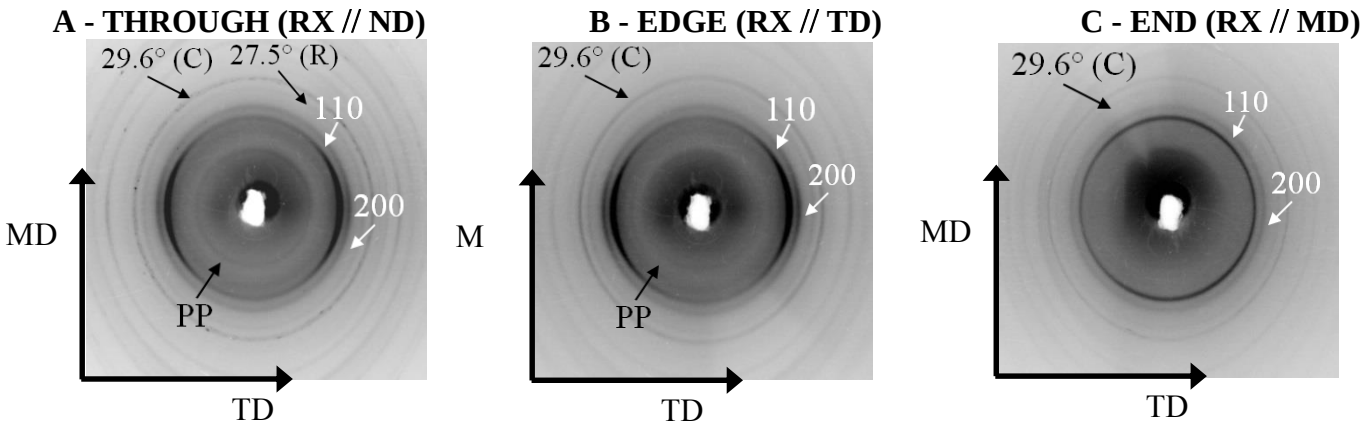

Figure 4.10 *2D X-ray diffraction of the embossed film, Film 2: through (A), edge (B), end (C). Shows the reflections 110 and 200 of the PE and the main reflection diffraction of calcium carbonate (C) and rutile (R).*

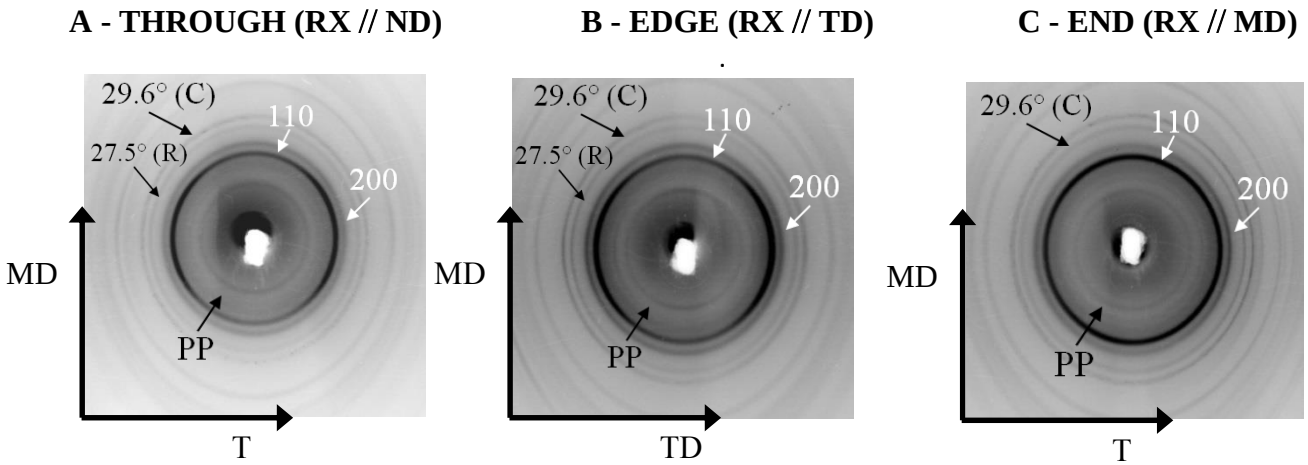

Figure 4.11 *2D X-ray diffraction of the embossed film, Film 3: through (A), edge (B), end (C). Shows the reflections 110 and 200 of the PE and the main reflection diffraction of calcium carbonate (C) and rutile (R).*

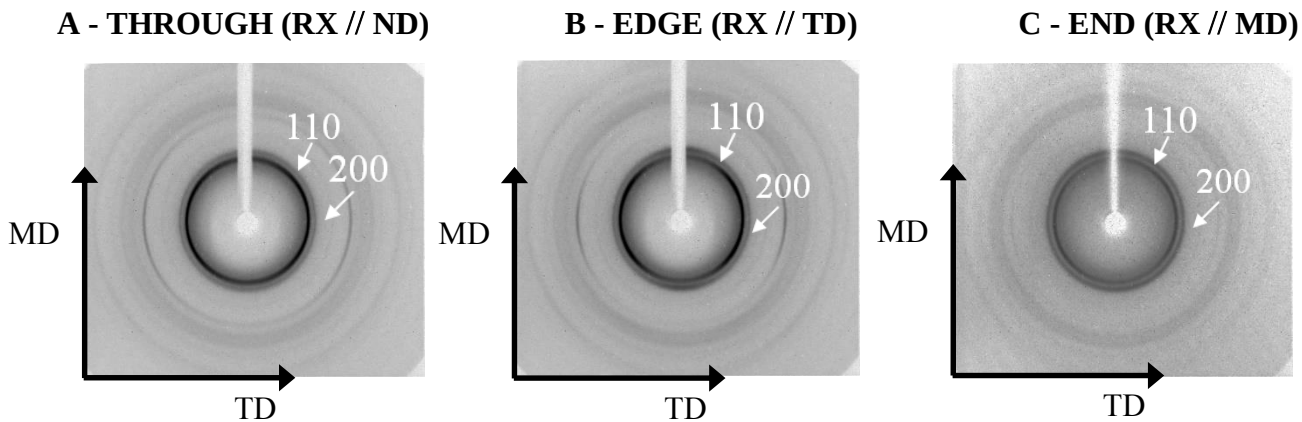

Figure 4.12 *2D X-ray diffraction of the sample Test 1: through (A), edge (B), end (C). Shows the reflections 110 and 200 of the PE*

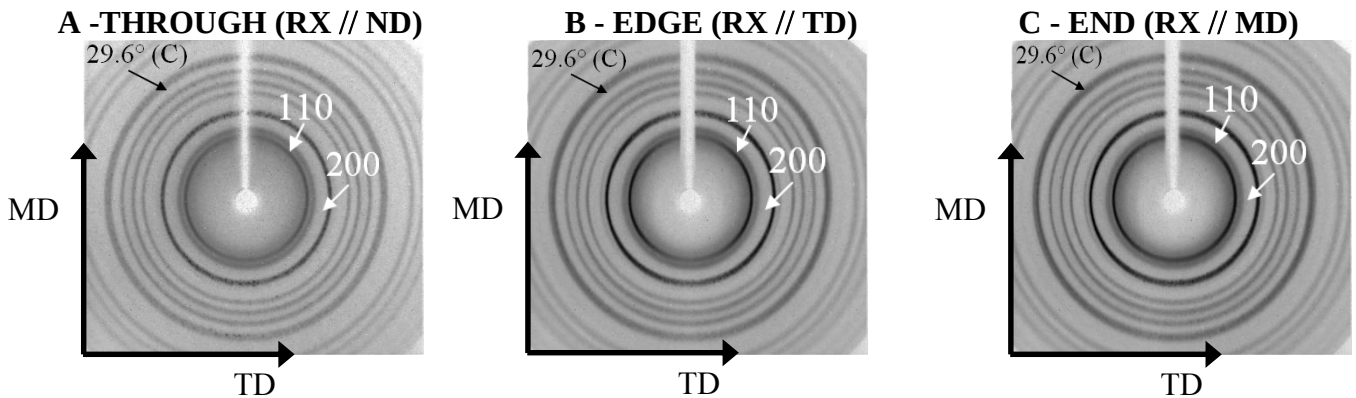

Figure 4.13 *2D X-ray diffraction of the sample Test 4: through (A), edge (B), end (C). Shows the reflections 110 and 200 of the PE and the main reflection diffraction of calcium carbonate (C)*

4.4 Morphological Analysis

4.4.1 Optical Microscopy of embossed film

The commercial embossed films have been analyzed by optical microscopy. This technique has allowed to identify the texture present on the surfaces of the films, due to embossing.

The images of the embossed Film 1, Film 2 and Film 3, at different enlargements, are reported in figures 4.14 - 4.16. The MD direction is vertical.

It is well visible for all the three films a regular and homogeneous micro-embossing pattern. In particular, Film 1 and Film 2 present a square shape motif (Figure 4.14 and 4.15), whereas Film 3 presents a circles shape motif (Figure 4.16).

The distances between the vertices of two consecutive squares (for Film 1 and Film 2) and two consecutive circles (for Film 3) in both MD and TD, and the dimensions of the side of the squares and the diameter of the circles have been measured and indicated in Figures 4.14 - 4.16. These measurements have provided an estimation of the percentage of embossed area for each sample, reported in Table 4.5.

The data of Table 4.5 indicate that the commercial embossed Film 1, having excellent best soft-touch perception (see Table 3.1) presents also the highest percentage of embossed area.

Table 4.5 P*ercentage of embossed area of the commercial Film 1, Film 2 and Film 3, determined by the optical microscopic imnages of Figures 4.14 - 4.16.*

Sample	% Embossed Area
Film 1	46.4
Film 2	31.0
Film 3	20.5

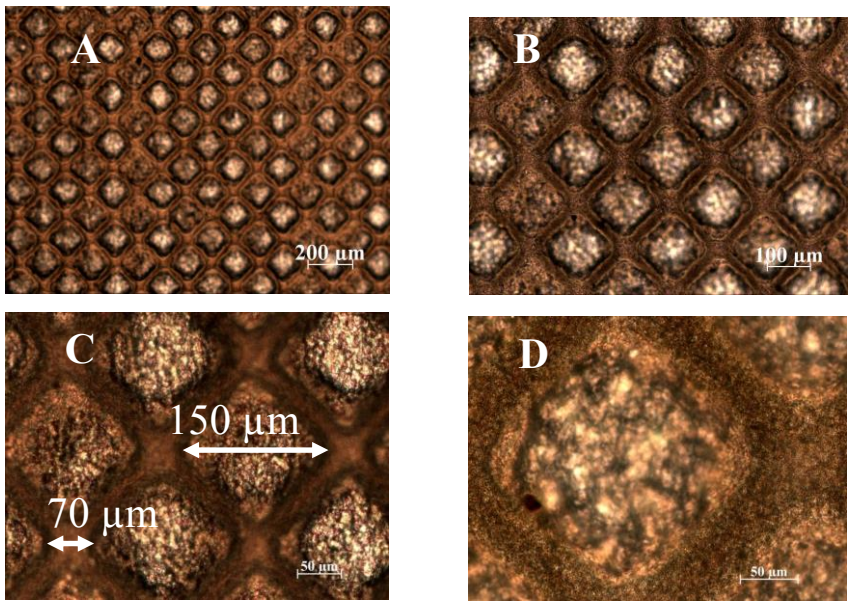

Figure 4.14 *Optical microscope images of the embossed film, Film 1, at 5x (A), 10x (B) 20x (C), 40x (D). The machine direction (MD) is vertical.*

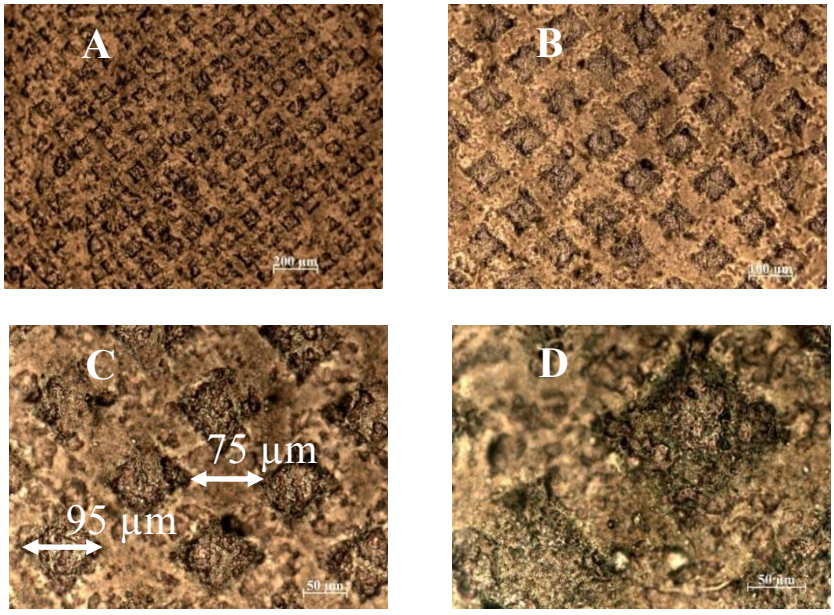

Figure 4.15 *Optical microscope images of the embossed film, Film 2, at 5x (A), 10x (B) 20x (C), 40x (D). The machine direction (MD) is vertical.*

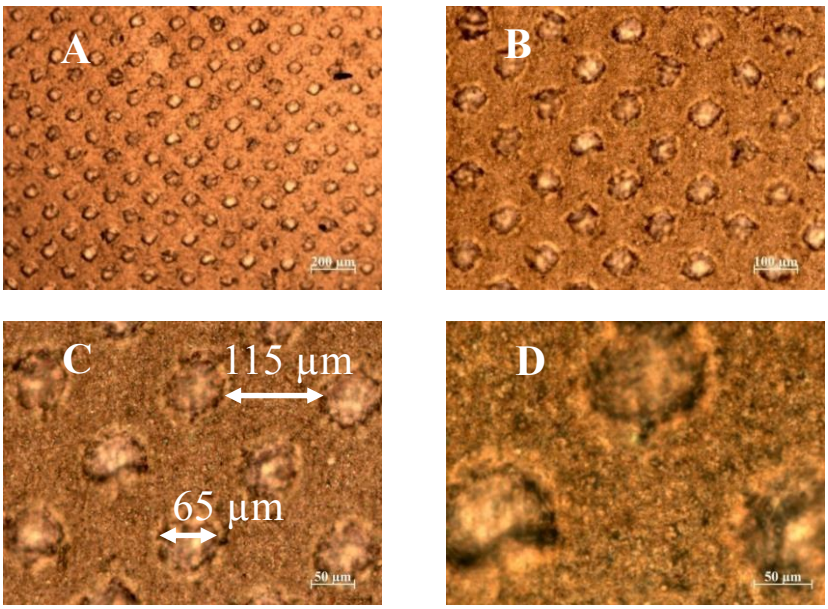

Figure 4.16 *Optical microscope images of the embossed film, Film 3, at 5x (A), 10x (B) 20x (C), 40x (D). The machine direction (MD) is vertical.*

4.4.2 Optical Microscopy of not embossed films

For smooth, not embossed, films (Samples Test 1 - Test 7) the optical microscopic images have been obtained in polarized light. The use of polarized light has allowed to highlight the presence of inorganic fillers, essentially calcium carbonate, that appears in the images as white spot.

The images of the sample Test 1, that does not contain inorganic fillers, and of samples Test 2 (with 20 wt% of CaCO3), Test 4 (with 20wt% of $CaCO_3$), Test 5 (with 30wt% of $CaCO_3$ and Talc) and Test 6 (with 40 wt% of $CaCO_3$ and small amount of the etherophase copolymer PE-PP1) are shown in Figures 4.17 and 4.18, as an example.

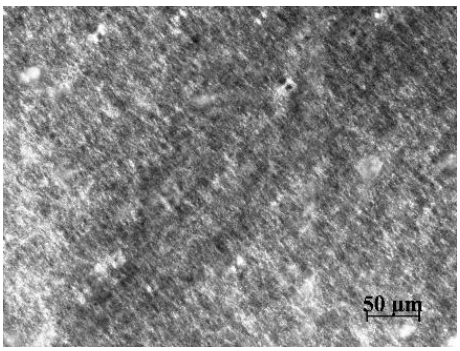

Figure 4.17 *Optical microscopic image in polarized light at enlargment 20x of the smooth film Test 1.*

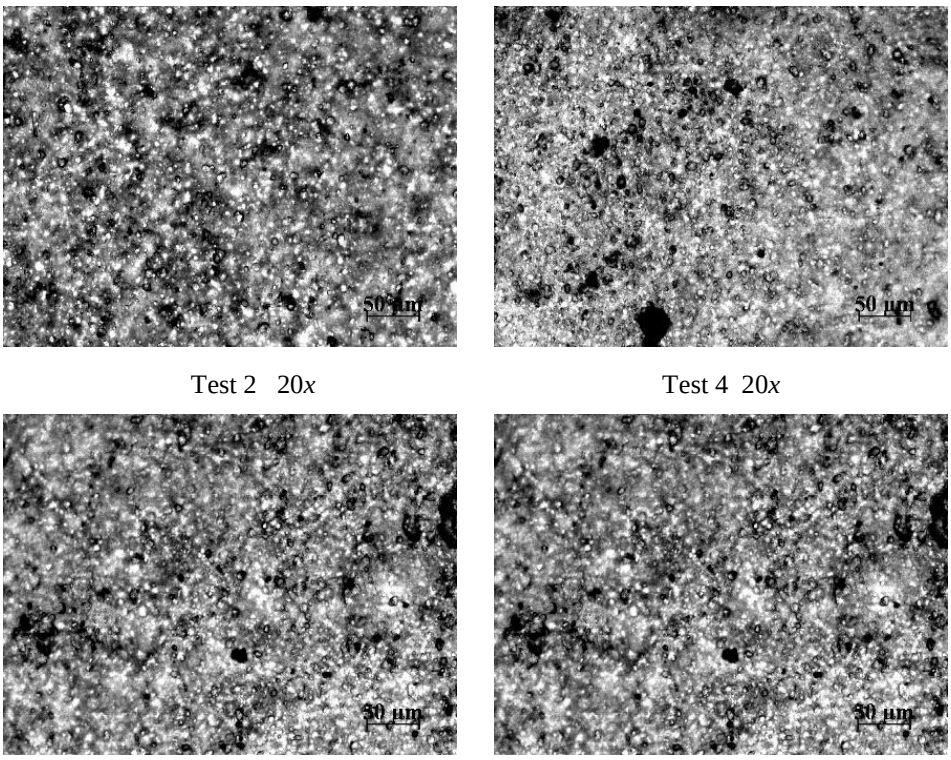

Test 2 20*x* Test 4 20*x*

Test 5 20*x* Test 6 20*x*

Figure 4.18 *Optical microscopic images in polarized light at enlargment 20x of the smooth films Test 2, Test 4, Test 5 and Test 6.*

It is apparent from the images of Figure 4.18 the presence of circular white particles, not visible in the image of Figure 4.17 relative to the sample Test 1 constituted by only PE. These are due to the inorganic fillers, calcium carbonate and talc, present in the samples Test 2, Test 4, Test 5 and Test 6. It is apparent for all samples a good dispersion of the inorganic fillers.

The distribution of the number of particles as function of their diameter have been determined from the images of Figure 4.18. The average values of the particle diameter, reported in Table 4.6, range for all samples from 4.3 to 5.5 μm.

Table 4.6 A*verage values of the diameter of particles of the inorganic fillers dispersed in the films.*

Sample	Average Diameter
Test 2 (20%$CaCO_3$)	**4.3 µm**
Test 3 (30%$CaCO_3$)	**4.4 µm**
Test 4 (40%$CaCO_3$)	**4.4 µm**
Test 4-2 (40%$CaCO_3$)	**5.0 µm**
Test 4-3 (40%$CaCO_3$)	**4.5 µm**
Test 5 (30%$CaCO_3$+Talc)	**5.4 µm**
Test 6 (40%$CaCO_3$+PE-PP1)	**5.3 µm**
Test 6 Bis (50%$CaCO_3$+PE-PP1 +PE-PP2)	**5.5 µm**
Test 7 (40%$CaCO_3$+PE-PP2)	**5.4 µm**

4.4.3 AFM Analysis

The not embossed films Test 1 - Test 5 have been analyzed by atomic force microscopy (AFM), in order to evaluate the surface roughness, given by the value of the average height, determined from the AFM topographical images recorded at different scanned areas (5x5, 20x20, 50x50, 100x100 µm), as show in the graph of Figure 4.19.

The most significant results are obtained for the largest scanned area 100x100 µm. For all samples the value of average height (roughness) increases with increasing the percentage of inorganic fillers. The greatest value is obtained for the sample Test 5, containing 30wt% of calcium carbonate and talc (Figure 4.19).

The values of average height of all analyzed sampes are reported in Table 4.7.

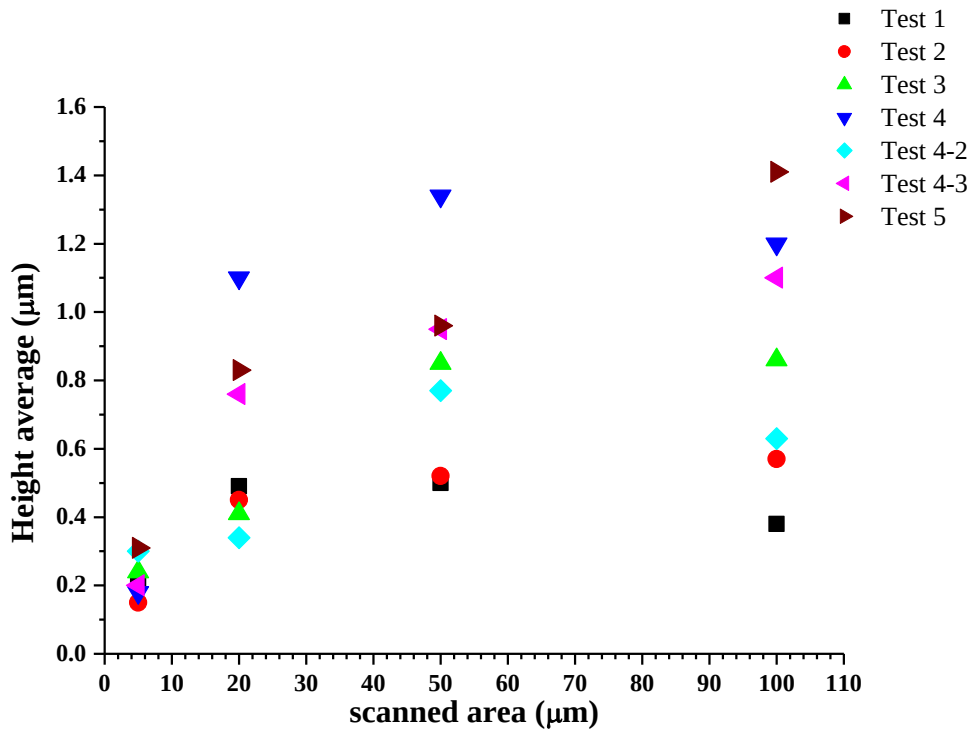

Figure 4.19 *Values of average height, determined from the AFM topographical images of the not embossed films (Test 1 -Test 5) as a function of different scanned areas.*

Table 4.7 *Values of the average hight determined from the AFM topographical images recorded at differet scanned areas of the samples Test 1 - Test 5.*

Sample	Size (µm)	Height average (µm)
■ Test 1 ($0\%CaCO_3$)	5	0.21
	20	0.49
	50	0.50
	100	0.38
● Test 2 ($20\%CaCO_3$)	5	0.15
	20	0.45
	50	0.52
	100	0.57
▲ Test 3 ($30\%CaCO_3$)	5	0.24
	20	0.41
	50	0.85
	100	0.86
▼ Test 4 ($40\%CaCO_3$)	5	0.36
	20	1.10
	50	1.34
	100	1.20
♦ Test 4-2 ($40\%CaCO_3$)	5	0.30
	20	0.34
	50	0.77
	100	0.63
◄ Test 4-3 ($40\%CaCO_3$)	5	0.20
	20	0.76
	50	0.95
	100	1.1
► Test 5 ($30\%CaCO_3$) (Talc)	5	0.31
	20	0.83
	50	0.96
	100	1.41

4.4.4 Profilometry

The roughness of the not embossed film has been determined also by a profilometer.

In particular, the values of average roughness (*Ra*) and mean square roughness (*Rq*) have been obtained for two different values of cut-off of 80 and 250 μm. Cut-off length refers to the distance a profilometer stylus travels across a surface when taking a measurement.

The values of average roughness (*Ra*) and square mean roughness (*Rq*) of all not embossed films are reported in Figures 4.20 and 4.21, as a function of two chosen different cut-off, and listed in Tables 4.8 and 4.9. The values of *Ra* and *Rq* of the embossed Film 3 are also reported for comparison.

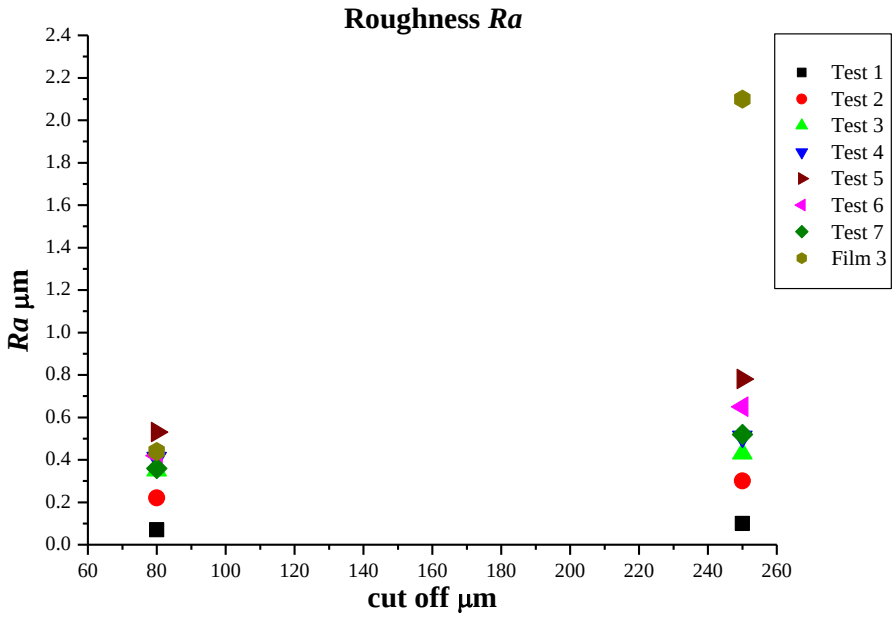

Figure 4.20 *Average roughness (Ra) of the samples Test1 - Test 7 as a function of two different value of cut-off. The average roughness of the embossed Film 3 is reported for comparison.*

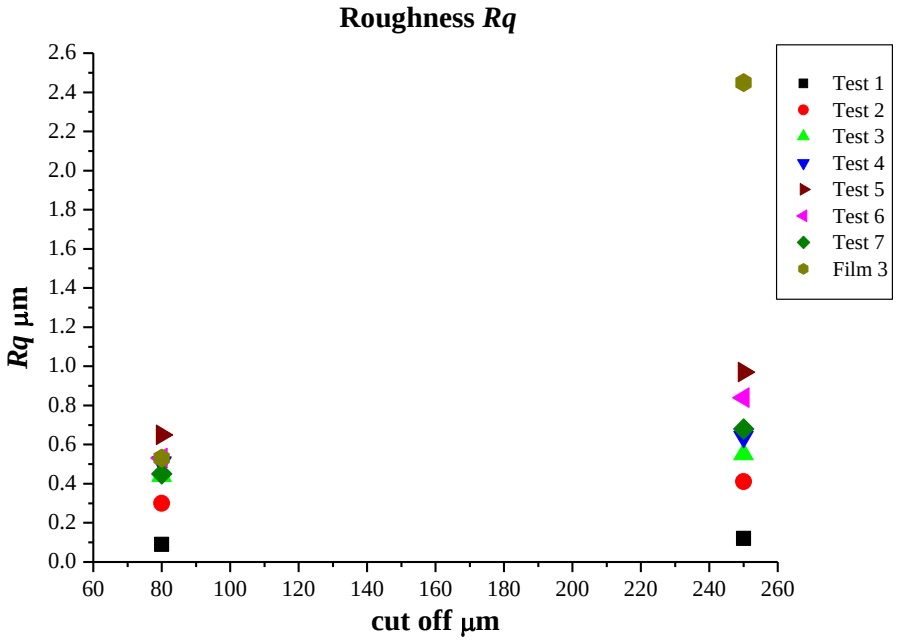

Figure 4.21 *Square mean roughness (Rq) of the samples Test1 - Test 7 as a function of two different value of cut-off. The Square mean roughness of the embossed Film 3 is reported for comparison.*

Table 4.8 *Values of average roughness (Ra) of the samples Test 1 - Test 7 and of the embossed Film 3, determined for two differet cut-off values.*

Roughness (*Ra*)	Cut-off 80µm	Cut-off 250µm
Test 1 (0% $CaCO_3$)	0.07 µm	0.1 µm
Test 2 (20% $CaCO_3$)	0.22 µm	0.3 µm
Test 3 (30% $CaCO_3$)	0.35 µm	0.43 µm
Test 4 (40% CaCO3)	0.41 µm	0.51 µm
Test 5 (30% $CaCO_3$ + Talc)	0.53 µm	0.78 µm
Test 6 (40% $CaCO_3$ + PE-PP1)	0.42 µm	0.65 µm
Test 7 (40% $CaCO_3$ + PE-PP2)	0.36 µm	0.52 µm
Film 3 (embossed)	0.44 µm	2.1 µm

Table 4.9 *Values of square mean roughness (Rq) of the samples Test 1 - Test 7 and of the embossed Film 3, determined for two differet cut-off values.*

Roughness (*Rq*)	Cut-off 80μm	Cut-off 250μm
Test 1 (0% $CaCO_3$)	0.09 μm	0.12 μm
Test 2 (20% $CaCO_3$)	0.3 μm	0.41 μm
Test 3 (30% $CaCO_3$)	0.44 μm	0.55 μm
Test 4 (40% CaCO3)	0.51 μm	0.64 μm
Test 5 (30% $CaCO_3$ + Talc)	0.65 μm	0.97 μm
Test 6 (40% $CaCO_3$ + PE-PP1)	0.53 μm	0.84 μm
Test 7 (40% $CaCO_3$ + PE-PP2)	0.45 μm	0.72 μm
Film 3 (embossed)	0.53 μm	2.45 μm

The data of Tables 4.8 and 4.9 indicate that the roughness increases with increasing of percentage of inorganic phase, in particular at value of cut-off of 250 μm. The gretest value of roughness is obtained for the sample Test 5, containing 30% of calcium carbonate and talc, in agreement to the AFM analysis. It is worth noting that the sample Test 5 reaches values of roughness about half of those of the embossed Film 3 (Tables 4.8 and 4.9), significantly high for a not embossed film.

4.5 Mechanical Properties

The mechanical tests have been recorded stretching the film specimens along the machine (blowing direction, parallel to the extrusion direction) (MD), and along the direction perpendicular to it (transverse direction TD).

The stress strain curves recorded at room temperature along MD and TD of the commercial embossed films and of the three sets of not embossed films

(samples Test 1 - Test 7) are reported in Figures 4.22 - 4.25, respectively. The average values of the mechanical parameters are listed in Tables 4.10 - 4.12.

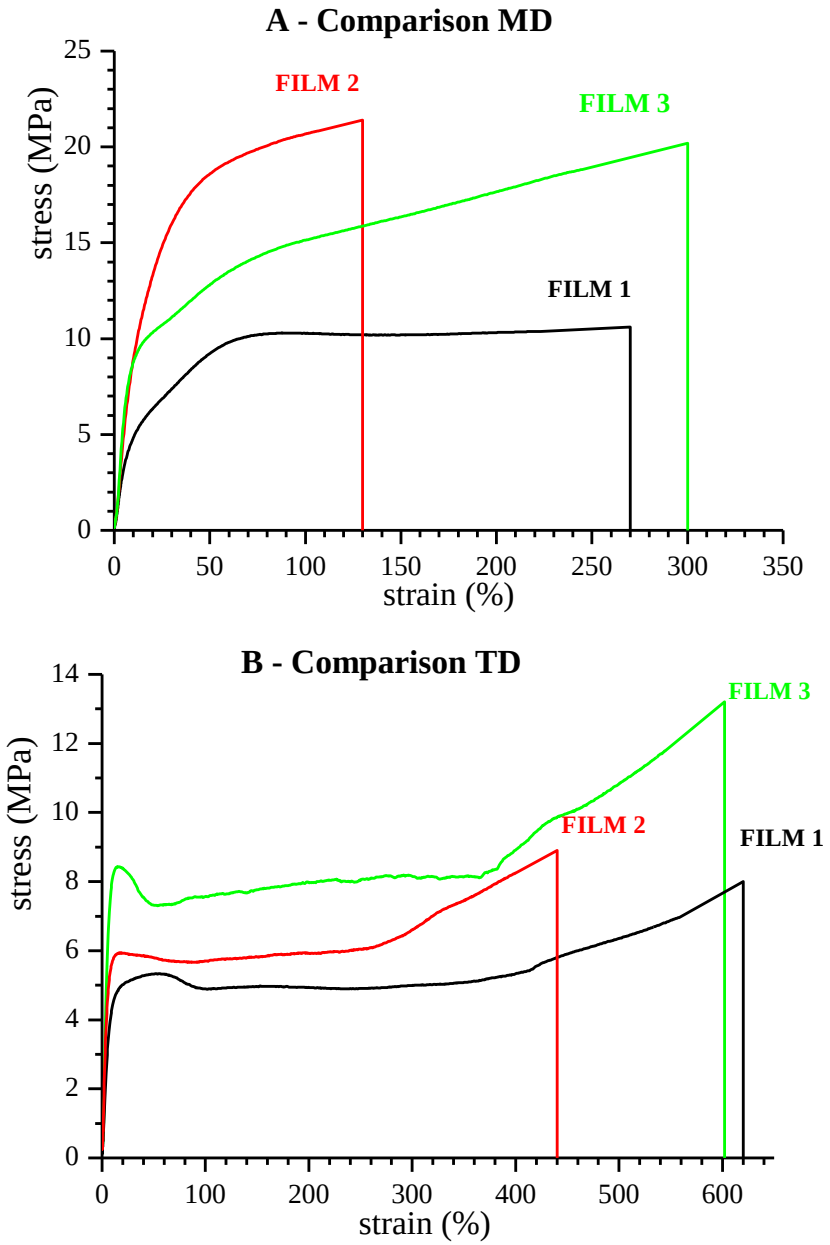

Figure 4.22 *Stress-strain curves recorded at room temperature of the embossed Film1 (black curves), Film 2 (red curves) and Film 3 (green curves). The mechanical tests have been recorded stretching the specimens along the blowing direction MD (A) and along the transverse direction TD, perpendicular to it (B).*

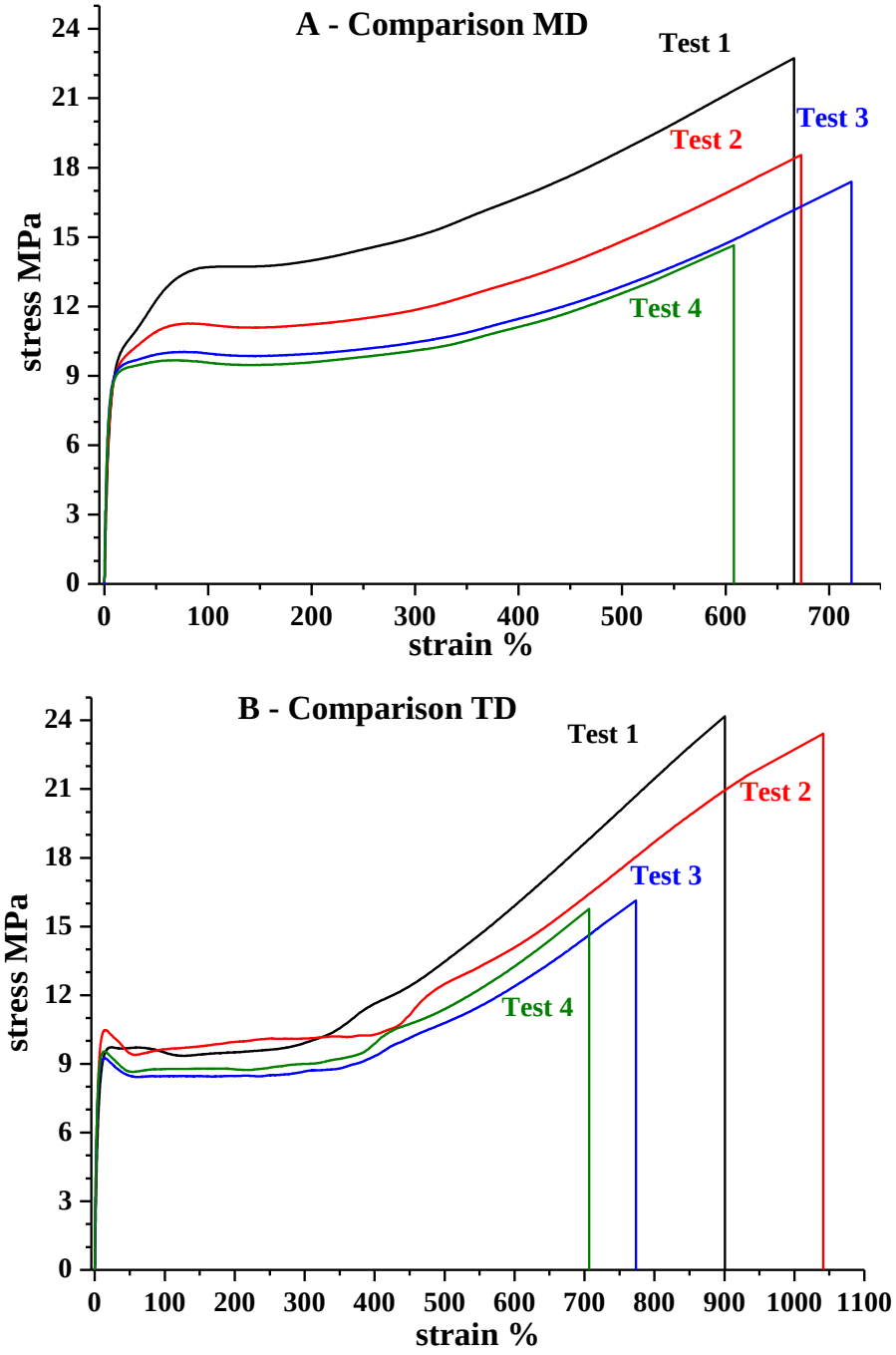

Figure 4.23 *Stress-strain curves recorded at room temperature of the first set of samples Test1 (black curves), Test 2 (red curves), Test 3 (blue curves) and Test 4 (green curves). The mechanical tests have been recorded stretching the specimens along the blowing direction MD (A) and along the transverse direction TD, perpendicular to it (B).*

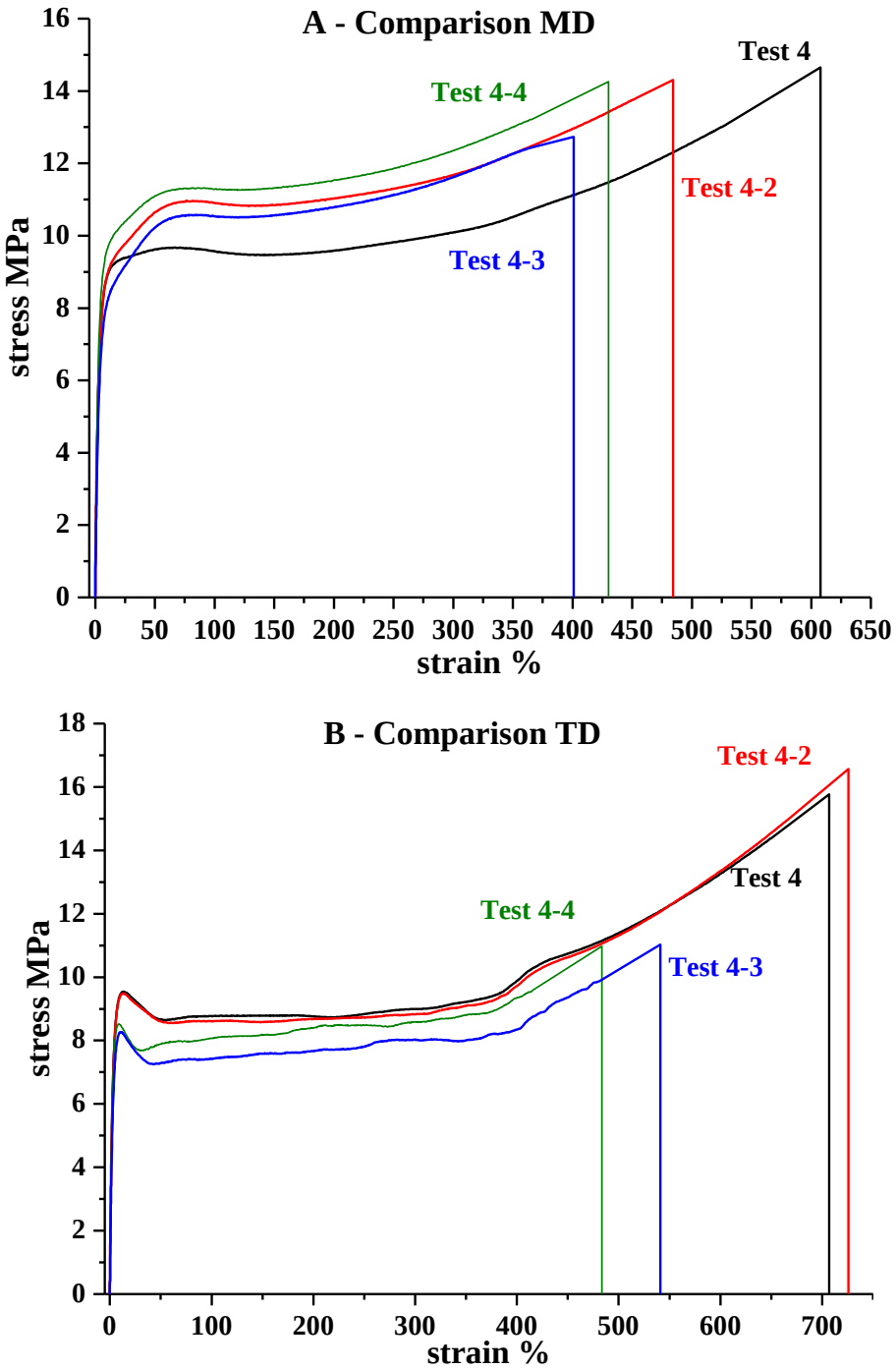

Figure 4.24 *Stress-strain curves recorded at room temperature of the second set of samples Test4 (black curves), Test 4-2 (red curves), Test 4-3 (blue curves) and Test 4-4 (green curves). The mechanical tests have been recorded stretching the specimens along the blowing direction MD (A) and along the transverse direction TD, perpendicular to it (B).*

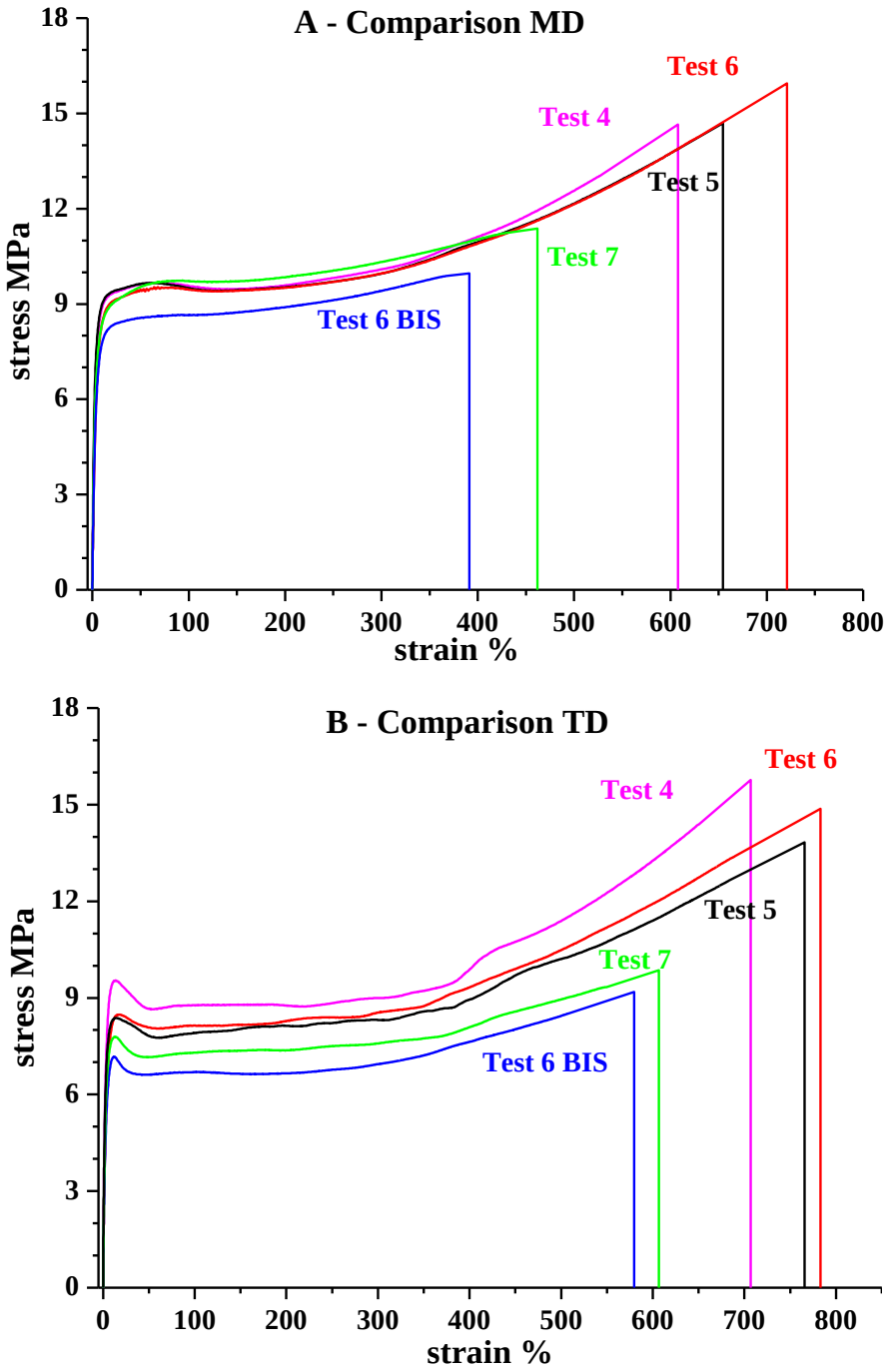

Figure 4.25 *Stress-strain curves recorded at room temperature of the third set of samples Test5 (black curves), Test 6 (red curves), Test 6BIS (blue curves) and Test 7 (green curves). The stress strain curves of the sample Test 4 (magenta curves) are also reported for comparison. The mechanical tests have been recorded stretching the specimens along the blowing direction MD (A) and along the transverse direction TD, perpendicular to it (B).*

Table 4.10: *Average values of Young's modulus (E), stress at yield (σ_y) and stress and strain at break (σ_b and ε_b) measured along MD and TD of the commercial embossed films. Thickness, values of percentage of embossed area, coefficient of friction (COF) and soft-touch perception of the samples are also reported.*

Sample	Thickness (μm)	% Embossed Area	*E* (MPa)	σ_y (MPa)	ε_b (%)	σ_b (MPa)	COF	Relative soft-touch perception
FILM 1 MD	35	46.4	62±6	5.1±0.6	270±40	10.6±0.3	0.58	High
FILM 1 TD			70±1	5.4±0.1	620±40	7.7±0.6		
FILM 2 MD	33	31.0	97±3	15.9±0.9	130±15	20.4±0.9	0.39	Medium high
FILM 2 TD			87±7	5.9±0.1	440±30	8.9±0.6		
FILM 3 MD	26	20.5	108±6	8.4±0.5	300±50	20±1	0.34	Medium
FILM 3 TD			130±4	8.5±0.5	600±40	13±1		

Table 4.11: *Average values of Young's modulus (E), stress and strain at yield (σ_y and ε_y) and at break (σ_b and ε_b) measured along MD and TD of the first and second sets of not embossed films. The values of percentage of $CaCO_3$, thickness (t) and coefficient of friction (COF) of the samples are also reported.*

Set	Sample	% $CaCO_3$	Thickness (μm)	*E* (MPa)	ε_y (%)	σ_y (MPa)	ε_b (%)	σ_b (MPa)	COF
I	**Test 1 MD**	0	70	169 ± 7	7.9 ± 0.3	9.6 ± 0.3	666 ± 39	23 ± 1	0.21
	Test 1 TD			168 ± 5	22.1 ± 1.6	9.7 ± 0.1	900 ± 28	24 ± 1	
	Test 2 MD	20	70	188 ± 8	6.1 ± 0.1	9.4 ± 0.1	673 ± 24	18.5 ± 0.7	0.41
	Test 2 TD			220 ± 20	14.8 ± 0.7	10.5 ± 0.8	1040 ± 70	23.4 ± 1	
	Test 3 MD	30	70	240 ± 10	5.5 ± 0.3	9.4 ± 0.3	721 ± 47	17.4 ± 0.8	0.41
	Test 3 TD			270 ± 8	13.2 ± 0.6	9.3 ± 0.5	773 ± 32	16.1 ± 0.8	
	Test 4 MD	40	70	244 ± 15	5.9 ± 0.4	9.3 ± 0.3	608 ± 47	14 ± 1	0.43
	Test 4 TD			260 ± 15	13.6 ± 0.5	9.5 ± 0.2	706 ± 45	16 ± 1	
II	**Test 4-2 MD**	40	50	259 ± 15	5.2 ± 0.4	9.1 ± 0.5	484 ± 26	14 ± 1	0.42
	Test 4-2 TD			251 ± 10	12.7 ± 0.5	9.5 ± 0.1	726 ± 37	16 ± 1	
	Test 4-3 MD	40	35	197 ± 12	5.5 ± 0.4	8.2 ± 0.4	401 ± 27	12.7 ± 0.7	0.42
	Test 4-3 TD			247 ± 30	10.4 ± 1.2	8.3 ± 0.6	541 ± 56	11 ± 1	
	Test 4-4 MD	40	25	241 ± 22	4.3 ± 0.2	9.7 ± 0.4	430 ± 42	14.3 ± 0.7	0.42
	Test 4-4 TD			263 ± 33	9 ± 1	8.6 ± 0.4	484 ± 37	10.9 ± 0.9	

Table 4.12: *Average values of Young's modulus (E), stress and strain at yield (σ_y and ε_y) and at break (σ_b and ε_b) measured along MD and TD of the third set of not embossed films. The values of percentage of $CaCO_3$, thickness (t) and coefficient of friction (COF) of the samples are also reported.*

Sample	New Additional Component	% $CaCO_3$	Thickness (μm)	*E* (MPa)	ε_y (%)	σ_y (MPa)	ε_b (%)	σ_b (MPa)	COF
Test 5 MD	Talc	30	70	309 ± 19	4.5 ± 0.2	9.3 ± 0.3	654 ± 29	14.7 ± 0.6	0.42
Test 5 TD				306 ± 17	13 ± 1	8.4 ± 0.4	765 ± 77	14 ± 1	
Test 6 MD	PE-PP 1	40	70	211 ± 10	6.8 ± 0.2	8.9 ± 0.2	721 ± 59	16 ± 0.7	0.53
Test 6 TD				224 ± 19	17 ± 2	8.5 ± 0.3	783 ± 77	15 ± 1	
Test 6 BIS MD	PE-PP 1 PE-PP 2	50	70	221 ± 13	6.6 ± 0.2	8.2 ± 0.2	391 ± 23	9.9 ± 0.3	0.53
Test 6BIS TD				223 ± 13	12 ± 1	7.2 ± 0.2	579 ± 57	9 ± 1	
Test 7 MD	PE-PP 2	40	70	256 ± 12	7.2 ± 0.3	8.8 ± 0.2	462 ± 34	11 ± 0.3	0.44
Test 7 TD				275 ± 13	13 ± 0.5	7.8 ± 0.2	607 ± 60	10 ± 1	

It is apparent that while the commercial embossed Film 2 and Film 3 present different mechanical behavior in MD and TD (Figure 4.22), the embossed Film 1 and the not embossed films (samples Test 1 – Test 7) present similar mechanical behavior along the two directions (Figure 4.23 - 4.25).

In particular, for the embossed Film 2 and Film 3 the values of deformation at break are generally higher in the transverse direction compared to those measured in the machine direction and the stress-strain curve recorded in MD presents values of Young's modulus and stress at any deformation greater than those recorded in TD (Figure 4.22 and Table 4.10). These differences are due to the presence of preferred orientations of the crystals of PE. In fact, the analysis of the two-dimensional X-ray diffraction patterns described in the paragraph 4.2, has shown that these films have an axial orientation of the crystals of PE, with the chain (*c*) axis preferentially aligned along the machine direction and the *a* and *b* axes cylindrically arranged around *c*. Therefore, the films show a greater resistance to the deformation along MD and this results in values of Young's modulus and stress at break higher in MD than in TD and values of strain at break smaller in MD than TD (Figure 4.22 and Table 4.10).

The Film 1 and the samples Test 1 - Test 7, instead, are essentially unoriented, or with low degree of crystalline orientations (see paragraph 4.2), and, as a consequence, show similar mechanical behavior along MD and TD (Figures 4.23 - 4.25 and Tables 4.11 and 4.12).

It is worth noting that the higher ductility of the films in the transverse direction is particularly important for these materials. In fact, one of the requirements of polyolefin-based films used as back-sheet in the healthcare application is the tear resistance especially along the tasverse direction. This requirement is fulfilled not only for the commerciaòl embossed films, but also for the new formulation and not embossed films, as evident by the values of strain at break measured along TD ranging from 600 to 1000 % (Tables 4.11 and 4.12).

The data Table 4.10 show that the embossed Film 1 present a value of Young's modulus less than that of Film 2 and Film 3. We recall that the thermal analysis showed that Film 1 is essentially constituted by HDPE, whereas the embossed Film 2 and Film 3, containing also small amounts of polypropylene and calcium carbonate, are essentially constituted by mixtures of LDPE and LLDPE. We should expect highest values of the Young's modulus for Film 1 with respect to Film 2 and Film 3, since HDPE is a material more rigid than LDPE and LLDPE. The values of modulus of Film 1 significantly lower than that of Film 2 and Film3 is, hence, attributable to the different embossed texture and, in particular, to the fact that Film 1 presents a greater percentage of embossed area (Table 4.10). In particular, the Young's modulus decreases with increasing the percentage of embossed area (Table 4.10) and, hence, with increasing the soft-touch performance. Moreover, the comparison of the other tensile parameters shows that with increasing the percentage of embossed area, and hence with increasing the softness of the films, the values of stress at yield and at break decrease and the values of COF increase (Table 4.10).

Hence, the analysis of the commercial embossed films has allowed to identify mechanical parameters, as Young's moduli, stress at yield and at break, coefficient of friction directly related to the quality of embossing and to the soft-touch perception. The values of Young's modulus and stress at yield and at break of the commercial embossed films are reported as a function of the percentage of embossed area in the graph of Figure 4.26.

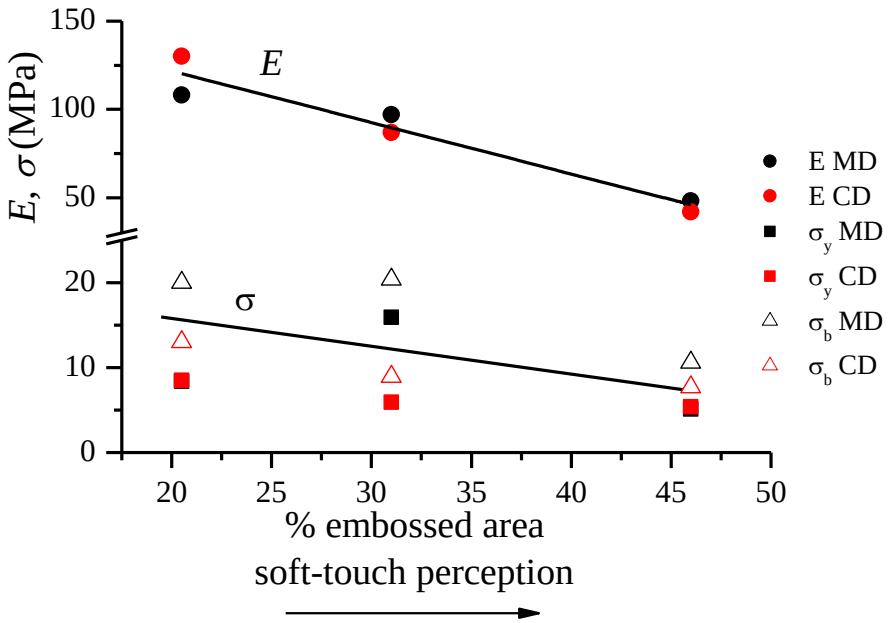

Figure 4.26 *Influence of the percentage of embossed area (and soft-touch perception) on the Young modulus and on the stress at yield and at break.*

The characteristics of soft-touch increase with decreasing of the Young's modulus and the tensile stress (Figure 4.26).

These results indicate that the soft-touch proprierty depends from the characteristic of the film surface (morphology), and from mechanical properties as Youing's modulus, yield strength, stress-strain behavior (rigidity *vs.* flexibility) and coefficient of friction. These properties can be directly related to soft-touch feeling (Figure 4.26).

Therefore, the physical properties that primarily influence our tactile perception of a material include surface texture, surface friction, and tensile properties; in particular, low values of Young's modulus and mechanical strenght are required for having films with good soft-touch performances.

In order to point out the dependance of the mechanical behavior of the films on the content of calcium carbonate and on the thickness, the Young's modulus, the stress at yeld and at break and the strain at break of the first and second sets of samples (Test1 – Test 4 and Test 4 – Test 4-4) are reported in Figure 4.27 as a

function of the concentration of calcium carbonate and in Figure 4.28 as a function of the film thickness.

It is apparent that the presence of calcium carbonate induces an increse of rigidity (*E*, Figure 4.27A) and a decrease of the stress at break (σ_b Figure 4.27C), whereas the stress at yield (σ_y Figure 4.27B) are almost constant with increasing the concentration of calcium carbonate. The ductility (ε_b, Figure 4.27D) is not much influenced by the presence of the inorganic filler and a decrease is obseved only for content of calcium carbonate higher than 20wt%.

The film thikness, instead, does not influence the tensile parameters, as indicated by the data of the second set of samples reported in Figure 4.28.

The addition of talc determines an increase of the rigidity of the film, as indicated by the increase of the values of Young's modulus both in MD and TD (Tables 4.11 and 4.12).

The addition of the elastomeric heterophasic PP-PE copolymer, instead, produces increase of ductility and decrease of rigidity (Tables 4.11 and 4.12), also for high content of calcium carbonate (Table 4.12).

The best result has been obtained for the sample Test 6 containing the elastomeric copolymers PP-PE 1 and 40wt% of calcium carbonate. The tensile parameters of this sample are reported in the graphs of Figure 4.27 for comarison. It is apparent that the presence of the elastomeric component of the etherophase copolymer produces in this film a decrease of rigidity and mechanical strenght, while maintaining high ductility, with respect to sample Test 4 containing same amount of inorganic filler (Figure 4.27).

The samples Test 6BIS and Test 7 the addition of the elastomeric copolymers do not produce improvement of the ductuility, probably because in these samples the percentage of inorganic filler has been increased in the central layers with respect to the sample Test 6 (Table 3.7), and this could weakens the structure of the film.

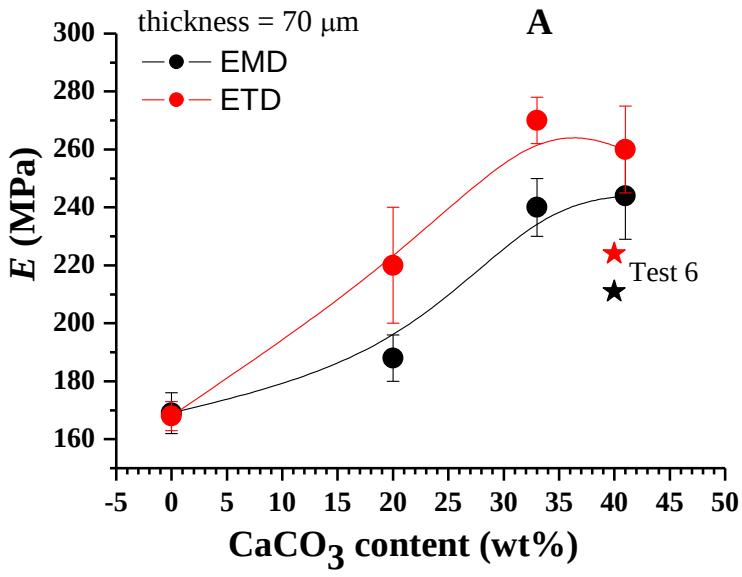
thickness = 70 μm
A
EMD
ETD
E (MPa)
300
280
260
240
220
200
180
160
Test 6
-5
0
5
10
15
20
25
30
35
40
45
50
CaCO3 content (wt%)

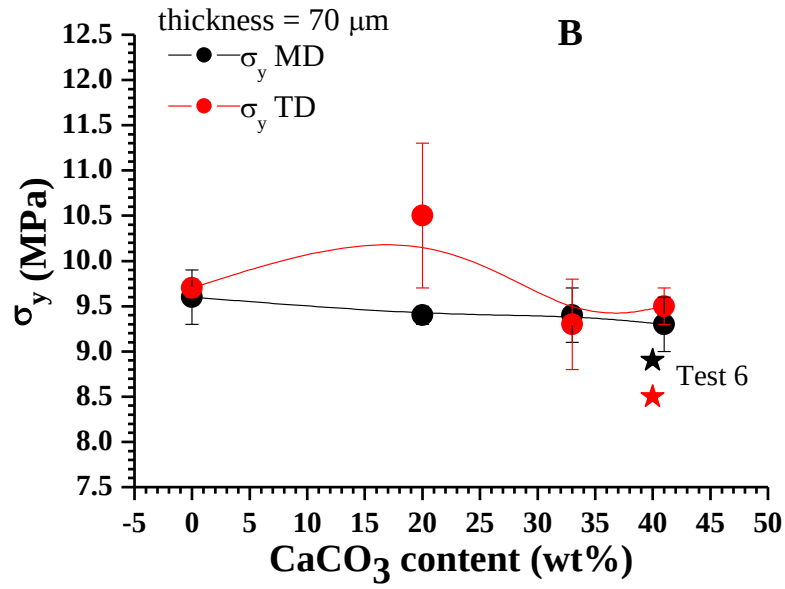
thickness = 70 μm
B
σy MD
σy TD
σy (MPa)
12.5
12.0
11.5
11.0
10.5
10.0
9.5
9.0
8.5
8.0
7.5
Test 6
-5
0
5
10
15
20
25
30
35
40
45
50
CaCO3 content (wt%)

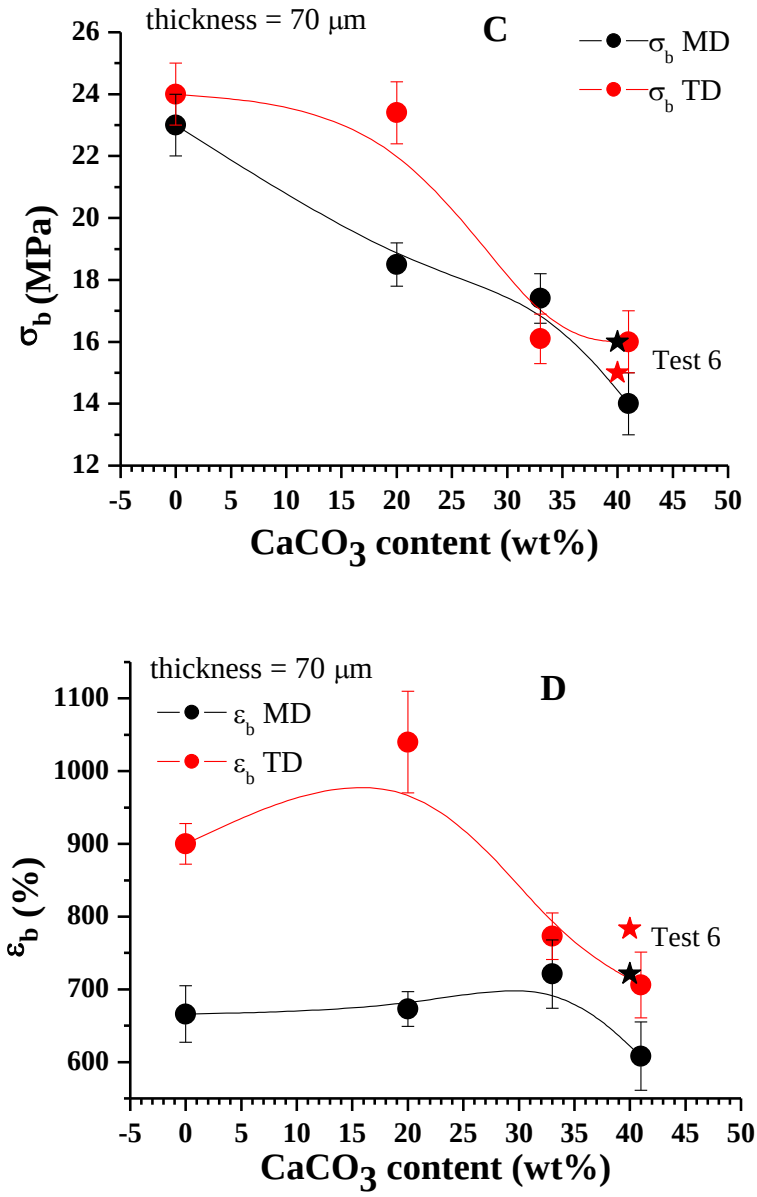

Figure 4.27 *Young's modulus E (A), stress at yield σ_y (B) and at break σ_b (C) and strain at break ε_b (D) determined in machine (MD) and tranverese direction (TD) for the first set of samples Test 1 – Test 4, as function of the concentration of calcium carbonate. The tensile parameters of the sample Test 6 are reported for comparisons.*

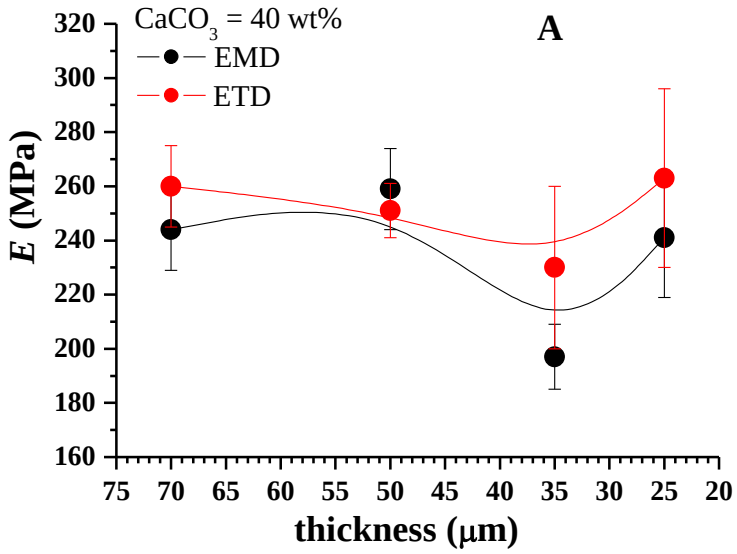
CaCO3 = 40 wt%
A
EMD
ETD
E (MPa)
320
300
280
260
240
220
200
180
160
75 70 65 60 55 50 45 40 35 30 25 20
thickness (μm)

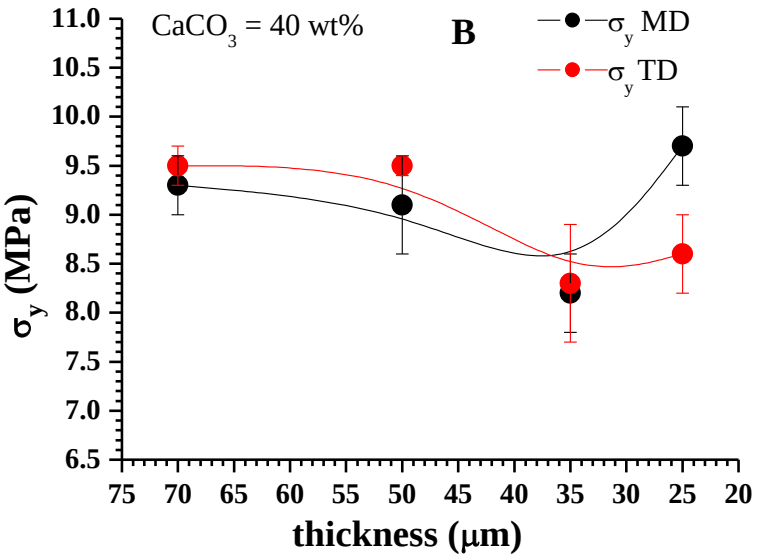
CaCO3 = 40 wt%
B
σy MD
σy TD
σy (MPa)
11.0
10.5
10.0
9.5
9.0
8.5
8.0
7.5
7.0
6.5
75 70 65 60 55 50 45 40 35 30 25 20
thickness (μm)

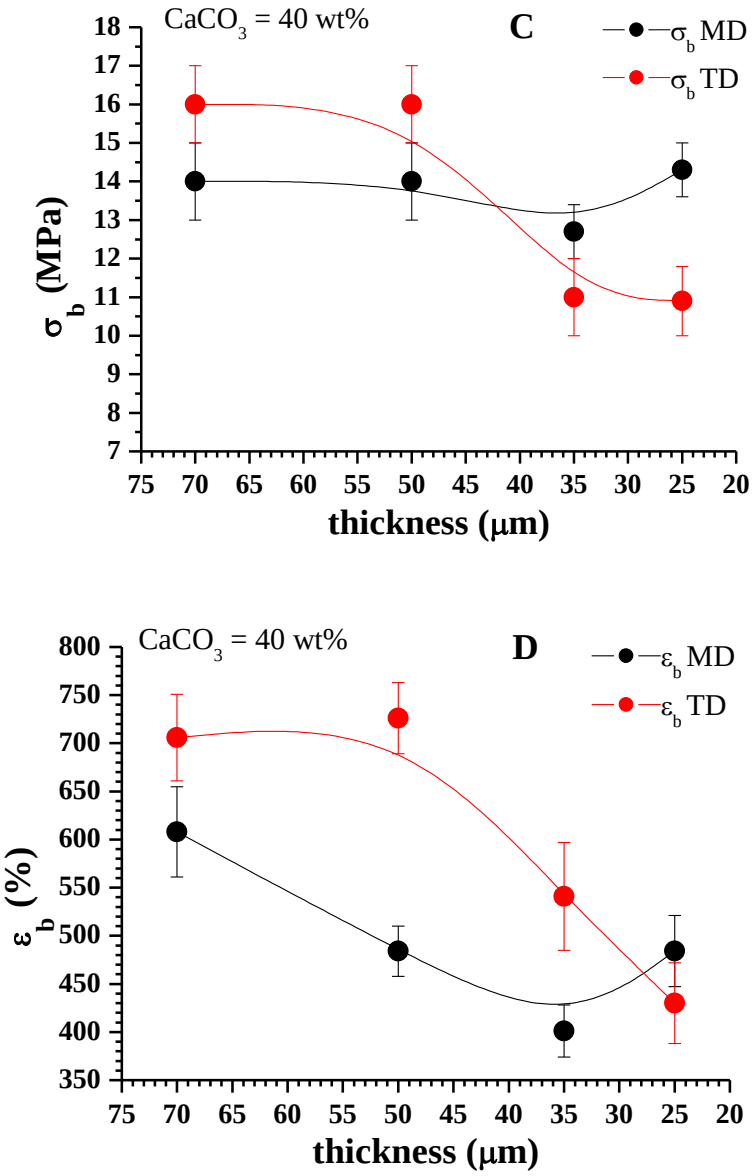

Figure 4.28 *Young's modulus E (A), stress at yield σ_y (B) and at break σ_b (C) and strain at break ε_b (D) determined in machine (MD) and tranverese direction (TD) for the second set of samples Test 4 – Test 4-4, as function of the film thickness.*

CHAPTER 5

Managment system of quality control

During my PhD I had the opportunity to spend a working-stage in the Blu Plast company in order to follow the entire production process of the main mono and multilayered films produced by Blu Plast and to contribute to the implementation of the management system of quality control.

The company produces polyethylene film with blow process for many technical and industrial applications. Its core business is focused on the production of:

- Shrink film, that are polymer plastic films that shrinking undergo by heat treatments. Thus, they can adhere perfectly to the object around which they are wrapped and they can keep the shape of the object once cooled.
- Laminated films, where the lamination is the technique of manufacturing a material in multiple layers, combining different materials. The terms LAMINATE, COUPLED and POLYCOUPLED are synonyms referring to thin multilayer structures obtained by combining existing materials for adhesion of paper, plastic film or aluminium.
- Thin films for healthcare applications obtained by extrusion, where techniques of multilayer coextrusion up to five layers, blending of polymers and specialty copolymers are joined to obtain film with good soft-touch performance.

For implementation of the management of quality control I have analyzed the main macro-structural defects of this film.

In fact, the main macro-structural defects, called technically “gels”, consist in small point-like regions, well visible with naked eyes on the film surface. They are caused by local presence of not well melted polymer particles, forming a clot. The presence of these “gels” may cause problems in the process, even using high extrusion temperatures. They determine discontinuities on the surface of the film, as show in Figure 5.1.

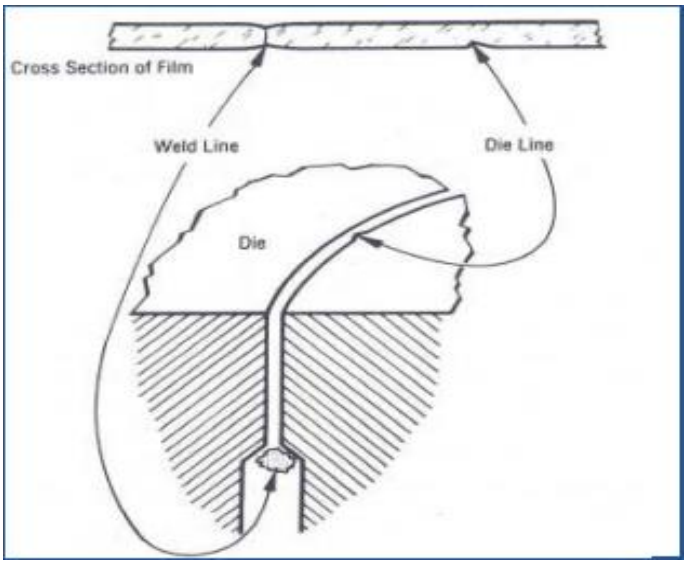

Figure 5.1 *Gel formation during extrusion*

One gel classification used widely in industry classifies gels into four main groups[39]. These groups are the Crosslinked/Oxidised gels, Cross Contamination gels, Unmixed/Non-homogenous gels and finally Fibers/Contamination gels.

- Crosslinked/Oxidised gels are the result of drastic molecular growth. This growth results in molecules of such a large size that they have much higher viscosity/elasticity compared to the rest of the melt. As a result the flow pattern of the melt is disrupted, especially after the

melt has left the die, resulting in a protrusion from the film which we call a gel. The actual molecule responsible constitutes less than 1/100th of the volume of protrusion. Crosslinked gels are primarily formed in the absence of oxygen and would therefore form inside the reactors of the polymer producer. Oxidised gels tend to form during extrusion, in the presence of oxygen.

- Cross Contamination gels are the result of unintended mixing between polymers of different density, molecular weight or comonomer type. The polymer mix is then extruded under conditions which do not allow adequate melting and mixing to occur. An example of this gel type would occur when using an extruder set up for LDPE film and running polymer (LDPE) contaminated by a small amount of HDPE. The HDPE would not fully melt under these conditions and would create gels.
- Unmixed/Non-homogenous gels are the result of polymer blends extruded under conditions of inadequate melting and mixing. Sources of these gels include poorly dispersed additives, polymer blends with very different melting points. An example of the latter would occur during the extrusion of a PP/HDPE blend.
- Fibres/Contamination gels result from floss (conveying of polymer using air), fibers from bagging material or contaminants picked up as a result of transport of the material.

For a LDPE or LLDPE the gels are visible when the molecules can grow until reaching a critical size, as show in Figure 5.2

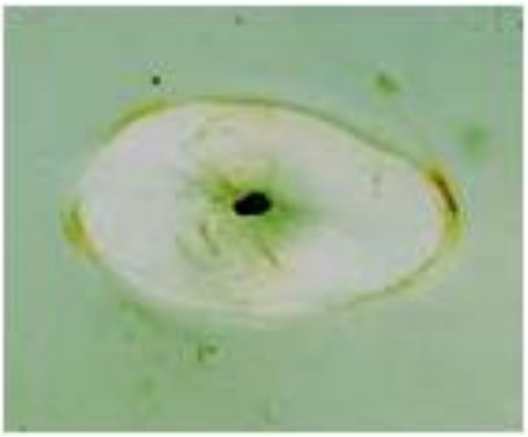

Figure 5.2 *Gel visible in a polyethylene film*

This molecular growth process is primed by free radicals and the degradation process starts as free radicals are formed. The degradation can comprise scission (breaking of molecules), oxidation (if oxygen is present), molecular growth, branching etc. The reaction conditions and molecular structure determine what of these processes dominates. With LDPE and LLDPE the dominat process is the molecular growth reaction.

It has been reported that two mechanisms are involved in the process of molecular growth. The first is molecular growth through the formation of ether groups. In this process a radical on a oxygen atom connected to a polymer molecule reacts with a radical on the carbon atom of another molecule. Another radical can form on the newly created larger molecule and repeat the process. In this manner the molecule can grow until the critical size and gel formation occurs. This mechanism was first proposed by a group from Melbourne University in Australia to explain the high concentration of ether groups found in gels that had been stuck inside an extruder.[40]

A second mechanism, crosslinking through vinyl groups (unsaturation), have been shown to be the most important process for crosslinking reactions. Vinyl groups are particularly capable of gel formation since they have high mobility and low steric hindrance compared to other types of unsaturated

groups.[41,42] The free radical formed after reaction with the vinyl group is available and molecular growth continues until it meets another free radical and the process is terminated. This mechanism is supported by works published by CIBA and GE.[41,42]

In order to detect and overcome these problems a new procedure for the management of quality control in production has been devised, with the use of a software named webMIP of Inno-Plast, a German company that deals with industrial automation for plastic manufacture. MIP (Management In Production) is the application for the WEB that transcribes the process data on the database and provides to people using a process information in real time.

The procedure consists of three phases of control:

1) Control in line with webMIP (during and after the production)
2) Control by testing cycles (beginning and during the production)
3) Control of the final product in laboratory (after production)

A generally screen image of the software webMIP, showing the information about the process, as data and time, formulation, thickness profile, is shown in Figure 5.3.

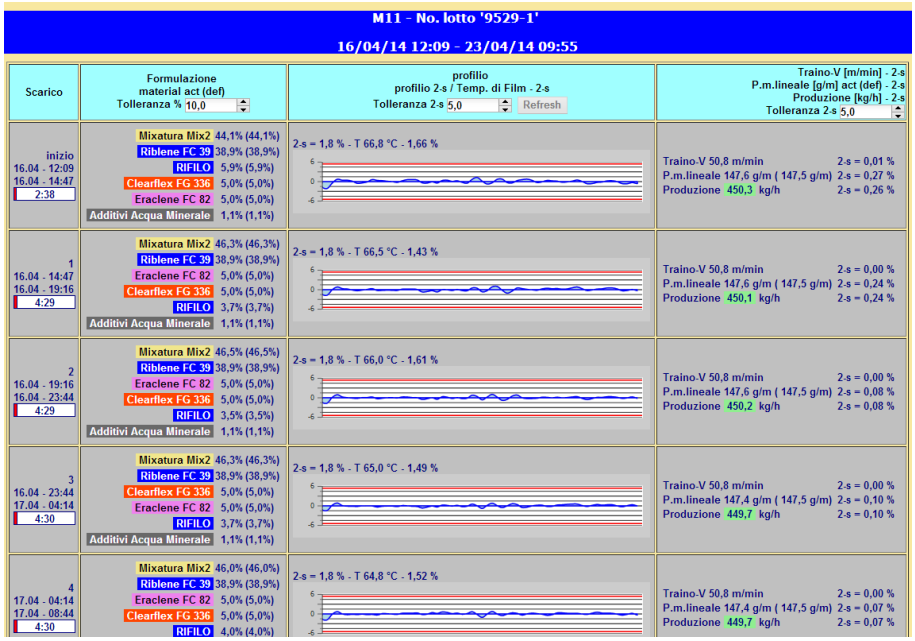

Figure 5.3 *Generally screen image of software webMIP*

The testing cycles consist of a series of control, to be performed at the beginning and durig the production, as show in Table 5.1. The samples are considered to conform and it can be sent to the customer only when passing the three phases of control.

Table 5.1 *Example of the testing cycles table used for the management of quality control at Blu Plast.*

		ORE																							
INDICARE DATA																									
N°	Tipo di Controllo	06	07	08	09	10	11	12	13	14	15	16	17	18	19	20	21	22	23	24	01	02	03	04	05
1	ORA INIZIO PROD.																								
2	Controllo Formula																								
3	Controllo Parametri																								
4	Grammatura																								
5	Tolleranza spessore																								
6	Rigature Film																								
7	Presenza grinze																								
8	Presenza geli																								
9	Allineamento bobina																								
10	Larghezza																								
11	Soffietti																								
12	Goffratura																								
13	Microforatura																								
14	Trattamento																								
15	Contro-trattamento																								
16	Saldatura in linea																								
17	Stampa/stampina																								
18	Colore																								
19	Campione Laboratorio																								

This procedure for management quality control complies with:

- UNI EN ISO 9001:2008 that sets out the criteria for a quality management system and is the only standard in the family that can be certified (although this is not a requirement). It can be used by any organization, large or small, regardless of its field of activity.
- UNI EN ISO 14001:2004 that sets out the criteria for an environmental management system and can be certified. It does not state the requirements for environmental performance, but maps out a framework that a company or organization can follow to set up an effective environmental management system. It can be used by any organization, regardless of its size, activity or sector.

CONCLUSION

The research activity of the present thesis work was focused on the characterization and developping of new polyolefin-based multilayered films used in healthcare applications. These films were made by blow extrusion process using a pilot plant at the company Blu Plast.

In particular, we have studied the structure and the physical properties of polyolefin films used in the industry as back-sheet of napkins and hospital draw sheets. These films should satisfy some requirements, such as high purity of the components, good mechine and lamination ability, good resistance to tear, in particular in the transverse direction (TD) respect to the blowing direction (MD), opacity and good characteristic of soft-touch. This latter term refers to the feeling of softness to the touch so that the film appears as a tissue and not as plastic when it is in contact with skin.

In general, in the industrial practice the characteristic of soft touch is obtained by the technique of micro-embossing, a mechanical treatment consisting in printing on the film surface a relief texture of the order of micrometers. In the case of plastic films the embossing has a drastic effect on the mechanical properties up to obtain film with higher flexibility and provides good soft touch performance. In fact, in the polyolefin films the micro-embossing not only imparts properties of soft touch, so that the material appears as a tissue, but can also have a drastic effect on the mechanical properties, producing local melting of the crystals up to obtain a film with improved flexibility. However, the embossing imply additional costs to the overall process.

The first objective reached was identify the physical properties responsible for the characteristic of soft touch of a polyolefin film and the parameters directly or indirectly related to it. This objective was achieved by analyzing

three commercial embossed films, commonly present on the market. The analysis of the surface by means of optical microscopy, combined to the study of the mechanical properties of these films, has established that the films with the highest percentage of embossing area have the best soft-touch feeling and low values of elastic modulus and stress at yield and at break and high value of deformation at break.

Therefore, the physical parameters directly related to the characteristics of soft touch are physical properties such as elastic modulus, yield point and strain at break of the films.

On these basis we have studied the possibility to obtain similar soft touch performances with polyethylene films without resorting to micro-embossing, and using a simple one stage process.

The soft touch properties of our films are controlled instead by resorting to blending, addition of fillers, co-extrusion and different specialty of polymers of low economic and environmental impact. Hence, different blends of various grades of polyethylene (PE), etherophasic copolymers PE-PP (PP standing polypropylene) and inorganic additives have been used in order to improve the characteristic of soft touch and the mechanical properties of the films, with thickness from 25 μm to 70 μm.

Three sets of not embossed multilayered PE-based films were produced in Blu Plast, by a pilot plant, using for all tests the same process parameters.

The films have been characterized as far as mechanical, thermal properties, morphology and crystallinity. The surface texture of the films have been also analyzed by optical microscopy, atomic force microscopy (AFM) and profilometry.

The properties of these films have been then compared to those of commercial micro-embossed polyethylene films.

The main result of the present investigation is that the sample Test 5 shows the best soft touch properties, due to addition of both talc and calcium

carbonate. Sample Test 5, in fact, reaches values of roughness about half of those of embossed films. The best mechanical performance are obtained, instead, by the film Test 6, containing an elastomeric etherophasic copolymers as additional component in the external layers.

The scale up of the results obtained for the films prepared at pilot plant to the industrial plan is now in progress at Blu Plast.

In conclusion, in this thesis work, it was possible to correlate the soft-touch characteristic of polyolefin films to physical and reliable parameters that can be used to measure the softness of a material. Moreover, smooth polyolefin-based films with improved resistance to tear and soft-touch properties with respect to standard films have been developed, with the advantage to avoid the additional costs of the embossing process.

Finally, the constant economic and commercial competition and the search for a product in line with the requirements of the European regulatory has determined the need to undertake a training course in order to qualify and organize, at best, the structure of the company. This led to the strategic decision to proceed with the implementation of a System of Quality Management.

During the last year of my PhD I had the opportunity to spend a working-stage in the Blu Plast company in order to follow the entire production process of the main mono and multilayered films produced by Blu Plast and to contribute to the implementation of the management system of quality control.

For implementation of the management of quality control I have analyzed the main macro-structural defects of the film. These defects are essentially caused by the presence of “gels” and grooves on the surface. The gels are overlapping of polymer chains in a single point. When the raw material includes gels, it may cause problems in the machine because, although the

high extrusion temperatures, these gels do not melt completely and determine the discontinuities on the film surface.

The gels as well as the grooves represent a deleterious fault, especially for films that need to be coupled or printing.

In order to detect and overcome these problems a new procedure for the management of quality control in production has been devised, by using a software named webMIP of Inno-Plast, a German company that deals with industrial automation for manufacture of plastic.

The procedure consists of three phases of control:

1) Control in line with webMIP (during and after the production)
2) Control by testing cycles (beginning and during the production)
3) Control of the final product in laboratory (after production)

The implementation of this procedure for management quality control was obtained thanks to certification of UNI EN ISO 9001:2008 and UNI EN ISO 14001:2004, moreover it has allowed the Blu Plat company to vie with competitors and to look up at the European market, where the required quality standards are very high.

Bibliography

1. Ullmann's Enciclopedy of Industrial Chemistry Wiley-VCH Verlag GmbH & Co. KGaA, Weinheim (2012) Hans-Georg Elias in *"Plastics, General Survey"*, vol.28, pag. 36.

2. Ullmann's Enciclopedy of Industrial Chemistry Wiley-VCH Verlag GmbH & Co. KGaA, Weinheim (2012) Kenneth S. Whiteley in "*Polyethylene*", vol. 29, pag. 1.

3. Herwig J., Kaminsky W., *Polym. Bull.* **1983**, *9*, 464.

4. Young L.J. in Bradrup and Immergut (eds.): *Polymer Handbook*, 2nd ed., Wiley, New York 1975, Section II, p. 105.

5. Mattice W.L., Stehling F.C. *Macromolecules* **1981**, *14*, 1479.

6. Encyclopedia of Polymer Science and Technology John Wiley & Sons, Inc. New York, 3rd ed. a) Elizabeth Benham and Max Mc Daniel in "*Ethylene Polymers, HDPE*" vol. 2, pag. 382. b) Norma Maraschin in "*Ethylene Polymers, LDPE*" vol. 2, pag. 412. c) D. M. Simpson and G. A. Vaughanin "*Ethylene Polymers, LLDPE*" vol. 2, pag. 441.

7. Mirabella F. M. Jr., Ford E. A. *J. Polym. Sci. Part B: Polym. Phys.* **1987**, *25*, 777.

8. a) Bunn, C. W. *Trans. Faraday Soc.* **1939**, *35*, 482; b) Seto, T.; Hara, T.; Tanaka, K. *Jpn. J. Appl. Phys.* **1968**, *37*, 31.

9. Natta G. *et al.* (**1955**) Italian Patent 554803 to Montecatini

Natta G. *et al.* (**1958**) *Polymorphism of crystalline titanium trichloride*, in: *Atti dell'Accademia Nazionale dei Lincei. Rendiconti. Classe scienze fisiche, matematiche e naturali, 24*, 121-129.

Natta G. *et al.* (**1959**) *Crystal structure of the* g *form of titanium trichloride*, in: *Atti dell'Accademia Nazionale dei Lincei. Rendiconti. Classe scienze fisiche, matematiche e naturali, 26*, 155-163.

Natta G. *et al.* (**1961**) *The different crystalline modifications of TiCl3, a catalyst component for the polymerization of* a-*olefins. I.* a-, b-, g-*TiCl3. II.* d-*TiCl3, J Polym. Sci., 51*, 399-410.

10. a) Hermans J. P., Henriqulie P. US Patent 3769233 (1973) to Solvay at Cie; b) Hermans J. P., Henriqulie P. US Patent 4210738 (1980) to Solvay et Cie.

11. Kashiwa N., Toyota A. AU 89462 82 (1981) to Mitsui Petrochem. Ind

12. Sinn H., Kaminsky W. *Advances in Organometallic Chemistry* **1980**, *18*, 99.

13. Ullmann's Enciclopedy of Industrial Chemistry Wiley-VCH Verlag GmbH & Co. KGaA, Weinheim (2012) T. Geoffrey Heggs in "*Polypropylene*", vol. 29, pag. 381.

14. Natta, G; Corradini, P. *Nuovo Cimento Suppl*., **1960**, *15*, 40.

15. Mencik, Z. *J. Macromol. Sci. Phys.* **1972**, *6*, 101.

16. Hikosaka M., Seto T., *Polym. J*., **1973**, *5*, 111.

17. Immirzi, A.; Iannelli, P. *Macromolecules* **1988**, *21*, 768.

18. Brückner, S.; Meille, S. V. *Nature* **1989**, *340*, 455.

19. Ferro, D. R.; Brückner, S.; Meille, S. V.; Ragazzi, M. *Macromolecules* **1992**, *25*, 5231.

20. Meille, S. V.; Ferro, D. R.; Brückner, S.; Lovinger, A. J.; Padden, F. J. *Macromolecules* **1994**, *27*, 2615.

21. Dorset; D. L.; McCourt, M. P.; Kopp, S.; Schumacher, M.; Okihara, T.; Lotz, B. *Polymer* **1998**, *25*, 6331.

22. Corradini, P.; Petraccone, V.; De Rosa, C.; Guerra, G. *Macromolecules*, **1986**, *19*, 2699.

23. Brückner, S.; Meille, S.V.; Petraccone, V.; Pirozzi, B. *Prog. Polym. Sci*., **1991**, *16*, 361.

24. Kardos, J. L.; Christiansen, W.; Baer, E. *J. Polym. Sci.* **1966**, *A-2* (4), 777.; Pae, K. D.; Morrow, D. R.; Sauer, J. A. *Nature (London)* **1966**, *211*,

514; Pae, K. D. *J. Polym. Sci.* **1968**, *A-2* (6), 657; Sauer, J. A.; Pae, K. D. *J. Appl. Phys.* **1968**, *39*, 4959; Morrow, D. R. *J. Macromol. Sci., Phys. Ed.* **1969**, *B3*, 53.

25. Lotz, B.; Graff, S.; Wittmann, J. C. *J. Polym. Sci., Polym. Phys.* **1986**, *24*, 2017; Kojima, M. *J. Polym. Sci.* **1967**, *5*, 245; Kojima, M. *J. Polym. Sci.* **1968**, *A-2* (6), 1255. Morrow, D. R.; Newman, B. A. *J. Appl. Phys.* **1968**, *39*, 4944.

26. Turner-Jones, A. *Polymer* **1971**, *12*, 487.

27. VanderHart, D. L.; Alamo, R. G.; Nyden, M. R.; Kim, M. H.; Mandelkern, L. *Macromolecules* **2000**, *33*, 6078.; Alamo, R. G.; VanderHart, D. L.; Nyden, M. R.; Mandelkern, L. *Macromolecules* **2000**, *33*, 6094.

28. Auriemma, F.; De Rosa, C.; Boscato, T.; Corradini, P. *Macromolecules* **2001**, *34*, 4815.

29. De Rosa, C.; Auriemma, F.; Circelli, T.; Waymouth, R. M. *Macromolecules* **2002**, *35*, 3622.

30. Auriemma, F.; De Rosa, C. *Macromolecules* **2002**, *35*, 9057.

31. Corradini, P.; Guerra, G. *Adv. Polym. Sci.* **1992**, *100*, 183.

32. Auriemma, F.; Ruiz de Ballesteros O.; De Rosa, C, Corradini, P *Macromolecules* **2000** *33*, 8764.

33. Enciclopedia degli idrocarburi Enrico Albizzati in "*Raffinazione e petrolchimica*", vol. 2, pg. 759.

34. a) Jang, B. Z.; Uhlmann, D. R.; Vander Sande, J. B. *J. Appl. Polym. Sci.*, **1984**, *29(11)*, 3409-3420. b) Jang, B. Z.; Uhlmann, D. R.; VanderSande, J. B. *J. Appl. Polym. Sci*. **1985**, *30(6)*, 2485-2504.

35. a) Cecchin, C.; Morini, G.; Pelliconi, A. *Macromol. Symp.***2001**, *173*, 195-209. b) Cecchin, C.; Marchetti, E.; Baruzzi, G. *Macromol. Chem. Phys.* **2001**, *202*, 1987-1994.

36. Cecchin, C. *Macromol. Symp.***1994**, *78*, 213.

37. Prentice, P.; Williams, J. G. *Plast. Rubber Compos Process. Appl.* **1982** 2, p 27; Fernado, P. L.; Williams, J. G. *Polym. Eng. Sci.* **1981** 21, p 1003; Narisawa, I. *Polym. Eng. Sci.* **1987** 27, p 41; Ma, D.; Li, X.; Luo, X.; Chin. J. Polym. Sci. **1994** 12, p 164; Bramuzzo, M. *Polym. Eng. Sci.* **1987** 29, p 1077.

38. Galli, P.; Haylock, J. C. *Makromol, Chem. , Macromol. Symp.* **1992**, *63*, 19.

39. Obijeski T.J., Dixon D.W. *Characterisation of gels in polyethylene film; Polymers, Lamination &Coatings Conference*; **1992**, p 61-69

40. Scheirs J., Bigger S.W., Delatycki O. *Efficiency of processing stabilisers using a micro-oxygen uptake technique; Polymer*, **1989**; *30*; p 2080-2087

41. Moss S., Zweifel H. *Degradation and Stabilisation of High Density Polyethylene during Multiple Extrusions; Polymer Degradation and Stability*, **1989** 25, p 217-245

42. Johnston, R. T.; Morrison, E. J. *Thermal scission and crosslinking during polyethylene melt processing*; (Dow Plastics, Freeport, TX 77541, USA). Adv. Chem. Ser., 249(Polymer Durability), 651-82 (English).